DEPARTMENT OF ELECTRICAL ENGINEERING
ELECTROPHYSICS

*Mode Locking of Free Electron Sources of Microwave and Millimeter Radiation**

Alan H. McCurdy

Department of Electrical Engineering, University of Southern California, Los Angeles, CA 90089-0271

Final Technical Report for AFOSR Grant # AFOSR-91-0388

for the period

September 30, 1991 to September 29, 1995

Prepared for the Air Force Office of Scientific Research,
Division of Plasma Physics AFOSR/NP ,
Bolling Air Force Base, Washington D.C. 20332-6448

* The research described in this report was carried out in collaboration with H. Wu, R. Liou, V. Kasibhotla, J. Plewa, and T. Phan of the University of Southern California.

UNIVERSITY OF SOUTHERN CALIFORNIA, UNIVERSITY PARK, LOS ANGELES, CALIFORNIA 90089

REPORT DOCUMENTATION PAGE

Form Approved
OMB No. 0704-0188

1. AGENCY USE ONLY (Leave blank)	2. REPORT DATE	3. REPORT TYPE AND DATES COVERED
	2-2-96	Final Technical 9-91 to 9-95

4. TITLE AND SUBTITLE

Mode locking of free electron sources of Microwave and millimeter radiation

5. FUNDING NUMBERS

62234N
0643/42

AFOSR-TR-96 0059

6. AUTHOR(S)

A.H. McCurdy

7. PERFORMING ORGANIZATION NAME(S) AND ADDRESS(ES)

University of Southern California
Electrical Engineering/ Electrophysics
M.C. 0271
University Park, Los Angeles, CA 90089-0271

8. PERFORMING ORGANIZATION REPORT NUMBER

9. SPONSORING/MONITORING AGENCY NAME(S) AND ADDRESS(ES)

AFOSR/NE
Building 410
Bolling AFB, DC 20332-6448
Attn: Dr. R.J. Barker

10. SPONSORING/MONITORING AGENCY REPORT NUMBER

AFOSR-91-0388

11. SUPPLEMENTARY NOTES

12a. DISTRIBUTION/AVAILABILITY STATEMENT

Approved for public release: Distribution unlimited

12b. DISTRIBUTION CODE

19960220 062

13. ABSTRACT (Maximum 200 words)

This report gives the results of theoretical and experimental work on mode locking gyrotron oscillators. A quasi-linear theory is predicts mode locking in the closed cavity gyrotron configuration. The dispersive properties of the electron beam are used to compensate for the electromagnetic dispersion of the cylindrical cavity. An rf modulation of the electron beam axial velocity is used to mode lock eight longitudinal TE_{11n} modes. It is shown that sub-nanosecond radiation pulses can be generated with substantial power. An improved cavity geometry is found which does not require electron beam compensation for mode locking. This tapered cavity is shown to generate short , mode locked radiation pulses via a nonlinear, large-signal theory. Optimum mode locking is found when the electron beam is strongly modulated. A particle-in-cell code (MAGIC) is used to simulate the tapered cavity locked oscillator. MAGIC is used to verify cold test results as well as predict oscillator performance with a modulated electron beam. It is found that short radiation pulses (trains of over 50 pulses) can be generated with moderate levels of rf modulation. The best results are found by using modulation of the electron density rather than the axial velocity. The oscillator and prebunching cavities are designed and experimental cold test si made of the oscillator cavity. Cold test results are compared with both a moving phase front theory and, indirectly, with MAGIC calculations. The prebunching cavity is simulated with MAGIC to determine resonant frequency and tuning range. Results are compared with circuit theory approximations.

14. SUBJECT TERMS

mode locking, gyrotron, maser

15. NUMBER OF PAGES

16. PRICE CODE

17. SECURITY CLASSIFICATION OF REPORT	18. SECURITY CLASSIFICATION OF THIS PAGE	19. SECURITY CLASSIFICATION OF ABSTRACT	20. LIMITATION OF ABSTRACT
unclassified	unclassified	unclassified	UL

NSN 7540-01-280-5500

Standard Form 298 (Rev. 2-89)
Prescribed by ANSI Std. Z39-18

DTIC QUALITY INSPECTED 1

DISCLAIMER NOTICE

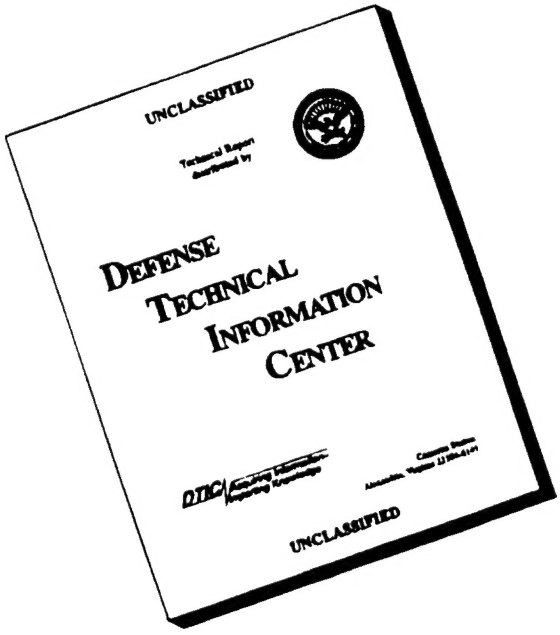

THIS DOCUMENT IS BEST QUALITY AVAILABLE. THE COPY FURNISHED TO DTIC CONTAINED A SIGNIFICANT NUMBER OF PAGES WHICH DO NOT REPRODUCE LEGIBLY.

Mode Locking of Free Electron Sources of Microwave and Millimeter Radiation

Abstract

This report gives the results of theoretical and experimental work on mode locking gyrotron oscillators. The theoretical work is outlined in the first three sections of the report. Experimental work is given in the final section. In Section I, a quasi-linear theory is outlined which predicts mode locking in the closed cavity gyrotron configuration. Here the dispersive properties of the electron beam are used to compensate for the electromagnetic dispersion of the cylindrical cavity. An rf modulation of the electron beam axial velocity is used to mode lock eight longitudinal TE_{11n} modes. It is shown that sub-nanosecond radiation pulses can be generated with substantial power. Section II covers an improved cavity geometry which does not require electron beam compensation for mode locking. This tapered cavity is shown to generate short , mode locked radiation pulses via a nonlinear, large-signal theory. Optimum mode locking is found when the electron beam is strongly modulated. At beam currents several times the start oscillation value, the character of the mode locking is found to change. A particle-in-cell code simulation of the tapered cavity locked oscillator is presented in Section III. The code MAGIC is used to verify cold test results as well as predict oscillator performance with a modulated electron beam. It is found that short radiation pulses (trains of over 50 pulses) can be generated with moderate levels of rf modulation. The best results are found by using modulation of the electron density rather than the axial velocity. Section IV includes the design and experimental cold test of the oscillator cavity, and the design of the prebunching cavity. Cold test results are compared with both a moving phase front theory and, indirectly, with MAGIC calculations. The prebunching cavity is simulated with MAGIC to determine resonant frequency and tuning range. Results are compared with circuit theory approximations.

This work has been published in part in:

H. Wu and A. H. McCurdy, "PIC Simulations of a Closed Cavity Mode Locked Gyrotron," to be published in IEEE Transactions on Plasma Science (June 1996).

A. H. McCurdy, "Nonlinear Theory of Large-signal Mode Locking in a Gyrotron Oscillator," Applied Physics Letters **66**, 1845 (1995).

A.H. McCurdy, "Synchronous Mode Locking in a Closed-cavity Electron Cyclotron Maser," Journal of Applied Physics 74, 3576 (1993).

This work has been presented at the following conferences:

A.H. McCurdy, "Synchronous Mode Locking in Gyrotrons," 1992 IEEE International Electron Devices Meeting, December 13 - 16, San Francisco, CA.

A. H. McCurdy, "Mode Locking in a Closed Cavity Gyrotron Oscillator," Seventeenth Int. Conf. on Infrared and Millimeter Waves December 14 - 18, 1992, Pasedena, CA.

A. H. McCurdy and H. Wu, "Nonlinear Theory of Large-Signal Mode Locking in a Gyrotron Oscillator," SPIE International Symposium on Optical Science, Engineering and Instrumentation: Intense Microwave Pulses III, San Diego, CA, 1995.

V. Kasibhotla and A.H. McCurdy, "Mode Conversion and Coupling in an Electron-Beam Driven Low Q Gyrotron," 22nd IEEE International Conference on Plasma Science, Madison, WI, 1995.

H. Wu, R. Liou, and A. H. McCurdy, "Pulsed Radiation Generation in Closed and Open Cavity Gyrotrons," 22nd IEEE International Conference on Plasma Science, Madison, WI, 1995.

V. Kasibhotla and A.H. McCurdy, "Mode Conversion and Coupling in a Low Q Gyrotron," 21st IEEE International Conference on Plasma Science, Santa Fe, NM, 1994.

H. Wu and A. H. McCurdy, "Study of Mode Locking in Tapered Cavity Gyrotron Oscillators," 21st IEEE International Conference on Plasma Science, Santa Fe, NM, 1994.

A.H. McCurdy, H. Wu, R. Liou, and V. Kasibhotla, "Mode Locking in Closed and Open Cavity Gyrotron Oscillators," 1994 Microwave Power Tube Conference, Monterey, CA.

A.H. McCurdy, "Mode Locking in a Closed Cavity Gyrotron Oscillator," Vacuum Electronics Review, Crystal City, VA, 1993.

A.H. McCurdy, "Mode Locking in Closed Cavity Gyrotrons," the 20th IEEE Int. Conf. Plasma Science, Vancouver, B.C., 1993.

H. Wu, V. Kasibhotla, T. Katsouleas, and A. H. McCurdy, "MAGIC Code Simulation of Mode Locking in Closed and Open Cavity Gyrotron Oscillators," the 20th IEEE Int. Conf. Plasma Science, Vancouver, B.C., 1993.

A.H. McCurdy, "Mode Locking of Free-Electron Sources of Microwave and Millimeter Wavelength Radiation," 1992 Microwave Power Tube Conference, Monterey, CA.

A.H. McCurdy, "Mode Locking of Free-Electron Masers," Bull. Am. Phys. Soc. 36, 1991.

Contents

SECTION I

Synchronous Mode Locking in a Closed Cavity Electron Cyclotron Maser

Abstract - Section I

It is theoretically demonstrated that mode locked operation can be achieved in a closed cavity electron cyclotron maser (gyrotron). This work is unique in two respects. First, the cavity provides a highly dispersive guiding structure for the electromagnetic wave, hence, the mode frequency spacing varies by an amount comparable to the average spacing between modes. The dispersive properties of the electron beam are used to compensate that of the cavity to allow eight longitudinal TE_{11n} modes to lock together. Second, the locking is obtained by rf modulation of the axial velocity of the electron beam. A numerical example shows that sub-nanosecond radiation pulses can be generated at 16 GHz with an order of magnitude increase in power level over the free-running maser.

I. INTRODUCTION

A problem encountered in the development of high power, high efficiency sources of coherent radiation in the microwave and millimeter wavelength regime is the competition between various electromagnetic modes. This problem is seen in devices such as free electron lasers, electron cyclotron masers (ECM), plasma based devices as well as the conventional slow wave devices such as traveling wave tubes. The physical mechanism for this mode competition lies in the nonlinear character of the electron beam from which the modes derive their energy. For applications requiring extremely narrow spectral widths, there is little substitute for single-mode operation. Hence much research has focused on the suppression of unwanted modes. However for some applications sharpness in the frequency spectrum is not important, it may in fact be desired that the signal be short-pulse or frequency modulated. For these applications it may be possible to utilize the microwave oscillator in the overmoded state. In general, the output of the overmoded oscillator is most useful if it is periodic. This requires a coupling between the modes to lock them into a common frequency interval. Thus coherent output is obtained with a concomitant modulation in either the amplitude or frequency. The technique of mode locking has been highly successful in laser oscillators.[1-3] Here we demonstrate that by using the method of synchronous mode locking in an ECM oscillator high peak power, short-pulse radiation is obtained. The mode locking is *synchronous* in that an external rf signal is applied to the gain medium (electron beam) to couple the modes.

There has been some previous work on mode locking of free-electron microwave devices. An early free electron laser experiment[4] utilized a 1.3 GHz pulsed electron beam and reported short pulse radiation output. It was later understood that these short pulses were the result of many locked cavity modes. However no tests of radiation output as a function of modulation parameters were reported (mode locking was an incidental part of the experiment). A general theoretical analysis of the nonstationary effects in FELs[5] predicted a wide range of behavior (such as is typically seen in nonlinear oscillators) such as mode locking, phase locking and stochastic regimes. Other FEL theory has also predicted mode locking.[6] Recent FEL experiments have reported self- mode locking[7] and inter-pulse locking via an external cavity.[8] The self-locking was intermittent (two locked radiation pulses out of 70) since the oscillator start-up conditions varied from pulse-to-pulse.

Self-mode locked ECMs have been described using the quasi-linear rate equation model.[9] Mode locking in a quasi-optical gyrotron using a time dependent phase perturbation in the cavity has also been considered.[10] In this case the phase change was caused by a secondary electron beam with a modulation imposed on the electron density. It was found in this study that mode locking in the linear regime could not be obtained when one beam was used for both the gain medium and the phase shift (the phase shift beam cannot be at the cavity center).

Here we describe the mode locking of ECMs, of the closed cavity type, using an external modulation signal. This method of mode locking is preferable in that enhanced oscillator stability and pulse-to-pulse coherence is obtained. Closed cavity ECM oscillators often oscillate in a single mode in the steady state, since the modes are strongly coupled. Even so, there are several reasons for considering the mode locking of such a device. First, short-pulse or frequency modulated output may be desired. Second, the time required for single mode operation to be obtained can be a substantial fraction of the pulsewidth.[11,12] Thus the ECM is, for all practical purposes, overmoded though it is approaching a single-mode state. One might anticipate that mode locking could enhance the performance of such an overmoded device. An interesting feature of the mode locking of an ECM of this configuration is that the structure guiding the electromagnetic wave is highly dispersive, hence the cavity modes are far from being equally spaced in frequency. In fact the *variation* in mode frequency separation of the modes which are eventually locked is on the order of the *average* mode frequency separation. It is shown here that the dispersive properties of the electron beam can be exploited to compensate that of the guiding structure. This result may have significance for mode locking in other dispersive systems. Another novel feature of this work is that mode locking is obtained via *velocity* modulation of the electron beam. This provides a temporal variation in the resonance condition (between the electron beam wave and the electromagnetic wave), hence having a much larger effect on the oscillator for a given size modulation signal than would be obtained with density modulation.

Applications for short pulse radiation in the millimeter and sub millimeter wavelength range include radar and time domain metrology. The attractive feature of the technique discussed here is that it may allow a wide range of radiation sources to provide short, highly reproducible radiation pulses. It is expected that the pulse-to-pulse noise prevalent in present high power sources of coherent radiation would not occur since the electron beam is CW.

II. THEORY

A. ECM rate equations including modulation

The gyrotron configuration considered here (see Fig. 1) is a circular cylindric cavity of radius r_w and length L supporting TE_{11n} modes.[13] The electron beam used is a zero temperature, annular one with an electron guiding center position R_0 and initial electron velocities perpendicular and parallel to the cavity longitudinal axis of $v_{\perp 0}$ and v_{z0}, respectively. It is assumed that the electromagnetic modes excited by the beam are those of the empty cavity structure. The cavity is electrically isolated and a low frequency (ω_m) voltage signal is applied between the cavity and the grounded beam channel.[14] This signal causes a temporal change in the axial electron velocity of the electron beam: $v_z(t) = v_{z0}[1 + \delta$

cos ($\omega_m t$)]. It is assumed that the cavity electric potential changes little in the time taken by an electron to traverse the cavity, $1 > (\omega_m L) / (2 \pi v_{z_0})$. The electron cyclotron maser (ECM) resonance condition between the cyclotron wave on the electron beam and the transverse electric electromagnetic wave is a sensitive function of the beam axial velocity. Thus the velocity modulation has a large effect on the amplitude and phase of the generated radiation and results of sufficient interest can be obtained by assuming small δ.

This problem can be analyzed using the rate equation model for the temporal evolution of the slowly varying power P_j and phase Ψ_j of the cavity modes:

$$\frac{dP_j}{dt} + \frac{\nu_j}{Q_j} P_j = -\nu_j P_j \, Im\{\chi_j\} \quad , \quad \frac{d\Psi_j}{dt} + \nu_j - \nu_j^0 + \frac{\nu_j}{2\,Q_j^0} = \frac{\nu_j}{2} Re\{\chi_j\} \qquad (1)$$

Here ν_j , ν_j^0 , and Q_j^0 are the frequency of oscillation, empty cavity resonant frequency, and Ohmic cavity quality factor of the j^{th} mode, respectively. The coupling losses from the cavity are included in Q_j. The electronic susceptibility c_j is computed from an integral over the cavity volume of the scalar product of the electron beam current density and the cavity electric field eigenmode.[12] This term characterizes the change in power level and phase of the cavity fields due to the electron beam. In deriving the rate equations, the instantaneous wave phase is $\nu_j t + \Psi_j(t)$. The steady state frequency of the j^{th} mode is defined: $\omega_j = \nu_j + \dot{\Psi}_j$. Since the frequencies of the oscillating modes will be nearly equally spaced (the beam dispersion is adjusted so that this is the case):

$$\omega_j = \omega_n + (q_j - q_n)\,\Delta\omega,$$

where ω_n is the oscillation frequency of a central mode, q_j and q_n are integers which distinguish the modes (in the case of axial mode competition they are the axial mode eigenvalues) and Dw is the frequency interval between modes. The frequency ν_j can be *defined* by:

$$\nu_j = \omega_n + (q_j - q_n)\,\omega_m.$$

The actual oscillation frequency is approximated:

$$\omega_j = \nu_j^0 - \frac{\nu_j}{2\,Q_j^0} + \frac{\alpha_j'}{2} \qquad (2)$$

where the nonlinear contributions to the frequency shift are assumed to be small. Using Eq. (2) and the definitions for n_j and w_j in Eq. (1) we find:

$$\frac{dP_j}{dt} - \left(\alpha_j'' P_j - \beta_j'' P_j^2 - \sum_{s \neq j} \theta_{j\,s}'' P_j P_s \right) = \delta \sqrt{P_j P_{j+1}}\, Im\left\{ \alpha_{j,j+1}\, e^{i(\Psi_{j+1} - \Psi_j)} \right\}$$

$$+ \delta \sqrt{P_j P_{j-1}}\, Im\left\{ \alpha_{j,j-1}\, e^{i(\Psi_{j-1} - \Psi_j)} \right\} \qquad (3)$$

$$\frac{d\Psi_j}{dt} - (q_j - 4)\,\Delta\nu - \frac{1}{2}\left(\beta_j' P_j + \sum_{s \neq j} \theta_{j\,s}' P_s \right) = -\frac{\delta}{2} \sqrt{\frac{P_{j+1}}{P_j}}\, Re\left\{ \alpha_{j,j+1}\, e^{i(\Psi_{j+1} - \Psi_j)} \right\}$$

$$-\frac{\delta}{2} \sqrt{\frac{P_{j-1}}{P_j}}\, Re\left\{ \alpha_{j,j-1}\, e^{i(\Psi_{j-1} - \Psi_j)} \right\}$$

where the TE_{114} has been chosen as the central mode ($q_n = 4$). Mode locking occurs when the time derivatives of the phases Ψ_j equal a constant. Primes and double primes represent the real and imaginary parts of the quantity, respectively. Here χ_j has been expanded in a power series in P, and only the lowest order saturation effects have been retained. $\Delta\nu = \Delta\omega - \omega_m$ is the detuning of the modulation signal frequency from the nominal cavity mode frequency separation. Inclusion of the external modulation in the rate equations results in new linear coupling between adjacent modes [through the coefficients $\alpha_{j,\,j+1}$ and $\alpha_{j,\,j-1}$ in Eq. (3)]. The linear coupling occurs because $\omega_{j \pm 1} - \omega_j \mp \omega_m \cong 0$. Thus when the rate equations are averaged over the fast time scale of the inter-mode beat frequencies, the adjacent linear mode coupling remains. Here we neglect coupling in the nonlinear terms β and θ.

B. Determination of the linear coupling coefficients

The rate equation coefficients, α, β, θ and $\alpha_{j,\,k}$ are computed by using the relativistic Lorentz force equations to determine the electron momenta, deriving the current density, and then performing the integration required to find χ_j.[15] For weakly relativistic ECM devices which support electromagnetic modes near cutoff, the Lorentz forces are transverse to the axial electron flow, the self-generated rf fields do not change the axial (z directed) electron velocity. The derivation of the linear cross-coupling coefficient for constant axial electron velocity has been given elsewhere.[16] Here we modify the former result to describe the case of a temporal dependence of the axial electron velocity which occurs when the external modulation signal is present. Following [16] the electron susceptibility can be written as:

$$\nu_j\, \chi_j = \alpha_j + \alpha_{j,k} \sqrt{\frac{P_k}{P_j}}\, e^{i[\Psi_k - \Psi_j + (\nu_k - \nu_j)t]} + \beta_j\, P_j + \ldots \qquad (4)$$

and the linear cross-coupling term is

$$\alpha_{j,k} = i \frac{2\,c\,(1-\beta_{\perp_0}^2)\,I_0\,\Gamma_j\,v_{z_0}}{\varepsilon_0\,\omega_j\,L\,\beta_{\perp_0}^2\,\omega_0\,v_z(t)}\,C_{m_k \ell_k}\delta_{m_j,m_k}\int_{z=0}^{\bar{L}} f_{q_j}^*(z) f_{q_k}(z)\,b_{0_j}(z,t)\,dz \qquad (5)$$

where $\Gamma_j = C_{m_j\,\ell_j}\,k_{m_j\,\ell_j}\,J_{m_j-1}(k_{m_j l_j} R_0)$, and the time-dependent terms are shown explicitly. Here I_0 is the dc electron beam current, ω_0 is a normalization frequency, c is the speed of light, $\beta_{\perp 0} = v_{\perp 0}/c$, L is the cavity length, and δ_{mn} is the Kronecker delta. The modal indices of the j^{th} cavity mode are given by m_j, l_j, and q_j (in the azimuthal, radial, and axial directions). C_{ml} is a modal normalization constant,[12] and k_{ml} is the perpendicular wave number. The integral is over the axial coordinate z, which has been normalized by $2\,v_{z0}/(\beta_{\perp 0}{}^2\,\omega_0)$. The normalized axial electric field eigenfunction $f_q = \sin(k_z z)$, (where $k_z = q\pi / \bar{L}$ and $\bar{L}$ is the normalized cavity length). The function $b_{0_j}(z,t)$ can be found by comparison with the known expression for the linear growth rate of the j^{th} mode:

$$b_{0_j}(z,t) = -\frac{\eta_j}{\gamma(t)\,v_z(t)}\frac{e^{i\Delta_j(t)\,z}}{f_q^*}\left\{\int_o^z f_q^*\,e^{-i\Delta_j(t)\,z'}\,dz' + i\frac{v_{z_0}}{v_z(t)}\int_o^z\int_o^{z'} f_q^*\,e^{-i\Delta_j(t)\,z''}\,dz''\right\} \qquad (6)$$

$$\text{where } \eta_j = \frac{e\,v_{z_0}}{2\,\beta_{\perp_0}^2\,\omega_j\,m\,v_{\perp_0}}\ , \text{ and } \Delta_j(t) = \frac{2}{\omega_0\,\beta_{\perp_0}^2\,v_z(t)}\left(\omega_j - \frac{\Omega_0}{\gamma(t)}\right)\ .$$

Here m is the electron rest mass, $\gamma(t)$ is the relativistic factor which depends on time through v_z and Ω_0 is the non-relativistic electron cyclotron frequency.

Equation (6) shows that modulation of the electron velocity causes the phase averaged electron perpendicular momentum to contain explicit time dependencies through the beam density variation (by charge continuity a velocity change is accompanied by a corresponding density change) and the resonance detuning parameter $\Delta_j(t)$. Because of the nonlinear dependence of Eq. (4) on v_z [through Eqs. (5) and (6)], harmonics of ω_m are generated in the electron beam current density which tend to couple all electromagnetic modes together. It is assumed here that only the fundamental harmonic is strong, hence the $\alpha_{j,k}$ couple only adjacent modes.

The time dependence of $\alpha_{j,k}$ is contained in the term $b_{0_j}(z,t)/v_z(t)$. This function can be expanded in a Fourier series in harmonics of the modulation frequency:

$$\frac{b_{0_j}(z,t)}{v_z(t)} = a_{0_j} + \sum_{n=1}^{\infty} a_{n_j} \cos(n\,\omega_m t \qquad (7)$$

where $a_{0_j} = \frac{\omega_m}{2\pi}\int_{t=0}^{\frac{2\pi}{\omega_m}} \frac{b_{0_j}(z,t)}{v_z(t)}\,dt$, $a_{1_j} = \frac{\omega_m}{\pi}\int_{t=0}^{\frac{2\pi}{\omega_m}} \frac{b_{0_j}(z,t)}{v_z(t)}\cos(n\,\omega_m t)\,dt$ etc.

Using Eq. (6) in (7), then into (5) and then (4) and averaging over the rapid time scale τ of beating between adjacent modes : $\tau = \frac{2\pi}{\omega_s - \omega_j} << \frac{P}{dP/dt}$, it is found that the time independent term a_{0j} averages to zero. The other terms are nonzero provided that

$\omega_s - \omega_j \cong n\,\omega_m$.

Keeping only the n = 1 term, consistent with the neglect of harmonics of w_m, we simplify the computation of $\alpha_{j,k}$ by linearizing in the velocity modulation amplitude, thereby assuming $\delta << 1$. The linear cross-coupling coefficients can be written:

$$\alpha_{j,k} = i\,\frac{I_0\, e\left(1-\beta_{\perp_0}^2\right)\Gamma_j\,\Gamma_k}{2\,\gamma_0\,\varepsilon_0\, m\,\beta_{\perp_0}^4\,\omega_0\,\omega_j\,L}\,\delta_{m_j,m_k}\,A_{j,k}$$

and $$A_{j,k} = \int_{z=0}^{L} dz\; f_{q_k}(z)\left\{2\int_{z'=0}^{z} dz'\, f_{q_j}^*(z')\, e^{-i\Delta^0{}_j(z'-z)}\left[1 + i\,r_j(z'-z)\right] + 3\,i\int_{z'=0}^{z} dz' \int_{z''=0}^{z'} dz''\, f_{q_j}^*(z'')\, e^{-i\Delta^0{}_j(z''-z)}\left[1+\frac{2}{3}\,i\,r_j(z''-z)\right]\right\}.$$

Here γ_0 is the relativistic factor (evaluated at the cavity entrance and using an axial velocity of v_{z_0}) and the normalized detuning Δ^0_j is defined as Δ_j evaluated with $\gamma(t) = \gamma_0$ and $v_z(t) = v_{z_0}$. Note that the $\alpha_{j,k}$ are complex since velocity modulation of the electron beam produces both phase and amplitude modulation in the radiation. The rotation factor

$$r_j = \frac{1}{\omega_0\beta_{\perp_0}^2}\left[\Omega_0\gamma_0\beta_{z_0}^2 - \left(\omega_j - \frac{\Omega_0}{\gamma_0}\right)\right]$$

describes the competing effect of the electron velocity change on the relativistic cyclotron frequency (first term) and the Doppler shift (second term). From the expression for $A_{j,k}$ it is clear that the coupling

becomes small when r_j is small (r_j multiplies the only non-oscillating terms in the integrals of $A_{j,k}$). The physical reason for this effect is that frequency of the cyclotron wave on the electron beam ($\omega_{beam} \cong \Omega_0/\gamma + k_z v_z$) is changed both through γ and v_z when the velocity is modulated (see Fig. 2). An increase of v_z will cause a decrease in the cyclotron frequency but an increase in the Doppler shift of the electron cyclotron wave as seen in the laboratory frame. For the low order modes, $q_j = 1, 2$ etc. the modulation is primarily due to the energy change while for the high order modes, $q_j = 6, 7, 8$ the modulation is due to the Doppler shift.

III. NUMERICAL RESULTS

A. ECM parameters

A numerical example is now given using the parameters: electron beam energy 40 keV, $I_0 = 2.5$ A, $R_0 = 0.35$ cm, $v_{\perp 0} / v_{z_0} = 1.0$, $r_w = 0.55$ cm, L = 15 cm, and quality factors of all modes 300. The open circles in Fig. 3 show the separation in cavity resonant frequencies as obtained from the waveguide dispersion relation $\omega = c\sqrt{k_{m\ell}^2 + k_z^2}$, (the resonant frequencies are near 16 GHz). The points nearly fall on a straight line since $k_{m\ell} >> k_z$ for this cavity (gyrotrons typically operate near cutoff). The contribution by the electron beam (for a choice of magnetic field of 5.858 kG) via the coefficients α'_j is shown by the × 's in the figure. The beam pushes up the frequency of mode TE_{11q_j} more than TE_{11,q_j-1} for small values of q_j while the opposite occurs for values of q_j greater than 5. A uniform mode separation of 270 MHz is obtained for the central six modes.

B. Conditions for equally spaced cavity modes

A general prescription can be given to make the mode spacing as uniform as possible. Since the electron beam must simultaneously compensate the uneven frequencies of many modes, many independent parameters must be adjusted. This parameter field can be limited by choosing a beam voltage so that the modal frequency pushing as a function of magnetic field has the features of Fig. 4(a). This figure indicates that the beam changes the frequencies of pairs of modes in the same way (note the overlap in the TE_{114} and TE_{115} curves, the TE_{113} and TE_{116} curves etc.). Thus the number of parameters required is reduced by a factor of two. The optimal mode spacing is achieved by varying the magnetic field until the relative frequency shift of the individual modes is correct to compensate the waveguide dispersion. The necessary absolute frequency shift is obtained by varying the beam current.

Beam frequency pushing of the kind shown in Fig. 4(a) is obtained by choosing a beam voltage such that resonance is simultaneously obtained for two modes centrally located in the frequency spectrum (the TE_{114} and TE_{115} modes in the example considered here). Figure 5 shows the resonance

between the beam and waveguide mode for this parameter choice. Because $\frac{\partial\omega}{\partial k_z} < v_z$ (v_z is the group velocity of beam wave) for $q_j < 4$, the TE_{11,q_j-1} modes are farther from resonance than the TE_{11q_j} modes; thereby incurring a smaller frequency shift. For $q_j > 5$, $\frac{\partial\omega}{\partial k_z} > v_z$ and the TE_{11q_j-1} modes are closer to resonance than the TE_{11q_j} modes; hence entailing a larger frequency shift. Since the TE_{114} and TE_{115} modes are both at resonance, they undergo an identical frequency shift. Thus the frequency difference between the "beam loaded" cavity modes will be approximately equal to the frequency difference between the "unloaded" TE_{115} and TE_{114} cavity modes. It should be noted that for large values of q_j, the associated TE mode has a large k_z and the effects of the time-varying magnetic field must be included.

By appropriate choice of the beam voltage and guide magnetic field, any two adjacent cavity modes can play the role of the TE_{114} and TE_{115} in this example. An alignment between modes of the type shown in Fig. 4(a) can be obtained by finding the w - intercept and slope of the beam wave which intersects the two chosen cavity modes (as in Fig. 5). It is easily shown that

$$\beta_z = \left\{ \frac{\sqrt{1+\left(\frac{k_{z_{n+1}}}{k_\perp}\right)^2} - \sqrt{1+\left(\frac{k_{z_n}}{k_\perp}\right)^2}}{\left(\frac{k_{z_{n+1}} - k_{z_n}}{k}\right)} \right\} \quad \text{and} \quad V_{beam} = \frac{m c^2}{e}\left\{\left[1-\beta_\perp^2-\beta_z^2\right]^{-\frac{1}{2}} - 1\right\} .$$

Also:

$$B_z = \frac{m c}{e}\left[1-\beta_\perp^2-\beta_z^2\right]^{-\frac{1}{2}}\left\{k_{z_{n+1}}\sqrt{k_\perp^2+k_{z_{n+1}}^2} - k_{z_n}\sqrt{k_\perp^2+k_{z_n}^2}\right\}\left(k_{z_{n+1}}-k_{z_n}\right)^{-1} .$$

Here $k_\perp$ is the perpendicular wavenumber and β is the ratio of the velocity to c. This computation is based on the resonance condition providing equal excitation to two modes at a given value of the beam parameters. This causes the adjacent modes to have equal growth rates. It has been found that in such a case the modes will also be frequency shifted by an equal amount (see Fig. 4). A comparison of the results of this approximation with the beam voltage and magnetic field predicted by linear theory to produce equal frequency pushing of the two chosen modes is shown in Fig. 6. The approximation slightly overestimates the optimal values of the parameters. This is because the ECM operation requires a slight detuning between the field frequency and cyclotron frequency for the maximum growth rate.

C. Mode locking results

The linear growth rates for the numerical example indicate that the TE_{111} and TE_{118} modes are below the start oscillation threshold for a magnetic field of 5.858 kG [see Fig. 4(b)]. As can be seen from Fig. 3, these two modes do not have the proper frequency spacing, thus will be difficult to mode lock. However, these modes are in the *hard excitation* regime (the self-saturation coefficients β''_j in Eq. (3) are negative) and can be easily excited by other modes. Hence it is necessary to further suppress them by lowering their modal quality factors to 150. In this way these modes are passively driven to a low level of oscillation. It is found that large modulation levels can transfer enough energy to drive these modes across their oscillation threshold, deleteriously affecting mode locked operation.

Figure 7 shows the mode locked radiation pulse envelope for three different values of normalized detuning $\Delta\nu$ (normalized to the nominal cavity mode spacing of 270 MHz) using $\delta = 0.1$ and B_z = 5.858 kG. This envelope is obtained by selectively coupling to one of the traveling waves in the maser cavity. The power is computed from:

$$P_{envelope}(t) = \sum_j \sum_k \sqrt{P_j}\,\sqrt{P_k}\cos\left[\left(q_j - q_k\right)\omega_m\, t + \Psi_j - \Psi_k\right] \quad . \tag{8}$$

The FWHM of the optimal pulse is about 500 ps with a power of greater than twelve times the free-running time averaged power level. A smaller secondary pulse is also generated. This is due to the steady state phases and amplitudes chosen by the modes. For the parameters chosen, the modal amplitude spectrum is not Gaussian (hence sidebands) and the phase separation is not np (hence asymmetry of sidebands). The optimum pulse is obtained for the largest allowable modulator frequency (a detuning of - 0.24 % is at the locking edge). Peak pulse size and pulsewidth degenerate substantially for other values of the detuning.

The size of the external signal required for mode locking is critical since, in practice, the available modulation power may be limited. The minimum modulator amplitude for locking of eight modes is shown as a function of detuning $\Delta\nu$ in Fig. 8, for several values of the magnetic field. Here the gyrotron is mode locked (for a fixed detuning) at any δ greater than that given by the curve. As in lasers, the minimum locking signal does not occur at $\Delta\nu = 0$. Figure 8 shows that this minimum depends on the magnetic field. The optimum (B = 5.848 kG, detuning of 1%) is found very close to the magnetic field at which the "beam loaded" cavity modes are equally spaced in frequency (as shown in Fig. 3). The required electron beam modulation is on the order of 5%. It is generally true that optimum pulse shape is obtained at the high frequency edge (lowest value of $\Delta\nu$) of the locking band.

Using the previously described method of dispersion compensation, it can be shown that the electron transit time is nearly half as long as the modulation period. This is done by setting the modulation frequency equal to the frequency separation between adjacent modes:

$$\omega_m \cong \omega_{n+1} - \omega_n \cong \frac{(2\,n+1)}{2\,\omega_n}\left(\frac{\pi}{L}\,c\right)^2, \quad \text{where } \frac{\omega_{n+1}-\omega_n}{\omega_n} << 1 \text{ has been assumed.}$$

The ratio of the electron transit time τ to the period of the modulation signal T is:

$$\frac{\tau}{T} = \frac{(2\,n+1)\,\pi\,c^2}{4\,\omega_n\,v_z\,L} \quad .$$

Using the fact that the waveguide and beam dispersion relations must intersect at ω_n and match in group velocity, ω_n and v_z can be expressed in terms of k_z. The relation

$$\frac{\tau}{T} \cong \frac{1}{2} + \frac{1}{4\,n} \qquad (9)$$

results. Because the transit time is so long the average effect of the modulator will be somewhat less than shown in Fig. 8. In order to more efficiently change the beam axial velocity, a separate cavity (perhaps of the re-entrant type used in klystrons) may be used to impress the modulation on the beam. Hence higher values of δ become experimentally accessible. The frequency band over which mode locking can be achieved is large, hence the modulator frequency need only be within a percent of the nominal cavity mode spacing (with $\delta \cong 0.1$).

Figure 9 gives the minimum value of modulation δ_{min} which will allow mode locking as a function of the magnetic field. The value of the detuning for which locking is obtained is also shown. The axial velocity modulation need only be on the order of 4% for locking at magnetic fields near 5.848 kG. The detuning needed for magnetic fields in this vicinity is near 1.25%. The detuning maximizes near the optimum value of δ_{min}.

The propagation of the radiation pulse in the cavity is shown in Fig. 10. The parameters are the same as the optimum pulse in Fig. 7 ($\delta = 0.1$, $\Delta\nu = -0.24$ %). The energy stored in the cavity fields (normalized to the time averaged free-running energy) is shown as a function of axial position in the cavity (position is normalized to cavity length). The temporal evolution of this energy profile over three-quarters of a modulation cycle is shown in the various figures (a) - (f). The energy is proportional to the power given by Eq. (8) with the additional term

$$\sin\left(\frac{q_j\,\pi\,z}{L}\right)\sin\left(\frac{q_k\,\pi\,z}{L}\right)$$

included because of the cavity standing wave fields. It can be clearly seen from the sequence 10(a) through 10(c) that a broad pulse, traveling to the right, reflects from the cavity end (z = L). The pulse shape is not constant in time, but peaks at the reflection point. The return trip proceeds in 10(d) through 10(f). Again the pulse broadens as it passes the cavity center and peaks upon reflection from the cavity

entrance. Correlating the time with Fig. 7, it can be seen that the pulse formation at the cavity entrance (t = 2.5 ns) coincides with the large pulse in Fig. 7. This pulse motion continues periodically in time with the pulse bounce time equal to the modulator period. The behavior observed here is similar to that previously noted in lasers with Fabry-Perot cavities. The primary difference is that the radiation envelope changes dramatically on its round-trip through the cavity due to the dispersion of the guiding structure. Equation (9) indicates that the electron transit time through the cavity is nearly half of the modulation period. From Fig. 10, it is seen that the pulse travels the length of the cavity in this same time. Hence the pulse interacts with a group of electrons as it traverses the cavity.

Since the radiation pulse peaks at the cavity ends, it is natural to attempt to couple the radiation from the cavity exit, z = L. Two problems are immediately apparent. If the output waveguide is of comparable size to the cavity cross-section, then dispersion effects will deteriorate the radiation pulse. On the other hand, if the output waveguide is large in cross-section then there will be spatial decoherence of the pulse as the lower order modes propagate at a larger angle to the cavity axis than the higher order modes. Clearly substantial design work is required to achieve an optimal output radiation pulse.

IV. CONCLUSION

In conclusion, it has been shown via quasi-linear theory that a gyrotron oscillator with a highly dispersive waveguiding structure can be mode locked by compensating with dispersion due to the electron beam. The required modulator signal level is not large and the frequency stability need only be on the order of 0.1 % (in order to stay in the region of optimal pulse production). In addition, no dramatic redesign of the oscillator cavity is necessary (though the TE_{111} mode must be damped). It is possible that this method may apply to other free-electron oscillators, especially ones which exhibit a monotonic change of $\frac{\partial \omega}{\partial k}$ with k. This method may allow generation of extremely short, reproducible radiation pulses (with high repetition rates) and high power levels in the microwave to submillimeter wavelength regime.

REFERENCES

1 L.E. Hargrove, R.L. Fork, and M.A. Pollack, Appl. Phys. Lett. **5**, 4 (1964).

2 O.P. McDuff and S.E. Harris, IEEE J. Quant. Electron. **QE-3**, 101 (1967).

3 See for example A. Yariv, *Optical Electronics* (Holt, Rinehart, and Wilson, New York, NY, 1985); A.E. Siegman, *Lasers* (University Science, Mill Valley, CA, 1986).

4 D.A. Deacon, L.R. Elias, J.M.J. Madey, G.J.Ramian, H.A. Schwettman, and T.I. Smith, Phys. Rev. Lett. **38**, 892 (1977).

5 Y.L. Bogomolov, V.L. Bratman, N.S. Ginzburg, M.I. Petelin, and A.D. Yunakovsky, Optics Comm. **36**, 209 (1981).

6 G. Dattoli, in *CAS Cern accelerator School: Synchrotron Radiation and Free Electron Lasers Proceedings* (CERN 90-03) 1989.

7 K. Toyoda and Y. Kawamura, Laser and Particle Beams **7**, 421 (1989).

8 D. Oepts et al., Phys. Rev. Lett. **68**, 3543 (1992).

9 G.S. Nusinovich, "Theory of Mode Interaction in the Gyrotron," KfK Rept. 4111, August 1986.

10 W.M. Manheimer and M.E. Read, Int. J. Electron. **61**, 1041 (1986).

11 B. Levush and T.M. Antonsen, Jr., Nucl. Inst. Meth. Phys. Res. **A285**, 136 (1989).

12 A.H. McCurdy and C.M. Armstrong, Phys. Fluids B **3**, 212 (1991).

13 This is a simplified closed-cavity gyrotron structure; A.H. McCurdy and C.M. Armstrong, Phys. Rev. Lett. **61**, 2316 (1988).

14 private communication with C.M. Armstrong.

15 G.S. Nusinovich, Int. J. Electron. **51**, 457 (1981).

16 A.H. McCurdy and J.S. Plewa, IEEE Trans. Plasma Sci. **20**, 139 (1992).

FIGURE CAPTIONS

FIG. 1. Closed cavity gyrotron with modulation signal V(t). Beam travels along the z-axis.

FIG. 2. Filamentary cyclotron wave (cylinder drawn for perspective).

FIG. 3. Dispersion compensation by electron beam. Open circles, empty cavity frequency spacing; × ' s, beam contribution; closed circles, beam-loaded cavity frequency spacing.

FIG. 4. Linear results for TE_{111} (solid), TE_{112} (dash), TE_{113} (chaindot), and TE_{114} (dot) in bold. TE_{115} (dot), TE_{116} (chaindot), TE_{117} (dash), and TE_{118} (solid) are also shown.

FIG. 5. Resonance condition for equally spaced cavity modes.

FIG. 6. Comparison of approximate and linear calculations of beam voltage and magnetic field required for alignment of modal growth rates.

FIG. 7. Mode locked radiation pulse. Modulator detuning of - 0.24% (solid), 0.58% (dot) and 2.1% (chaindot).

FIG. 8. Mode locking bandwidth. Minimum modulator strength required to mode lock at a given detuning (normalized to cavity mode spacing). (Solid, B = 5.868 kG; chaindot, 5.858 kG; dot, 5.848 kG; dash, 5.838 kG).

FIG. 9. Minimum modulation amplitude needed for mode locking at a given magnetic field. Also shown is the detuning at which the mode locking is found.

FIG. 10. Propagation of radiation pulse through cavity. Axial field energy profiles at times of (a) 0.0 ns, (b) 0.5 ns, (c) 1.0 ns, (d) 1.5 ns, (e) 2.0 ns, and (f) 2.5 ns.

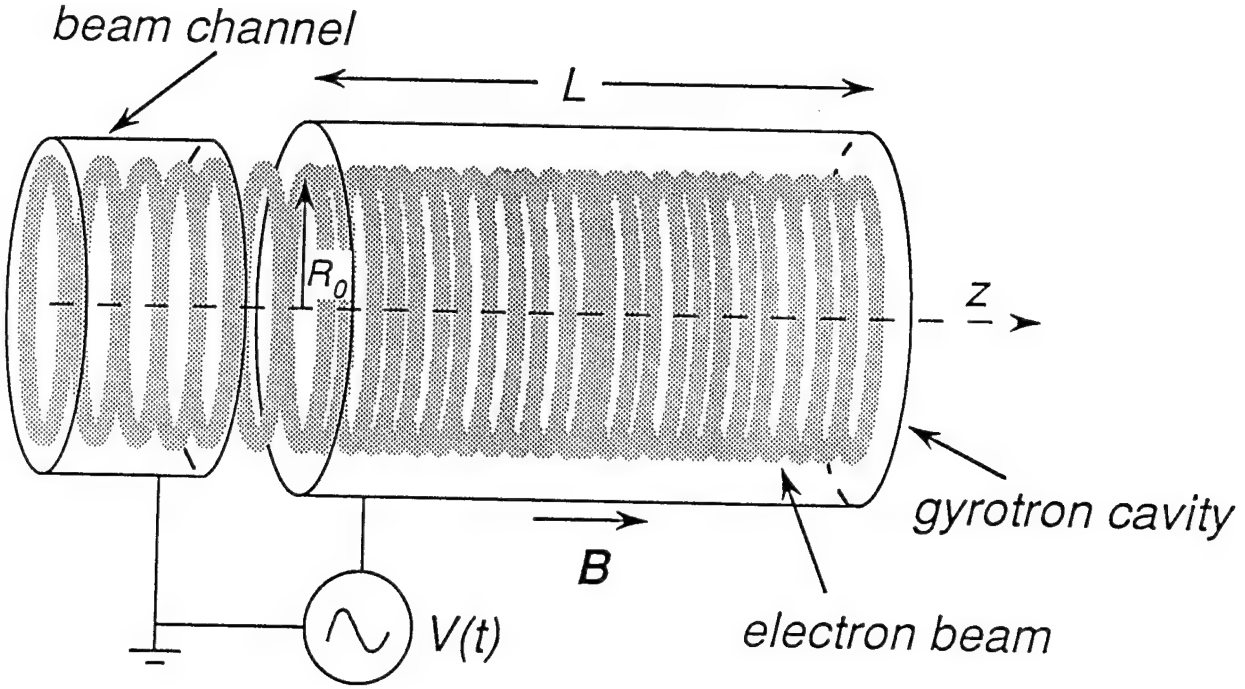

FIG. 1

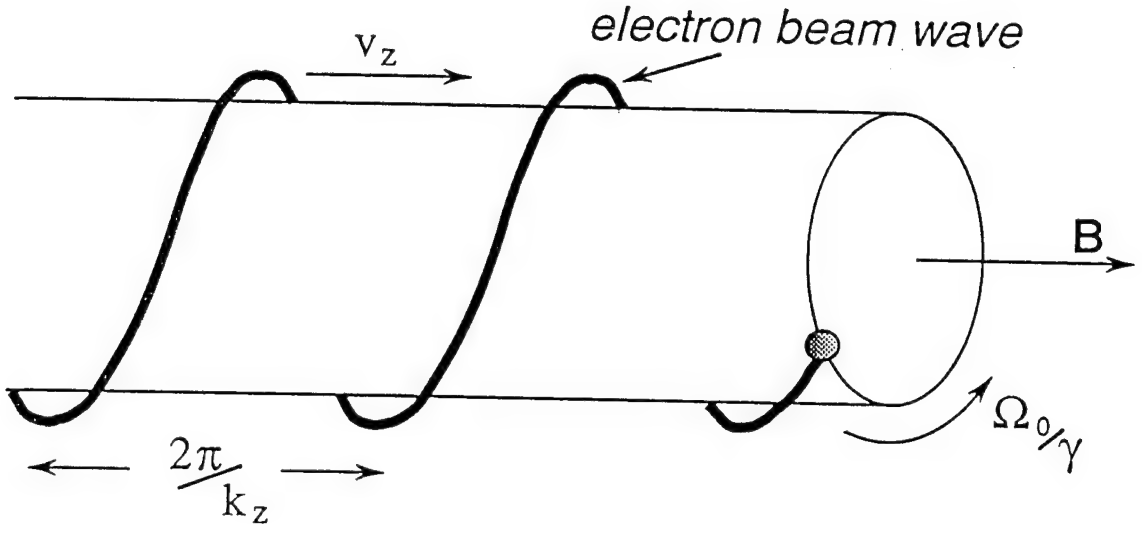

FIG. 2

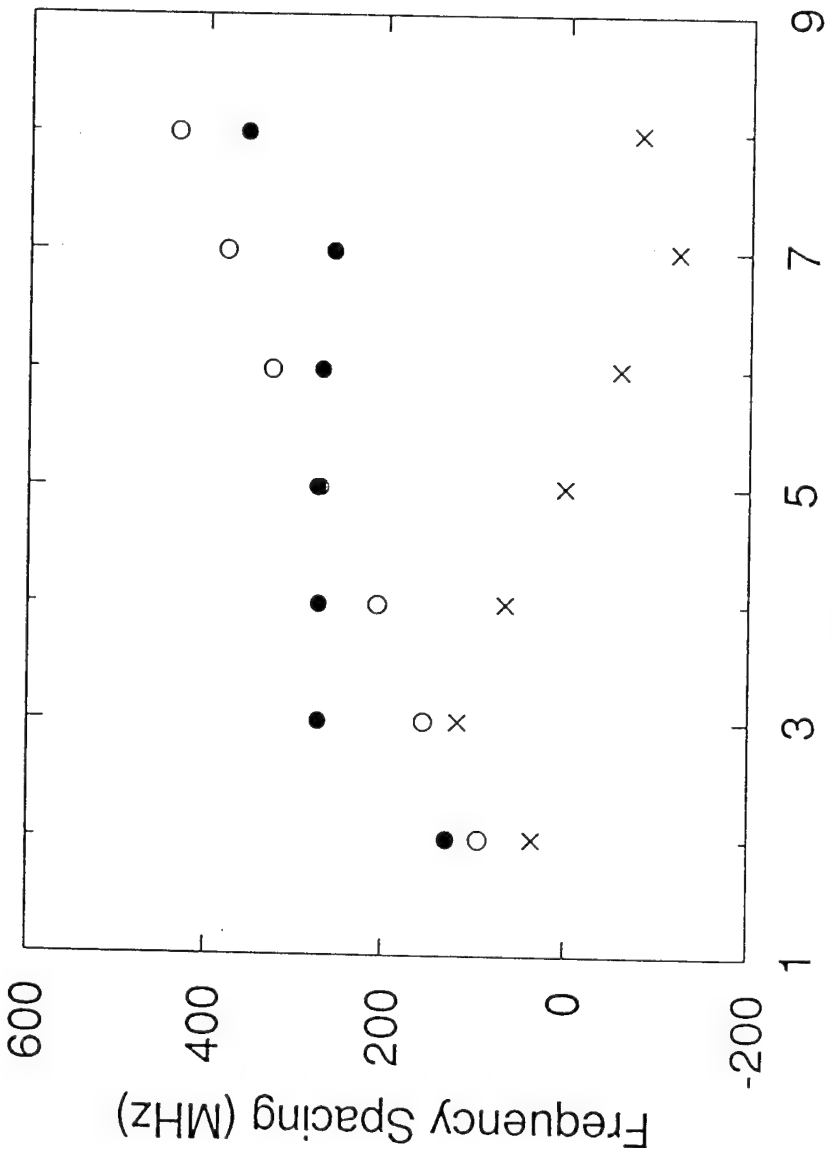

FIG. 3

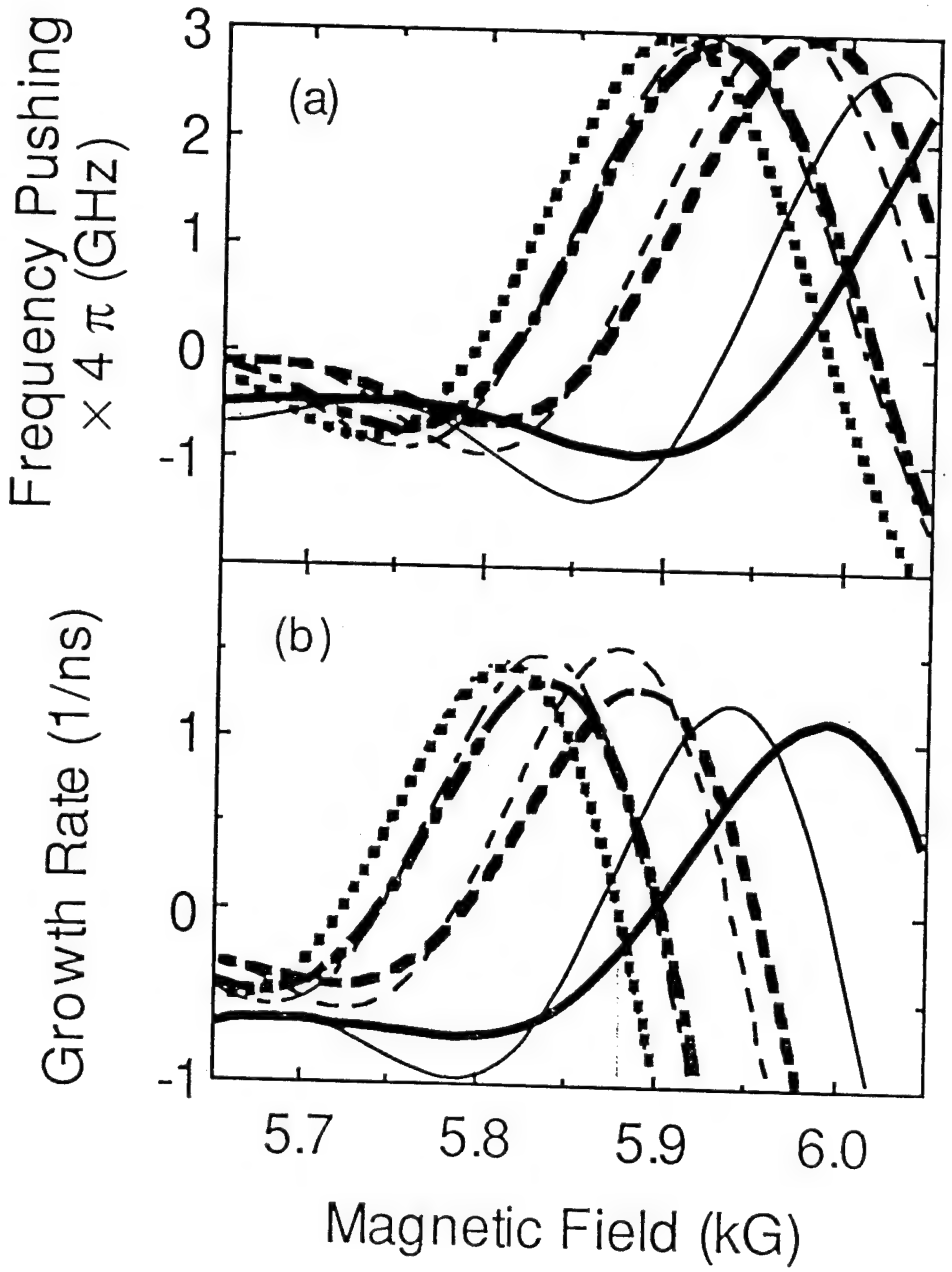
Frequency Pushing
× 4 π (GHz)
3
2
1
0
-1
(a)
(b)
Growth Rate (1/ns)
1
0
-1
5.7
5.8
5.9
6.0
Magnetic Field (kG)

FIG. 4

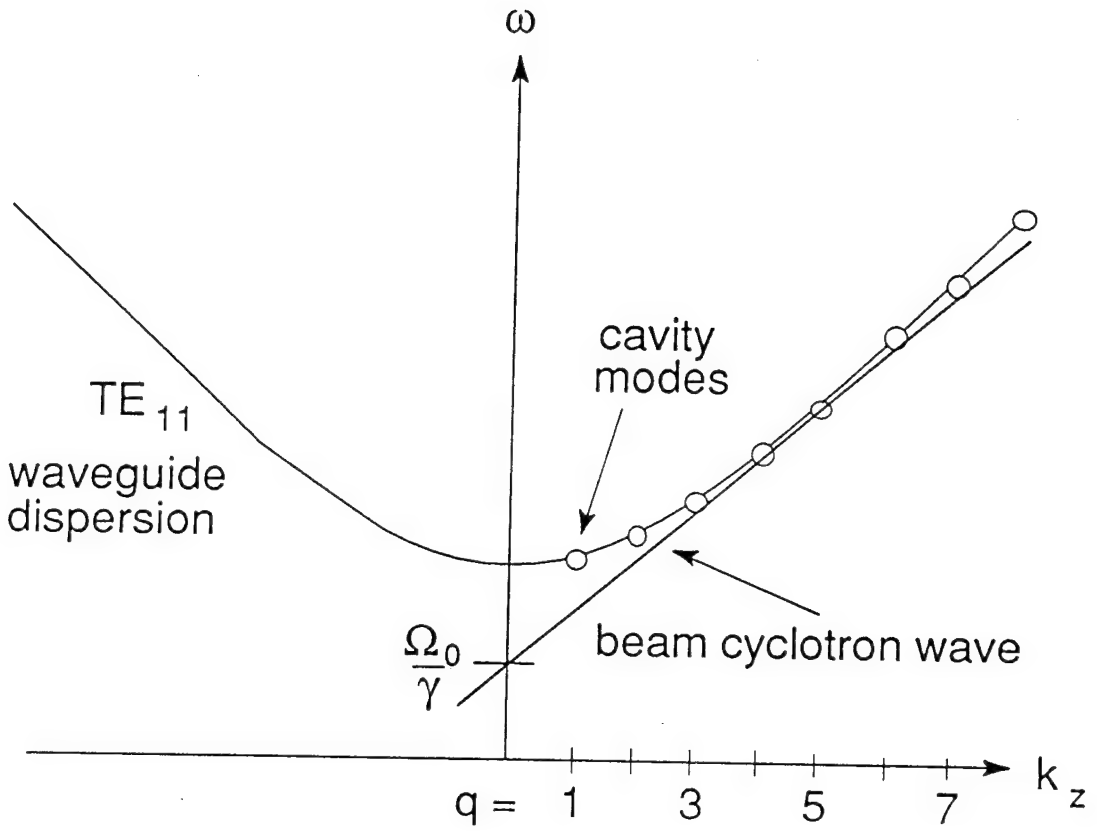
ω
cavity
modes
TE 11
waveguide
dispersion
Ω0
γ
beam cyclotron wave
q = 1 3 5 7
k z

FIG. 5

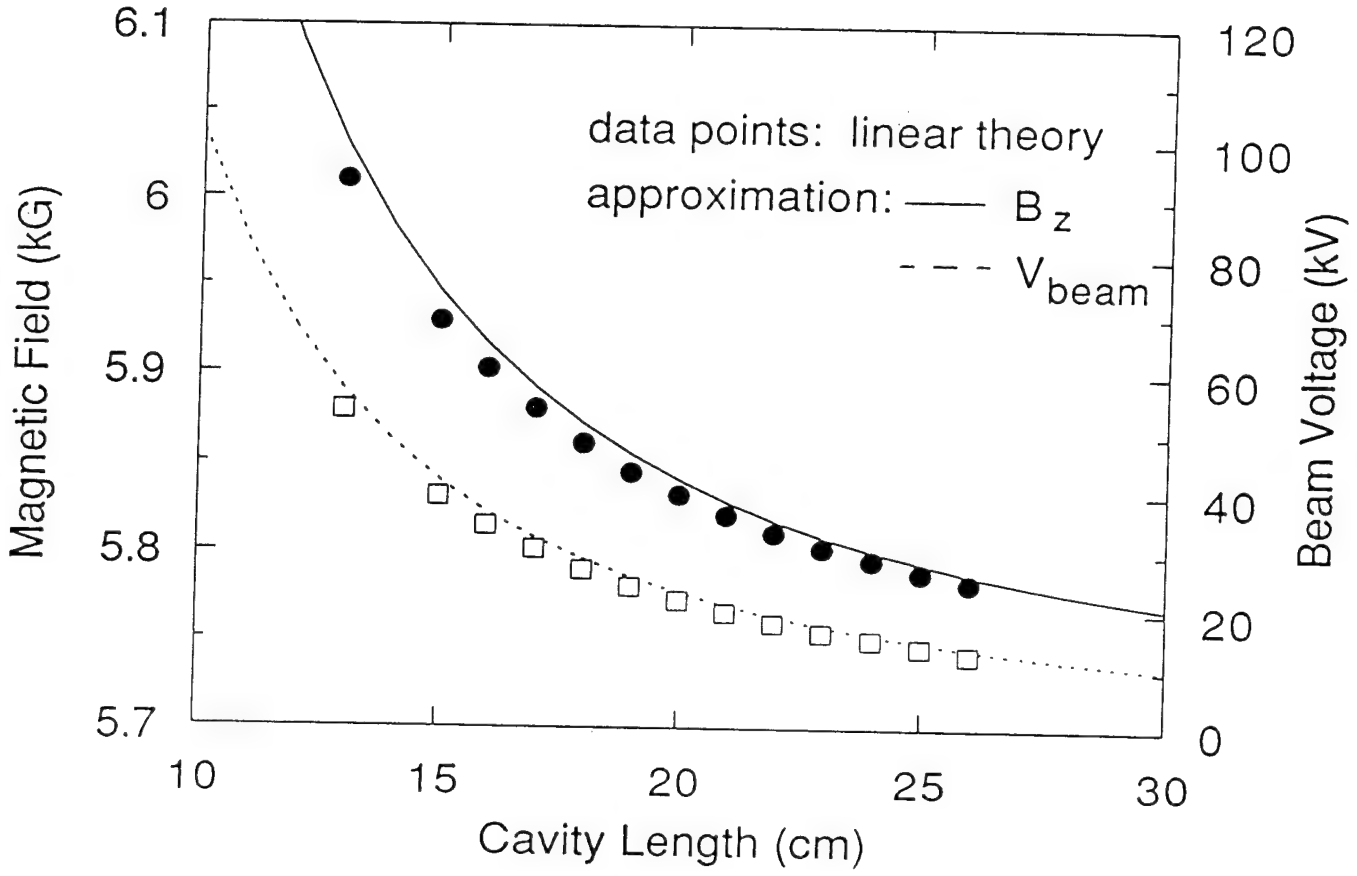
6.1
6
5.9
5.8
5.7
Magnetic Field (kG)
10
15
20
25
30
Cavity Length (cm)
120
100
80
60
40
20
0
Beam Voltage (kV)
data points: linear theory
approximation: —— B_z
- - - V_{beam}

FIG. 6

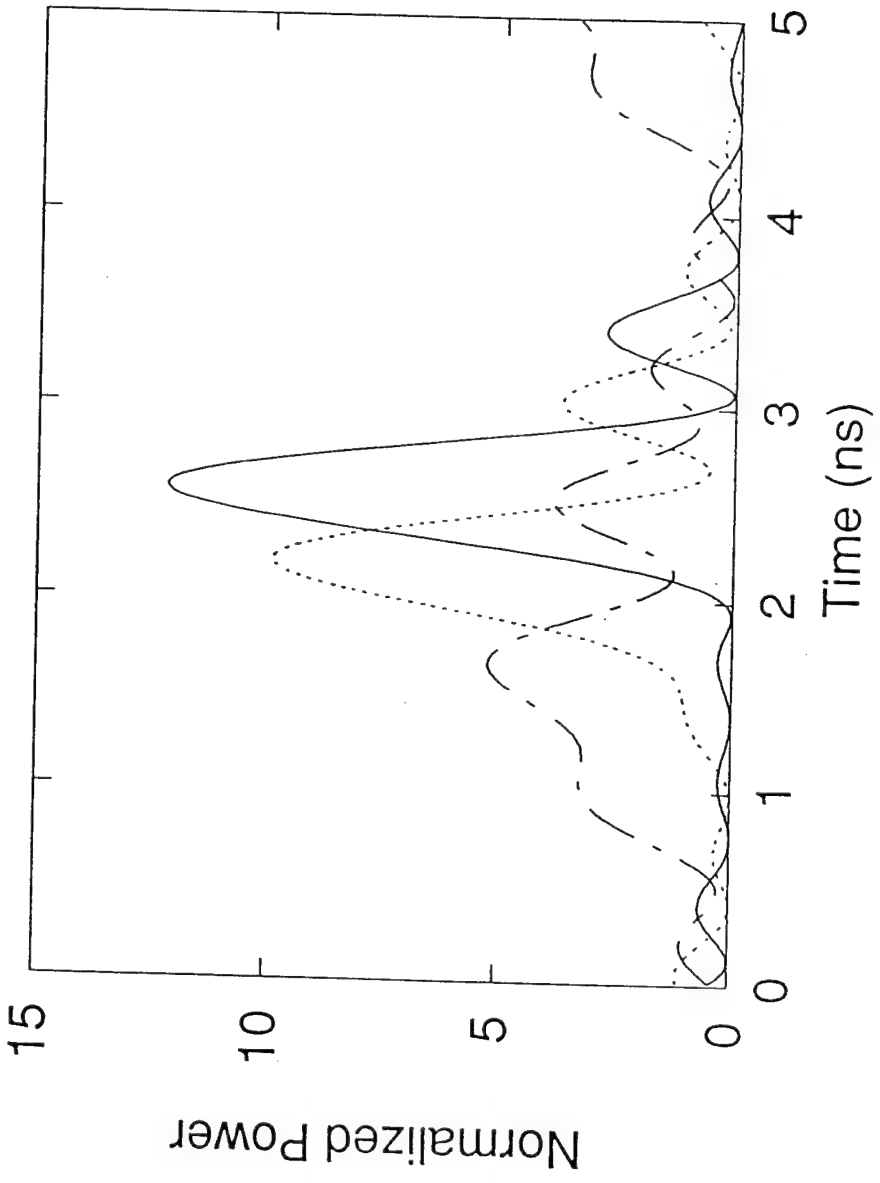

FIG. 7

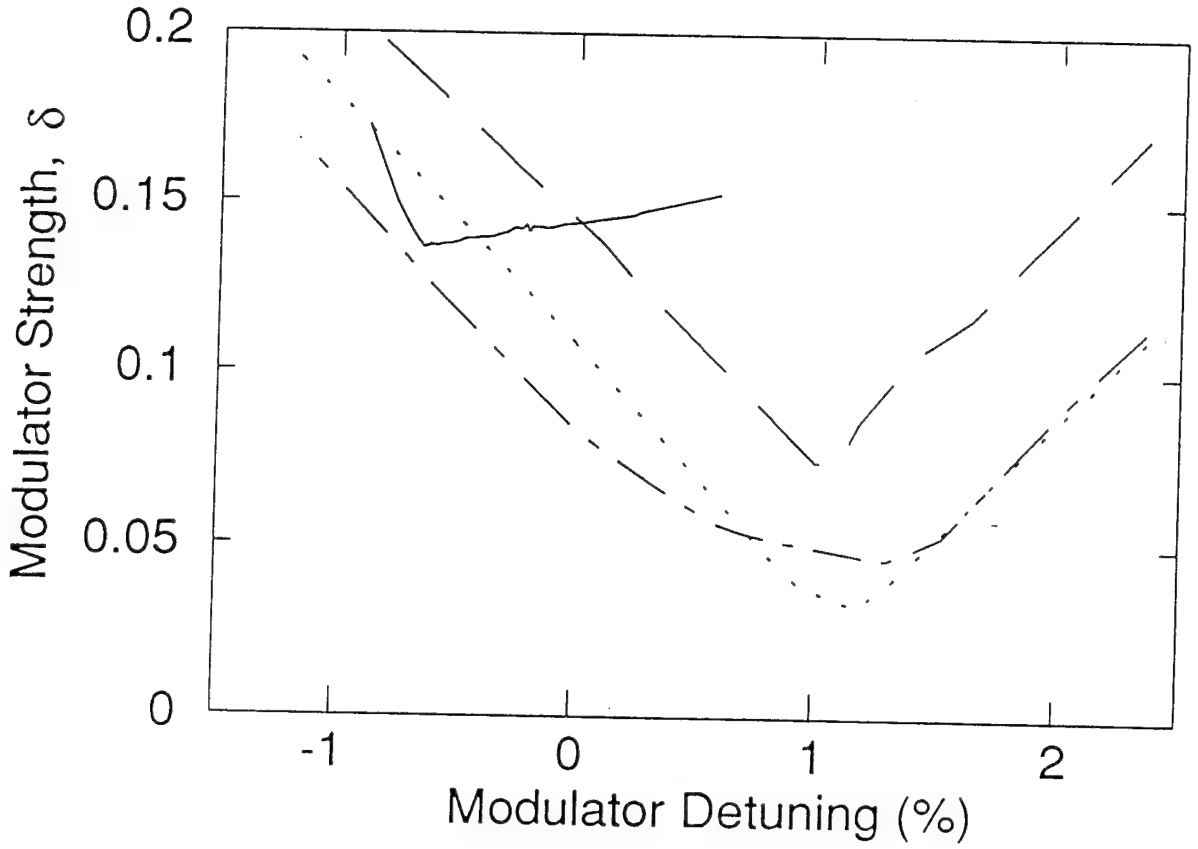
0.2
0.15
0.1
0.05
0
Modulator Strength, δ
-1
0
1
2
Modulator Detuning (%)

FIG. 8

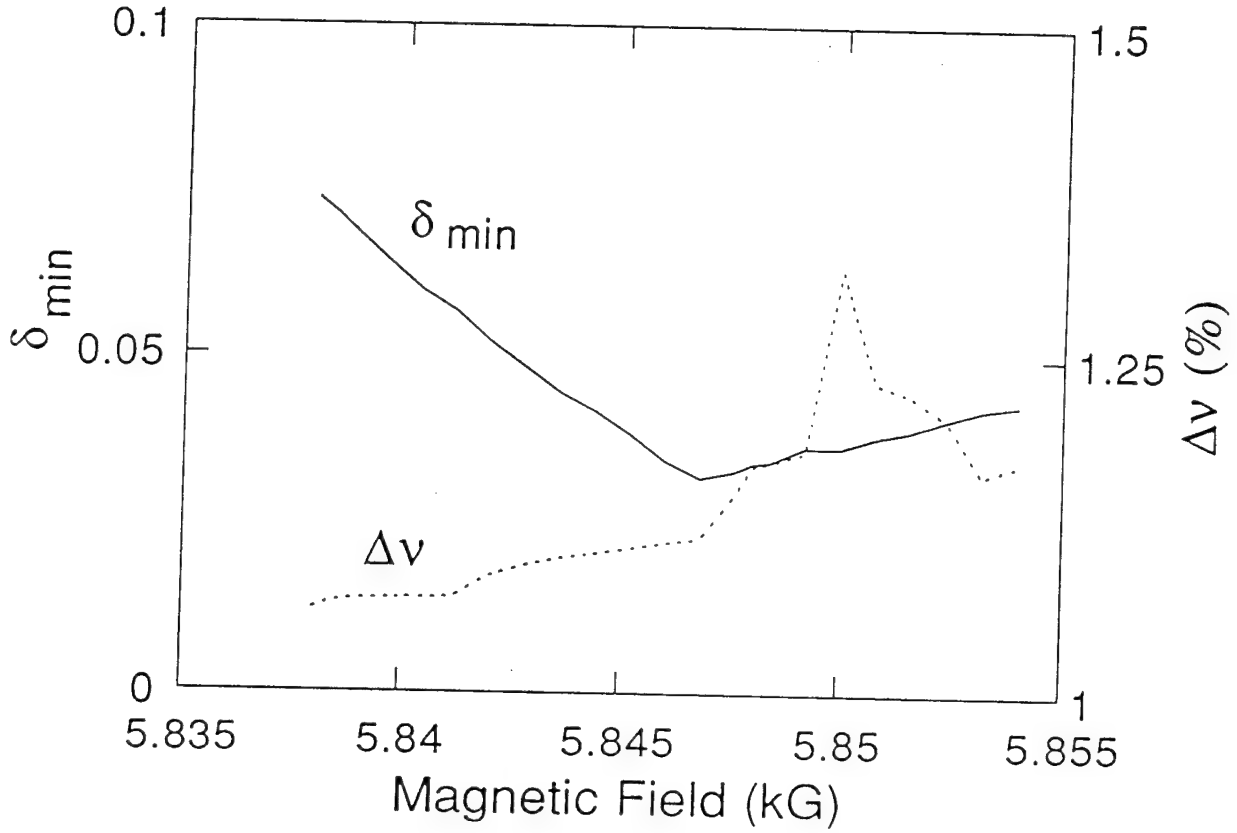
0.1
0.05
0
δ_{min}
1.5
1.25
1
$\Delta\nu$ (%)
δ_{min}
$\Delta\nu$
5.835
5.84
5.845
5.85
5.855
Magnetic Field (kG)

FIG. 9

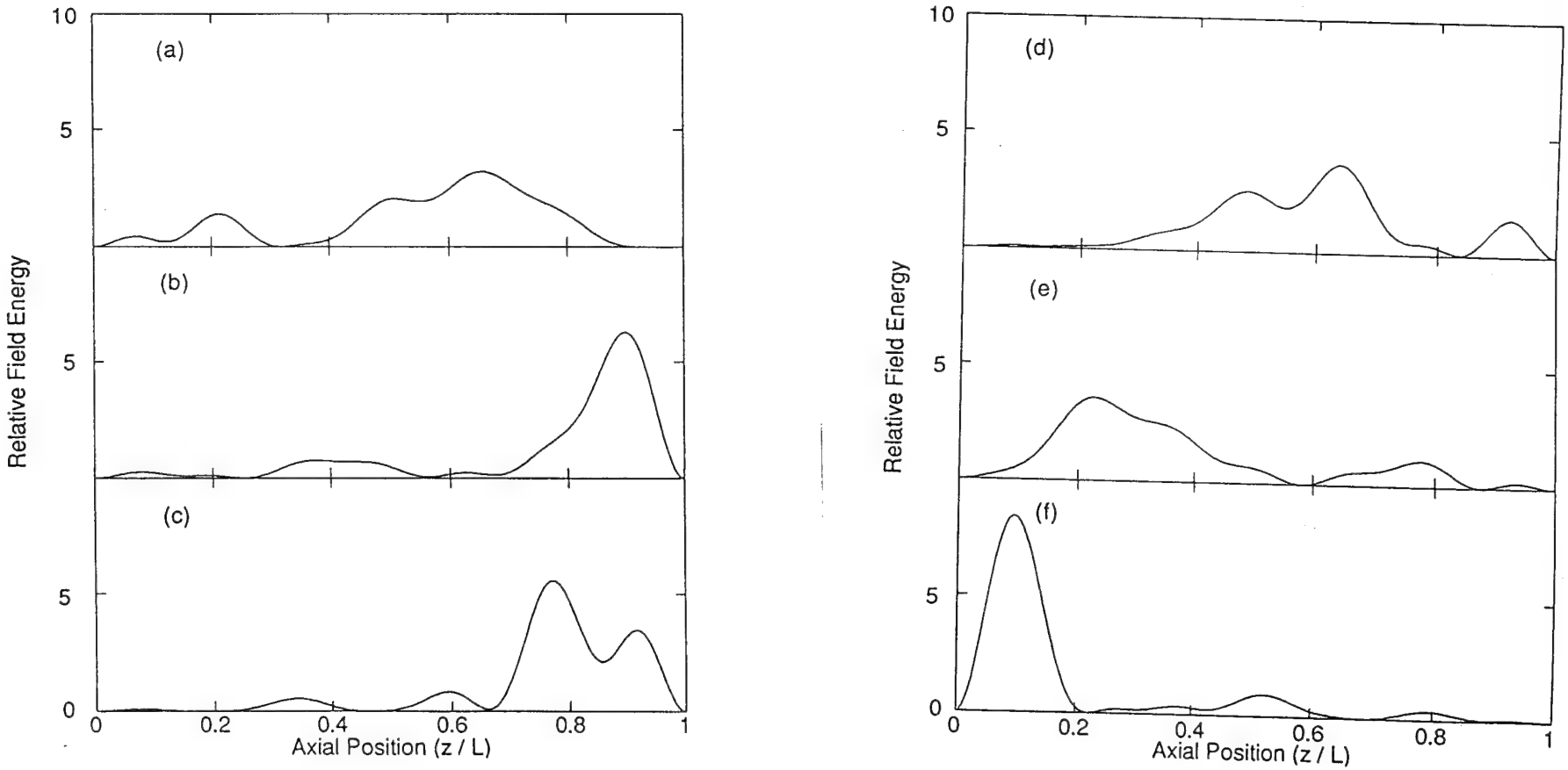
(a)
(b)
(c)
(d)
(e)
(f)
Relative Field Energy
Axial Position (z / L)
10
5
0
0.2
0.4
0.6
0.8
1

FIG. 10

SECTION II

Nonlinear Theory of Large-signal Mode Locking in a Gyrotron Oscillator

Abstract - Section II

Nonlinear, time-dependent calculations have been carried out for closed-cavity gyrotron oscillations using a strongly modulated electron beam. It is found that radiation pulses of width 200 ps can be generated with carrier frequency of 18 GHz at over 10% efficiency. The gyrotron features a tapered wall radius to allow an equidistant spectrum of cavity modes. Evidence of a disruption in locking is found at electron beam currents several times the start oscillation value.

I. INTRODUCTION

The mode locking technique has provided short radiation pulses in the optical frequency range.[1] Recent work has studied the extension of this technique into the microwave frequency range to address applications such as radar, Fourier Transform Spectroscopy, plasma diagnosis, and time domain metrology. Experimental and theoretical studies have been done on mode locking the free-electron laser (FEL).[2,3] Because of the low required operating voltage and soft constraints on the electron beam, interest has developed in generating short pulses from the gyrotron. Quasi-linear theory indicates that gyrotron modes can be synchonized[4,5] and a two-beam quasioptical gyrotron calculation predicted mode locking.[6]

It is shown in this letter that extremely short radiation pulses, at kilowatt power levels and good efficiency, may be obtained by mode locking a tapered cavity gyrotron using an electron beam with a modulated current density. The theory used is a nonlinear time-dependent one which has proven successful in describing low gain gyrotrons.[7] In this case, a sequence of axial TE_{11n} modes are excited by an electron cyclotron electron beam wave which is matched in phase and group velocity to these modes. The features of the oscillator cavity are outlined in the following, as well as mode locking results as a function of beam current pulsewidth, pulse repetition frequency and amplitude.

II. THEORY

The schematic of the mode locked gyrotron is indicated in Fig. 1. Here a gyrating electron beam (beam voltage 100 kV, current 1.0 - 5.0 A, perpendicular-to-parallel electron velocity ratio of 1.0) is generated by a magnetron injection gun and passes through a re-entrant modulation cavity, a cutoff drift section, then into a tapered cavity gyrotron oscillator. The modulation cavity is similar to a bunching cavity in a klystron and provides a small modulation in the electron velocity via a time varying axial electric field in the gap. The modulation frequency is 280 MHz, the nominal frequency separation between modes in the gyrotron cavity. The drift section produces a strong axial current density modulation.

The tapered gyrotron cavity is designed so that the TE_{11n} modal set is equally spaced in frequency. This is possible by using a slowly changing cavity radius which cuts off each mode at a different axial location. It is assumed in the calculation that the modes are exactly equally spaced at 280 MHz and the quality factors are equal (1500). (An appropriate *nonlinear* taper can provide the equidistant frequency spacing and cavity loading sets the quality factors). The modal electromagnetic field structure can be well approximated by using that of a linearly tapered cavity. The analysis is done with weakly nonuniform wavequide theory.[8] For the example chosen, the cavity straight section has a length of 8.5

cm and radius 0.55 cm while the taper is 10.0 cm in length with a taper angle of 0.5^{o}. Sixteen axial modes, with resonant frequencies between 16 and 20 GHz, are included in the computation. A 6.15 kG magnetic field puts the TE_{115} mode above threshold at a beam voltage of 100 kV using a current pulsetrain with a 2.0 A amplitude, 0.119 ns pulsewidth, and 280 MHz pulse repetition frequency. The nearby axial modes are near the start oscillation threshold, and are excited as the TE_{115} mode grows. The next higher transverse electric mode TE_{21} has a cutoff frequency of 26 GHz and is not excited.

The analysis of the modal evolution relies on the slow time scale equations for the electron momentum and the amplitude and phase of the electromagnetic field.[7] This analysis considers the field profiles fixed and includes the rf magnetic field. The Lorentz force equations for the electrons equations of motion are time averaged over all time scales faster than $2\pi/(\omega_n - \Omega)$, where ω_n and Ω are the field and relativistic cyclotron frequencies, respectively. The fields are expanded in cavity eigenmodes as

$$\mathbf{E}(\mathbf{r},t) = \frac{1}{2}\sum_n A_n e^{i(\omega_n t + \psi_n)}\,\mathbf{e}_n(\mathbf{r},t) + \text{c. c.}$$

and

$$\mathbf{B}(\mathbf{r},t) = \frac{i}{2}\sum_n A_n e^{i(\omega_n t + \psi_n)}\,\frac{\nabla \times \mathbf{e}_n(\mathbf{r},t)}{\omega_n} + \text{c. c.}$$

where $\mathbf{e}_n$ is the cavity eigenfunction and A_n and Ψ_n are modal amplitudes and phases which vary slowly on the time scale of the mode growth. The rate equations for the fields are

$$\dot{\Psi}_n = \frac{\omega_n^{o\,2} - \omega_n^2}{2\,\omega_n} - \frac{\omega_n}{2\,Q_n} + \frac{\chi_n''}{A_n} \quad \text{and} \quad \dot{A}_n = -\frac{\omega_n A_n}{2\,Q_n} + \chi_n'$$

where $$\chi_n = \chi_n' + i\,\chi_n'' = \frac{I_o\,\omega_n\,k_{\perp n}\,C_n\,J_{m-1}(k_{\perp n} R_o)}{4\,\pi\,\varepsilon_o} \int_{z=0}^{L} \left\langle \frac{p_\perp\, e^{i\vartheta}}{\gamma\, v_z} \right\rangle_{t_o,\,\phi_o,\,\theta_o} f_n(z)\,dz.$$

includes the power flow from, and the frequency shifting effects of the electron beam. Here I_o is the dc beam current, $k_{\perp n}$ the perpendicular wavenumber, C_n a constant defined elsewhere,[9] R_o the electron beam guiding center, $p_\perp$ the electron perpendicular momentum, L the cavity length, f_n the z-dependent part of the cavity eigenfunction, and $\vartheta = (m - 1)\,\theta_o - \Lambda - \Psi_n$ where Λ is the slowly varying relative phase between the electron and the electromagnetic wave. The average is taken over electron entrance time, t_o, and the electron initial gyrophase and guiding center angles, ϕ_o and θ_o.

The Lorentz force and rate equations are solved iteratively. The input current is varied periodically in time with period T. Because the radiation fields are periodic (in the locked state) on a time

T it is necessary to average over all electrons which enter the cavity during that time (t_o varies from 0 to T). This effectively averages the results over the modulator period, T.

The temporal evolution of power and frequency for eight modes is shown in Fig. 2. The beam current is given a square pulse modulation varying between zero and 2.0A at a frequency of 280 MHz. The current pulsewidth is 0.119 ns. Here, the mode locked state is achieved in 200 ns. The bold curve (Fig. 2(a)) shows the TE_{115} evolution, which excites other modes during its growth. In the absence of current modulation, it is found that a single mode oscillation is eventually obtained. When modulation is applied, power is continually pushed from the central TE_{115} to the satellite modes as in inhomogeneously broadened lasers.[10] The frequency shifts of all the modes are identical, as seen in Fig. 2(b), and near zero. The steady-state response seen in Fig. 2 indicates that the gyrotron output power is periodic in time. This does not guarantee large or narrow radiation pulses since the modal phases play a key role. Results similar to Fig. 2 were observed for a wide range of modulation amplitudes (including sinusoidal modulation) with frequency near 280 MHz.

A field summation gives the temporal dependence of the power output and is shown in Fig. 3 (same beam/cavity conditions as Fig. 2). Radiation pulses are obtained at a power level of over 25 kW with a FWHM (ΔT) of 220 ps. The electronic efficiency is 13 %. The pulse shape is close to Gaussian, with a small trailing secondary pulse. This secondary pulse originates in non-optimal phasing of the cavity modes. It is found that the phasing of the higher order modes (with index 8 - 16) is weak. This is due to the spatial extent of the beam current pulse (~ 1 cm). In order to control the phase of a given mode, the pulselength should be much smaller than the guide wavelength. This criterion is not satisfied for the higher order modes included in this study. The radiation pulse is observed at the cavity output just after the electron beam pulse exits the cavity. This timing is reminiscent of the radiation *lethargy* seen in FEL's.[11] Since the electron current pulse is exactly synchronous with the mode spacing, this lethargy effect should be at its maximum. It was not found that this type of narrow pulse output could be obtained with sinusoidal current density modulation.

Figures 4 and 5 measure the *degree* of mode locking by assigning a figure of merit, $\xi = (\mathcal{E}_{\Delta T}\, T\, P_{peak}) / (\mathcal{E}_T\, \Delta T\, P_{beam})$, to each pulseshape, where E_{DT} is the energy delivered between the pulse half-power points, $\mathcal{E}_T$ is the energy delivered per modulator period, and P_{peak} and P_{beam} are the peak radiation and beam powers, respectively. It can be seen from Fig. 4 that optimal pulses are generated at a modulator frequency slightly below the nominal cavity mode spacing and the frequency range over which good pulses can be obtained is about 1 MHz. Figure 5 indicates that optimal pulse formation is obtained with a current pulselength near 0.1 ns. Shorter pulses are observed to generate poorer pulses with lower power and growth rate (until sustained oscillation is not achieved). This degradation may be due to the current pulselength being shorter than the *slippage* length (defined as the beam axial velocity divided by the average frequency detuning of the electromagnetic wave from the cyclotron wave). This slippage is required for energy transfer to the fields and is analogous to that found in FEL's.

The mode locking dynamics are dependent on current pulse amplitude. In this study, the temporal evolution of the gyrotron is followed for 1 μs. For the 280 MHz, 0.119 ns current pulse train described earlier, start oscillation occurs near a peak beam current of 0.8 A. The radiation power (and growth rate) are found to steadily increase as the current is raised to 2.0 A. At 2.0 A, a low frequency, low amplitude beat signal emerges during the last 100 ns of the simulation, indicating that the mode locked state is not stable. At currents above 2.0 A the onset of this instability occurs earlier in time. Above 2.5 A the instability leads to a new mode locked state on a time scale of 1 μs. At progressively higher currents the instability continues to occur earlier in time but with a shorter duration. The high current mode locked states generally include more power in the high order modes, but the modal phases are not well controlled and the pulse shapes are inferior to those at low current. Further work is being done to characterize the instability.

IV. CONCLUSION

In conclusion, it has been shown via nonlinear theory that a closed-cavity gyrotron oscillator with a tapered waveguiding structure can be mode locked by an electron beam with strong current density modulation. The required peak current level is not large and the modulation frequency stability need only be on the order of 0.3 % (in order to stay in the region of optimal pulse production).

REFERENCES

1 A.E. Siegman, *Lasers* (University Science, Mill Valley, CA, 1986).

2 F. Ciocci, R. Bartolini, A. Doria, G.P. Gallerano, E. Giovenale, M.F. Kimmitt, G. Messina, and A. Renieri, Phys. Rev Lett. **70**, 928 (1993).

3 E. Jerby and G. Bekefi, IEEE J. Quant. Electron. **29**, 2845 (1993).

4 A.H. McCurdy, J. Appl. Phys. **74**, 3576 (1993).

5 G.S. Nusinovich, "Theory of Mode Interaction in the Gyrotron," KfK Rept. 4111, August 1986.

6 W.M. Manheimer and M.E. Read, Int. J. Electron. **61**, 1041 (1986).

7 A.W. Fliflet, R.C. Lee, S.H. Gold, W.M. Manheimer, and E. Ott, Phys. Rev. A **43**, 6166 (1991).

8 R.J. Temkin, Int. J. Infrared Millimeter Waves **2**, 629 (1981).

9 A.W. Fliflet, M.E. Read, K.R. Chu, and R.Seeley, Int. J. Electronics **53**, 505 (1982).

10 D.J. Kuizenga and A.E. Siegman, IEEE J. Quant. Electron. **QE-6**, 709 (1970).

11 H. Al-Abawi, F.A. Hopf, G.T. Moore, and M.O. Scully, Opt. Commun. **30**, 235 (1979).

FIGURE CAPTIONS

FIG. 1. Schematic of mode locked gyrotron showing 1) electron beam, 2) MIG gun, 3) bunching cavity, 4) drift tube, 5) tapered gyrotron cavity, 6) rf input, 7) microwave output.

FIG. 2. Gyrotron modal evolution showing a) power and b) oscillation frequency shift from the empty cavity resonant frequency. Curves are labeled by the axial mode index.

FIG. 3. Radiation output pulse corresponding to case shown in Fig. 2.

FIG. 4. Pulse formation at different modulation frequencies.

FIG. 5. Pulse formation at different current pulsewidths.

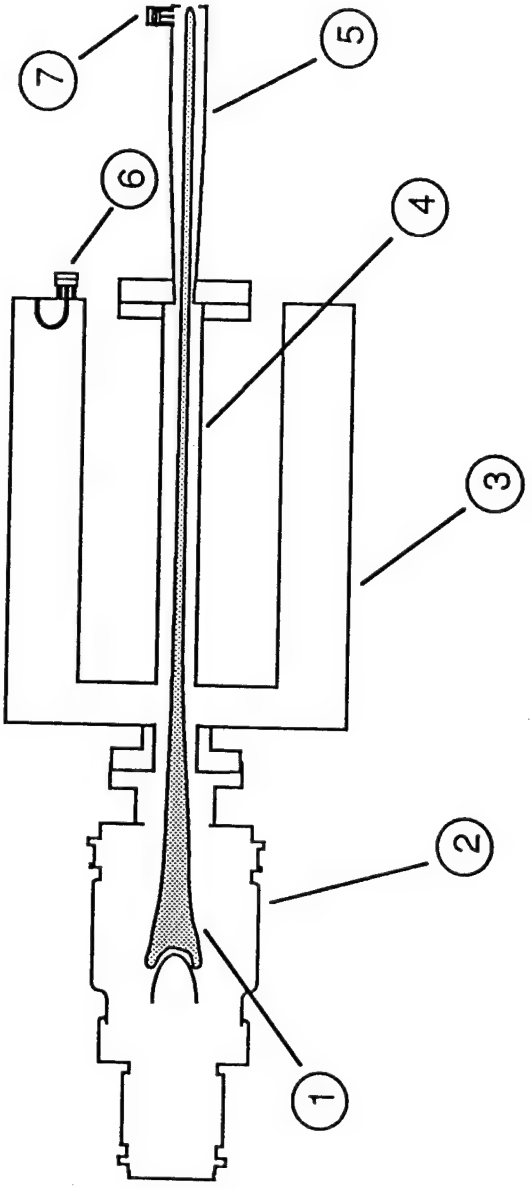

FIG. 1

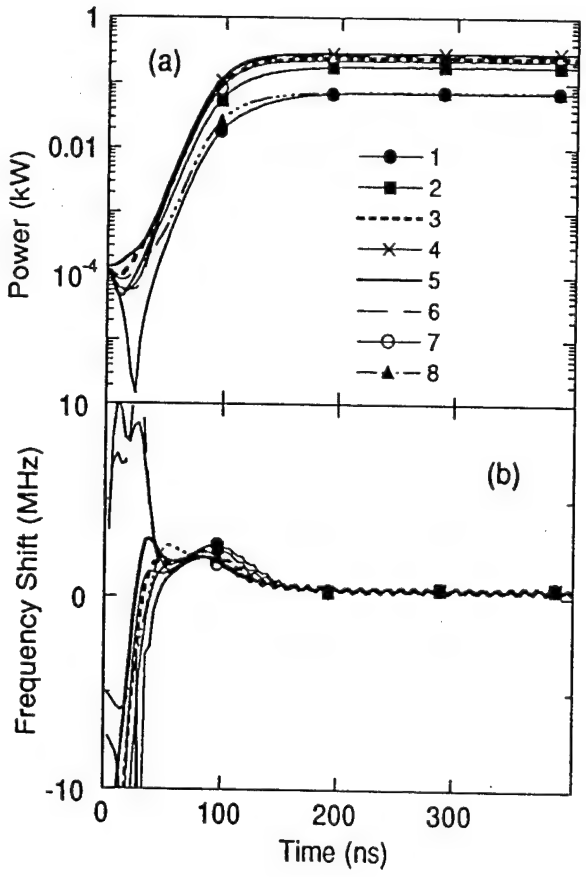
(a)
(b)
Power (kW)
Frequency Shift (MHz)
Time (ns)
1
0.01
10^{-4}
10
0
-10
0
100
200
300
1
2
3
4
5
6
7
8

FIG. 2

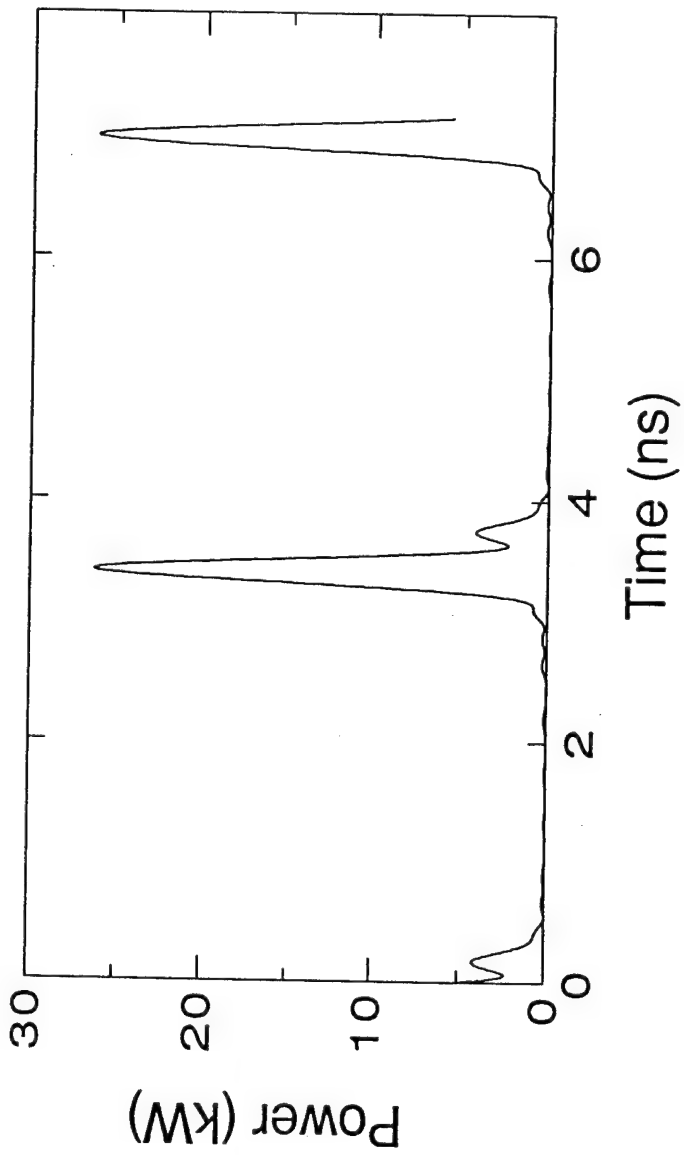

FIG. 3

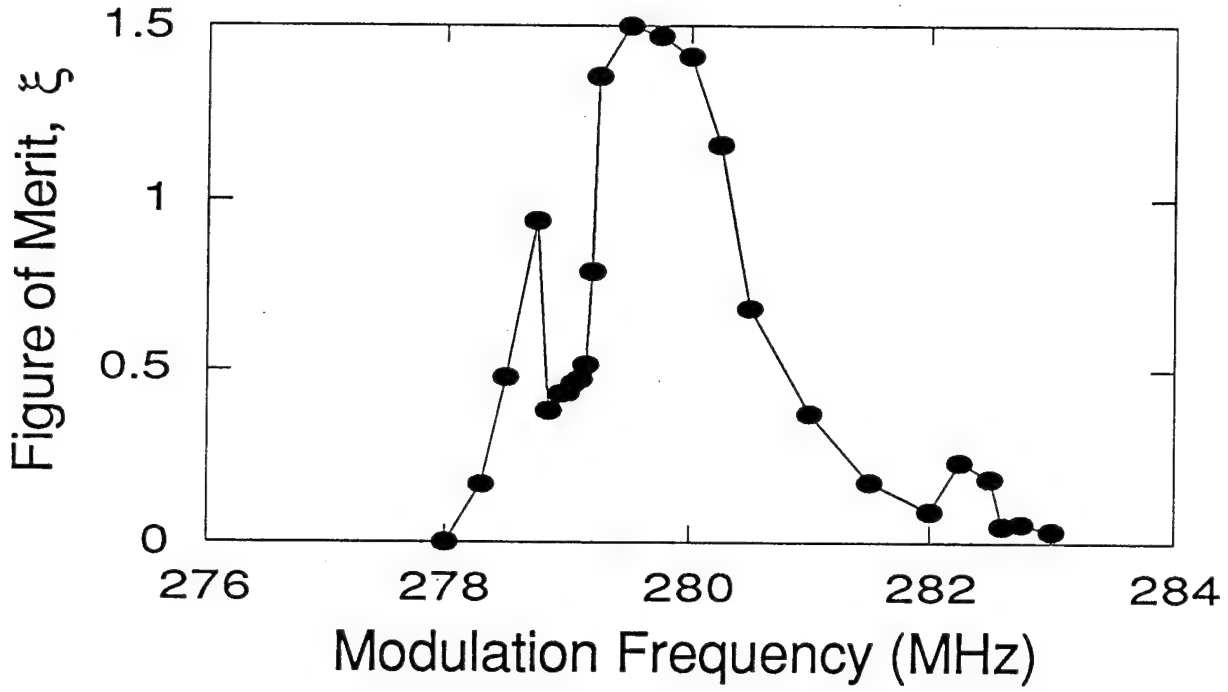
Figure of Merit, ξ
1.5
1
0.5
0
276
278
280
282
284
Modulation Frequency (MHz)

FIG. 4

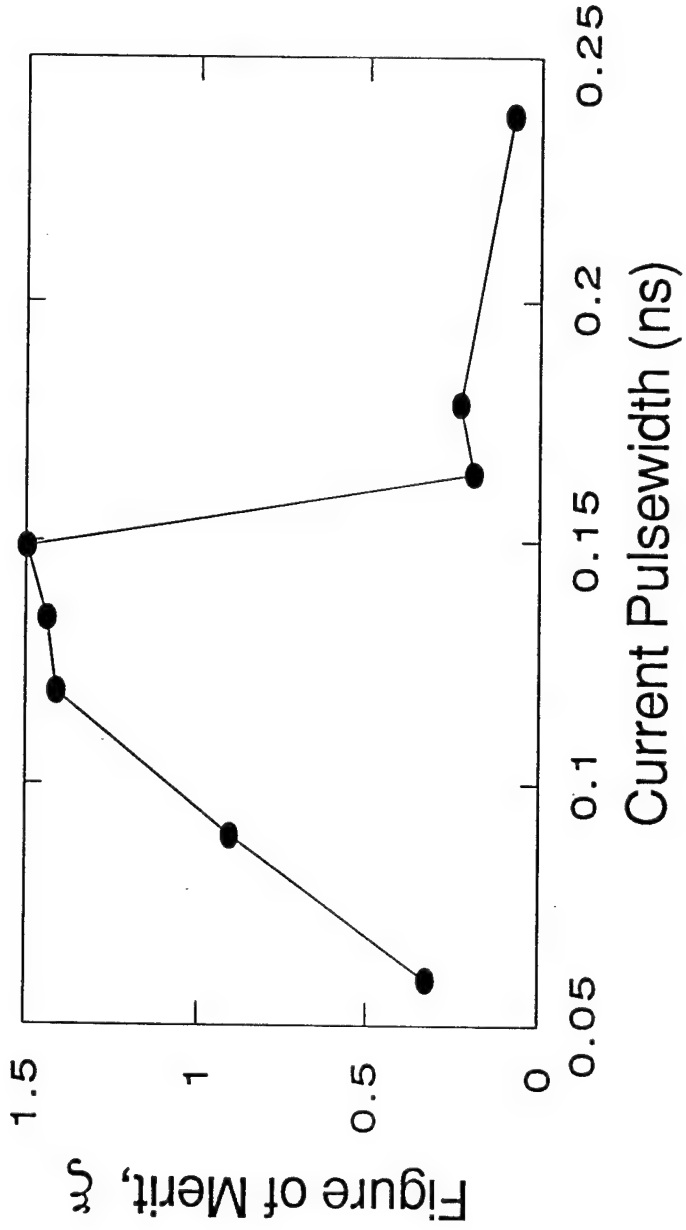
Figure of Merit, ζ_f
1.5
1
0.5
0
0.05
0.1
0.15
0.2
0.25
Current Pulsewidth (ns)

FIG. 5

SECTION III

PIC Code Simulation of Pulsed Radiation in a Tapered Closed-Cavity Gyrotron

Abstract - Section III

MAGIC, a two-and-one-half-dimensional PIC code, has been used to investigate mode locking in closed-cavity gyrotrons. A cavity, with equally spaced modal frequencies, composed of a radially tapered section and a straight section of waveguide, is designed, built and cold-tested. Experimental cold test results agree well with the MAGIC PIC code simulations. Using a sinusoidal current density modulation with an amplitude of 5% of the d.c. current and frequency of 280 MHz, the simulation results show radiation output in a train of narrow pulses (FWHM ~ 1 ns) at a 280 MHz repetition rate. Though the gyrotron does not appear to be mode locked, uniform pulse trains of 30-50 pulses can be obtained.

I. INTRODUCTION

The generation of high power coherent radiation using electron beams is a topic of current research interest [1]. Pulsed free electron lasers (FELs) [2] and electron cyclotron masers (ECMs or gyrotrons) [3], [4] have generated high power at high frequencies (> 1 MW at frequencies > 100 GHz). The general problems in pulsed operation include pulse-to-pulse reproducibility and synchronization, efficiency, and repetition rate. Phase locking may provide phase synchronism between successive electromagnetic pulses. A number of theoretical studies and experimental results on phase locking in FELs have been reported recently [5]-[7]. Periodic short pulses were observed in the oscillation of the waveguide mode FEL [8], and microsecond to subpicosecond pulses have been produced with a FEL oscillator [9], [10]. Gyrotron oscillators can produce both large average power and large peak power at lower voltages and with higher efficiency than FELs. Most gyrotron oscillator work has been on long pulse or CW operation driven by the microwave source requirement for electron cyclotron resonance heating of fusion plasmas. For high-power gyrotron operation, high current is usually required [11]. This often puts many electromagnetic modes above the start oscillation threshold. These modes will compete with each other for energy. In solving the gyrotron mode competition problem, much research has focused on the suppression of unwanted modes [12]. However little work has been done to utilize the gyrotron in the overmoded state [13]-[15]. Mode locking is a technique for generating short-pulse periodic output from an overmoded oscillator.

This work follows on a quasi-linear theory [16] of mode locking in closed cavity gyrotrons. The various electromagnetic modes are coupled together through modulation of the electron beam. Thus coherent output is obtained with a concomitant modulation in either the amplitude or frequency. Mode-locking is defined as those situations in which the mode sidebands are arrayed all in phase, or nearly so, regardless of their amplitudes, and coupled modes lead to the kind of short-pulse output in [17], where rate equations are derived for the time evolution of the amplitudes and phases of the electromagnetic modes in an overmoded laser. The mode locking technique has been highly successful in laser oscillators.

The applications for short pulse microwave source include radar imaging of isolated targets, atmospheric sensing, Fourier transform spectroscopy, plasma diagnosis, and other time domain measurements. It has been shown through the quasi-linear theory that a gyrotron oscillator with a highly dispersive wave guide structure can be mode locked by compensating with dispersion due to the electron beam. Nonlinear theory indicates that the modal frequency shifts are quite different from quasi-linear predications which make beam compensation difficult. An alternative approach to mode lock the gyrotron is to taper the cavity. This paper presents such a tapered cavity gyrotron design, along with results from experimental cold test and MAGIC PIC code simulations. The results indicate the possibility of short pulsed radiation output at high repetition rate in such a device.

II. TAPERED CAVITY DESIGN

The gyrotron electron beam can typically excite many electromagnetic modes. Because the beam is a nonlinear gain medium, the various modal frequencies will combine to form "beat" notes at the sum and difference frequencies. These beat frequencies when combined with resonant frequencies may be close to the frequencies of nearby modes. If the amplitudes of the combination frequencies become strong enough, they can "phase lock" adjacent modes so as to make the frequency separation between modes equal to a constant. Optimal "AM" mode locking will occur if the phase difference between adjacent modes is 0 or π. However, if the frequency spacing between modes is very nonuniform, the combination frequencies will not be near enough to modal frequencies to produce locking. The above discussion illustrates that roughly uniform frequency spacing between cavity modes is a prerequisite to lock the modes.

The dispersion relation for TE_{mnp} modes in a cylindrical gyrotron cavity with radius r_w and length L is

$$\omega_{mnp}^2 = \frac{\chi_{mn}^2}{r_w^2}c^2 + k_z^2 c^2$$

where χ_{mn} is the nth root of the equation, $J'_m(x) = 0$, and $k_z = p\pi/L$. Because the cylindrical waveguide is highly dispersive near cutoff, the modes are unequally spaced in frequency. In order to mode lock such a device, the cavity geometry may be modified.

It is shown here that a cavity composed of a radially tapered section and a straight section of waveguide can obtain an equidistant frequency spectrum. Such a cavity configuration is shown in Fig. 1. This structure is similar to that previously used in wide-band gyrotron traveling-wave amplifiers [18]. The straight section has a circular cross-section of radius r_w and length L. The tapered section has a linearly varying radius $r_w(z)$ and a length L'. An annular, gyrating electron beam is injected into the cavity from the tapered side. Many modes can be excited because the tapered geometry expands the frequency range over which gyrotron interaction can occur. Different modes will penetrate different distances into the taper because the turning point of the wave depends on wave cutoff frequency. With proper taper design (choice of cutoff positions and untapered cavity length), a set of modes with equally spaced resonant frequencies can be realized.

The dimensions of the tapered cylindrical cavity are determined using the WKB theory of [19]. The relation between taper angle and resonant frequency separation for $r_w = 0.92$ cm and L' = 11.25 cm is depicted in Fig. 2. The design parameters are chosen to be comparable to those to be used in an experiment. The frequency separation between adjacent modes is sensitive to the choice of taper angle when the taper angle is small, and it is insensitive when the angle is large. The frequency interval between two adjacent low order modes becomes insensitive to the change of taper angle at intermediate

angles. The choice of taper angle is limited on the high side by the number of equally spaced, low order modes and on low side by machining constraints. A satisfactory taper angle in this case is 0.6^0. Because of assumptions made in [19] only those resonant frequencies near cutoff are accurate.

The resonant frequencies of any mode in a tapered cylindrical cavity can be the determined by the moving phase front method (MPF). For a wave frequency to be resonant, the round trip phase change (product of frequency and travel time, plus the phase changes at the ends) must equal a multiple of 2π.

For the tapered cavity of Fig. 1, the z-component of the phase velocity v_ϕ :

$$v_\phi(z) = \frac{\omega}{k_z(z)} = \frac{c}{\sqrt{1 - \omega_c^2(z)/\omega^2}} \tag{1}$$

where $\omega_c = \frac{c\chi_{mn}}{r_w(z)}$ and $r_w(z)$ is a known function of z in the tapered region.

The round trip time is

$$\tau = \frac{2L}{v_\phi} + 2\int_{z=0}^{z=-L'(\omega)} \frac{dz}{v_\phi(z)} \tag{2}$$

where $L'(\omega)$ is the position of wave cutoff in the tapered guide.

Including the $\pi/2$ phase shift at cutoff (z = -L') and the π change at the short circuit (z = L), the total phase change is

$$\Delta\phi = \omega\tau + 3\pi/2. \tag{3}$$

This method is directly applicable to nonlinear tapers. For a cavity supporting TE_{01n} modes with parameters: L = 11.25 cm, r_w = 0.92 cm and taper angle $\alpha = 0.6^0$, the resonant frequency differences are shown in Fig. 3. It can be seen that the resonant frequency spacing predicted by MPF is quite uniform except for the first two modes. It can also be seen that WKB predictions agree best with MPF ones for the first few modes. The frequency spacing predicted by WKB becomes lower than that by MPF at larger mode number n. This is because the WKB theory overestimates $L'(\omega)$, the position of cutoff, for each mode in the taper section. This error becomes worse at higher frequency. Therefore the frequency separation between high order modes is predicted by WKB to be smaller than is actually the case.

III. CAVITY SIMULATION AND TEST

To verify the design parameters a computation of mode resonant frequencies is carried out using MAGIC, a two and one-half dimensional electromagnetic and relativistic PIC code [20]. The resonant frequencies are found by exciting a time-dependent current-density source inside the cavity to drive electromagnetic fields. The frequency spectrum of this source is approximately a square function so that resonant frequencies are excited equally in amplitude. Such a source can be formed via an inverse Fourier transform of the square function and takes the following form:

$$i(t) = \frac{\sin(\omega_0 t)}{\omega_0 t}\cos(\omega_c t) \qquad \text{for } 0 \le t \le T$$

$$i(t) = 0 \qquad \text{for } t > T$$

where ω_c is the central frequency, and $\omega_c+\omega_0/2$ and $\omega_c-\omega_0/2$ are upper and lower frequency limits of the square function, respectively. For ω_c = 21 GHz, ω_0 = 2 GHz and T = 40 ps, ten TE_{01n} modes can be excited equally (n = 1 to 10). Other forms of current-density sources, such as a sine wave function superposed on a square function, are used to selectively excite resonant modes.

Mission Research Corporation has added a new SHIM command to the MAGIC code to deal with linearly tapered cavities [21]. It adds a small, perfectly-conducting layer to a conformal conductor. The thickness of the layer is typically a fraction of the cell size; thus it can provide a perfect linear taper boundary which is not restricted by cell size. Since the grid need not resolve the taper, a coarse grid can be used and the total simulation time is reduced. Code grid sizes are chosen as Δz = 0.55 mm and Δr = 0.11 mm to have enough resolution (about 30 cells per wavelength) to distinguish different modes and maintain 5:1 maximum step size ratio. Since good resolution is required in the radial direction, Δr sets the overall minimum scale length in the problem. Finer grid sizes require a smaller time step to satisfy the Courant condition ($\Delta r > c\,\Delta t$, where Δt is the temporal step size), resulting in unacceptably long computation time. The total simulation time is 100 ns which is long enough for phase mixing effect to take place in the electromagnetic fields. Resonant frequencies are found through FFT of the time history of the fields.

The MAGIC simulation results for TE_{01n} modes in the closed tapered cavity are shown in Fig. 4, along with cavity resonant frequencies computed by MPF. The MAGIC results have a resolution of about 10 MHz which is limited by the total simulation time. It can be seen from Fig. 4 that the two results agree very well.

Because of the symmetry requirements of MAGIC, only two-dimensional modes (such as the azimuthally symmetric TE_{01n} set) can be simulated. However, the planned experiment will use TE_{11n}

modes since the available electron beam size is small (TE_{11n} modes will allow maximum utilization of field-beam interaction) and TE_{11n} modes are fundamental ones in the circular cavity. The TE_{11n} design is indirectly compared to the MAGIC results using the MPF method since it has been benchmarked to MAGIC.

A tapered cavity supporting TE_{11n} modes with a nominal cutoff frequency of 16 GHz was built and cold-tested. The tapered section is made of copper with length L' = 10.17 cm. The straight section is brass with length L = 8.52 cm. The taper angle, α, is measured to be 0.5^o. The field profile inside the cavity is calculated using WKB theory. Three probe positions are chosen to sample the various modes. The field amplitudes of modes n=2 and 6 are near their maximum at probe # 1, modes n=1, 7 and 8 are near their maximum at probe # 2, and modes n=3, 4 and 5 are near their maximum at probe # 3.

The cold test measurement results and the MPF predictions are depicted in Fig. 5. The experimental sources of error include $\pm$10 MHz from the frequency measurement and a slightly elliptical cross-section of the tapered section. The uncertainty in MPF calculation is found by using the probable maximum and minimum taper angles corresponding to dimensional uncertainties. It can be seen that two set of data are in excellent agreement.

Tapered cavities with various sizes of apertures in the untapered end have also been simulated. Resonant frequency shifts with respect to closed cavity resonances were studied. Simulation shows that for a given aperture size, the quality factor Q roughly decreases as $1/n^2$. A simple heuristic argument indicates the dependence should be: $Q \sim 1/n^2\lambda^3$, where λ is the modal resonant wavelength [19]. The resonant frequencies should be down shifted by approximately $\Delta f \sim f/2Q$ [22], where f is the modal resonant frequency. The simulation results for a circular aperture of radius $0.95r_w$ are compared with the heuristic relations in Fig. 6.

MAGIC simulations including both a beam and an aperture were not done because of difficulties in simulating the beam at a partially open boundary. This problem can be avoided by including the collector region in the simulation, which separates the beam from the radiation. However, a simulation of this size is beyond the limits of the available computer resources.

IV. PULSE RADIATION OUTPUT

Once equally spaced resonant frequencies are obtained a simulation including the electron beam can proceed. A broad-band gyrotron interaction occurs when the phase and group velocities of a beam cyclotron wave are matched to those of the electromagnetic wave. Matching the beam wave $\omega = \frac{\Omega}{\gamma} + k_z v_z$ to the TE_{014} and TE_{015} resonant frequencies (via eq. (1)), the z-component of the electron velocity can be determined:

$$v_z = \frac{d\omega}{dk_z} = \frac{2\pi(f_{015} - f_{014})}{k_{z_{015}} - k_{z_{014}}} \qquad (4)$$

where f_{01n} and $k_{z_{01n}}$ are the resonant frequency and axial wave number of the TE_{01n} mode, respectively.

If a d.c. electron beam is used, the simulation shows that a single TE_{014} mode is dominant after 66 ns. An FFT of the last 40 ns of the simulation shows that the TE_{014} mode power is 20 times the next largest one (TE_{015}). The result also shows the frequency separation between modes is not exactly equal.

Electron beam modulation is used to couple modes together so that the frequency separation between modes becomes identical. Simulations including axial velocity modulation were performed using different modulation amplitude and frequency. No stable output pulsing is observed. This is possibly due to excessive detuning of the beam wave.

More success was achieved with current modulation. The electron beam parameters are 50 KeV beam energy, 10 A current, and the initial electron guiding center is 0.35 cm away from the symmetry axis. The external axial magnetic field is 7.46 kG. A sinusoidal current density modulation with an amplitude of 5% of the d.c. current level and frequency of 280 MHz is imposed on the input beam to model the effect of a prebunching cavity. Due to computer time constraints, the simulation time is confined to 80 ns. The output radiation, shown in Fig. 7 (a), consists of a train of narrow pulses (FWHM ~ 1 ns) at a 280 MHz repetition rate. The vertical axis is the total instantaneous electromagnetic energy calculated over a 1.1 cm wide cylindrical volume near the end of the untapered cavity. The frequency spectrum of the field component E_θ averaged over the radial direction is shown in Fig. 7 (b). In a mode locking case, the full width τ (between zero amplitude points) of the pulse is given by $2T / N$, where T is the modulation period and N is the number of modes locked [16]. τ is about 1 ns for $1/T = 280$ MHz and $N = 7$. τ can be written in another way using the fact that the number of oscillating modes N is approximately $\Delta\bar{\omega} / \Delta\bar{\omega}_0$, where $\Delta\bar{\omega}$ is the bandwidth over which the oscillator excites modes and $\Delta\bar{\omega}_0$ is the frequency spacing between modes: $\tau = 2 / \Delta\bar{\omega}$. τ is found to be 1 ns for $\Delta\bar{\omega} = 2$ GHz in Fig. 7 (b). Therefore, the pulse width in Fig. 7 (a) is comparable with that of the mode locked case. Fig. 7 (b) shows the frequency interval between adjacent modes is almost identical to the modulation frequency. Correspondingly, the output pulses are spaced in time by the modulation period T. This is again an indication of possible mode locking. The energy of radiation pulses increases in time in Fig. 7 (a) because each of eight modes is growing in its early stage. At later time it is observed that energy is saturated and amplitudes of radiation pulses vary sinusoidally at very low beat frequencies. Since the pulses in Fig. 7 (a) are not perfectly time periodic, we cannot conclude that the gyrotron is mode locked.

Radiation pulse transport in the tapered cavity is shown in Fig. 8. The pulse bounce time is found to be 3.6 ns, which is very close to the modulation period (Fig. 8 shows one half cycle with the pulse moving right to left). It can be seen that the narrow pulses are broadened while propagating

towards the tapered section since the waveguide is dispersive. The spatial pulsewidth is estimated by multiplying the temporal (~ 1 ns) pulsewidth by the pulse group velocity (v_z), and is found to be ~ 8 cm. This is consistent with the results displayed in Fig. 8. When the broadened pulse propagates towards the short-circuit end, however, the pulse narrows as the modal waves regain phase synchronism. The small scale oscillations are primarily due to numerical noise. Abrupt rise of current (0 to 10 A instantly) excites a wide frequency spectrum in the simulation. Also the MAGIC centered-difference field algorithm does not suppress numerical noise efficiently.

Figs. 9 and 10 measure the quality of the radiation pulses by assigning a figure of merit, ζ, to each pulseshape, where

$$\zeta = \frac{\bar{\varepsilon}_P}{\bar{\varepsilon}_T} \frac{\tau}{\Delta\tau} \frac{\bar{\varepsilon}_P}{IV_{beam}\tau}.$$

$\bar{\varepsilon}_P$ is the averaged energy delivered between the pulse half-power points and $\bar{\varepsilon}_T$ is the averaged total energy delivered between the pulses. τ is the pulse peak-to-peak period and $\Delta\tau$ is the FWHM of the pulse. This figure of merit is high for high power, narrow pulses. It can be seen from Fig. 9 that optimal pulses are generated at a modulating frequency of 280 MHz while good pulses can be formed using a frequency as high as 283 MHz. The optimal modulation frequency and the tuning range (3 MHz) are comparable to slow-time scale theory results [23]. Figure 10 indicates that optimal pulse formation is obtained with a 5% amplitude modulation. Small amplitude modulation is observed to generate very poor pulses because the modulation is too weak to sufficiently couple the modes. Large modulation reduces noise level between pulses, but generate pulses with low energy. The reason for the decrease in energy could be the large fluctuation of current density. In analogy with single mode gyrotron operation, it is expected that the efficiency of each mode will be optimum over a small range of beam current. If the modulation pushes the current outside of this range, the efficiency of each mode decreases and the energy in the pulses decreases.

Figures 9 and 10 also display a measure of the uniformity of the pulse-train. The parameters of measurements include pulse FWHM, height and period. The standard deviation σ of each measurement for ten pulses is calculated and an associated figure of merit, υ, is assigned:

$$\upsilon = \frac{\Sigma_{\Delta\tau}}{\sigma_{\Delta\tau}} \frac{\Sigma_h}{\sigma_h} \frac{\Sigma_{period}}{\sigma_{period}},$$

where Σ denotes the minimum standard deviation of pulse FWHM, height and period in each category, respectively. The maximum value of υ is unity. In an ideal mode-locking case every pulse should be identical thus the standard deviation is zero. It can be seen from Figs. 9 and 10 that for 5% modulation

the pulse train is quite uniform for modulation frequency between 280 MHz and 283 MHz. In this range the figure of merit, ζ, is also high. If the modulation frequency is fixed at 280 MHz, for 5% or more modulation, the uniformity of the pulse-train is good. Stronger modulation is seen to produce more uniform pulses. It can be concluded from Figs. 9 and 10 that pulse formation is rather sensitive to modulation frequency and a minimum 5% amplitude modulation is required to produce good pulses.

V. CONCLUSION

It has been shown via nonlinear simulation that a closed-cavity gyrotron oscillator with a tapered waveguiding structure can generate a train of narrow radiation pulses at the repetition rate of the modulation frequency. The cavity dimensions are determined so that an equidistant resonate frequency spectrum is obtained. The tapered-cavity gyrotron with equally spaced modal frequencies is designed, built and cold-tested. The optimal modulation frequency and amplitude for given cavity dimensions are found to be 280 MHz and 5%, respectively. For this case, the simulation results show radiation output in a train of narrow pulses (FWHM ~ 1 ns) at a 280 MHz repetition rate. Though the gyrotron does not appear to be mode locked, uniform reproducible pulse trains of 30-50 pulses are obtained.

References

[1] V. L. Granatstein and I. Alexeff, *High-power microwave sources*, Dedham, MA: Artech house, 1987.

[2] L.-Y. Lin and T. C. Marshall, "High power spike pulses emitted from a microwave FEL," *Nucl. Instrum. Methods Phys. Res.*, vol. A331, pp. 144-148, 1993.

[3] G. Gantenbein, E. Borie, G. Dammertz, H.-U. Nickel, B. Piosczyk and M. Thumm, "Experimental results and numerical simulations of a high power 140 GHz gyrotron," *IEEE Trans. Plasma Sci.*, vol. 22, pp. 861-870, 1994.

[4] W. C. Guss, M. A. Basten, K. E. Kreischer, R. J. Temkin, T. M. Antonsen, Jr., S. Y. Cai, G. Saraph, and B. Levush, "Influence of sideband oscillations on gyrotron efficiency," *IEEE Trans. Plasma Sci.*, vol. 22, pp. 871-877, 1994.

[5] D. Oepts and W. B. Colson, "Phase locking in an infrared short-pulse free-electron laser", *IEEE J. Quantum Electron.*, vol. 26, pp. 723-730, 1990.

[6] D. Oepts, R. J. Bakker, D. A. Jaroszynski, A. F. G. van der Meer, and P. W. van Amersfoort, "Induced and spontaneous interpulse phase locking in a free-electron laser," *Phys. Rev. Lett.*, vol. 68, pp. 3543-3546, 1992.

[7] E. Jerby and G. Bekefi, "AM mode-locking of a free-electron laser oscillator," *IEEE J. Quantum Electron.*, vol. 29, pp. 2845-2851, 1993.

[8] K. Totoda and Y. Kawamura, "Experimental study of free electron laser using cold relativistic electron beams," *Laser Part. Beams*, vol. 7, pp. 421-431, 1989.

[9] F. Ciocci, R. Bartolini, A. Doria, G. P. Gallerano, E. Giovenale, M. F. Kimmitt, G. Messina, and A. Renieri, "Operation of a compact free-electron laser in the millimeter-wave region with a bunched electron beam," *Phys. Rev. Lett.*, vol. 70, pp. 928-931, 1993.

[10] F. Glotin, R. Chaput, D. Jaroszynski, R. Prazeres, and J. M. Ortega, "Infrared subpicosecond laser pulses with a free-electron laser," *Phys. Rev. Lett.*, vol. 71, pp. 2587-2590, 1993.

[11] S. H. Gold, A. W. Fliflet, W. M. Manheimer, R. B. McCowan, W. M. Black, R. C. Lee, V. L. Granastein, A. K. Kinkead, D. L. Hardesty, and M. Sucy, "High peak power K-band gyrotron oscillator experiment," *Phys. Fluids*, vol. 30, pp. 2226-2238, 1987.

[12] B. Levush and T. M. Antosen, Jr., " Mode competition and control in high-power gyrotron oscillators," *IEEE Trans. Plasma Sci.*, vol. 18, pp. 260-271, 1990.

[13] W. M. Manheimer and M. E. Read, "Sub-nanosecond pulselength millimeter wave generation with a phase modulated quasi-optical gyrotron," *Int. J. Electron.*, vol. 61, pp. 1041-1048, 1986.

[14] G. S. Nusinovich, "Theory of mode interaction in the gyrotron," *KfK Report* No. 4111, August 1986.

[15] A. T. Lin, C. C. Lin, Z. H. Yang, K. R. Chu, A. W. Fliflet, and S. H. Gold, "Simulation of transient behavior in a pulse-line-driven gyrotron oscillator," *IEEE Trans. Plasma Sci.*, vol. 16, pp. 135-141, 1988.

[16] A. H. McCurdy, "Synchronous mode locking in a closed cavity electron cyclotron maser," *J. Appl. Phys.*, vol. 74, pp. 3576-3583, 1993.

[17] A. E. Siegman, *Lasers* , Mill Valley, CA: University Science, 1986.

[18] L. R. Barnett, Y. Y. Lau, K. R. Chu, and V. L. Granatstein, "An experimental wide-band gyrotron traveling-wave amplifier," *IEEE Trans. Electron Devices*, vol. ED-28, pp. 872-875, 1981.

[19] R. J. Temkin, "Analytic theory of a tapered gyrotron resonator," *Int. J. Infrared and Millimeter Waves*, vol. 2, pp. 629-649, 1981.

[20] B. Goplen, L. Ludeking, D. Smithe, and G. Warren, "User-Configurable MAGIC for Electromagnetic PIC Calculations," *Computer Physics Communications*, vol. 87, pp. 54-86, 1995.

[21] B. Goplen and L. Ludeking, private communication.

[22] J. C. Slater, *Microwave electronics*, New York, NY: D. Van Nostrand Company, 1950.

[23] A. H. McCurdy, "Nonlinear theory of large-signal mode locking in a gyrotron oscillator," *Appl. Phys. Lett.*, vol. 66, pp. 1845-1847, 1995.

Figure Captions

Fig. 1 Tapered cavity configuration.

Fig. 2 Frequency difference between adjacent TE_{01n} modes as a function of taper angle for parameters: $r_w = 0.92$ cm, $L' = 11.25$ cm and $L = 7.5$ cm. Δnm denotes frequency difference between mode TE_{01n} and mode TE_{01m}.

Fig. 3 Equally spaced TE_{01n} modal frequencies around 280 MHz. Frequency difference between adjacent modes is calculated by WKB (circle) and MPF (dot).

Fig. 4 MAGIC simulation results (triangle) and MPF calculation (circle) of TE_{01n} mode resonant frequencies for same parameters as Fig. 2 with $\alpha = 0.6^0$.

Fig. 5 Cold test measurements (circle) and MPF calculation (triangle) of TE_{11n} mode resonant frequencies for $r_w = 0.55$ cm, $\alpha = 0.526^0$, $L' = 10.17$ cm and $L = 8.52$ cm.

Fig. 6 Quality factor, Q, and frequency shift, $\Delta\bar{\omega}$ as a function of TE_{01n} mode number n for the tapered cavity with an aperture in the end.

Fig. 7 Time evolution of (a) electromagnetic energy and (b) frequency spectrum of azimuthal field E_θ from MAGIC simulation.

Fig. 8 Radiation pulse transport in tapered cavity for one half of the modulation cycle. Pulse position at time (a) 0 ns, (b) 0.8 ns, and (c) 1.8 ns. E_θ at $r = r_w/2$ is shown. Pulse moves from right to left.

Fig. 9 Degree of pulse formation at different modulation frequencies. ζ and υ measure the quality and uniformity of the radiation pulses, respectively.

Fig. 10 Degree of pulse formation at different modulation amplitudes. ζ and υ measure the quality and uniformity of the radiation pulses, respectively.

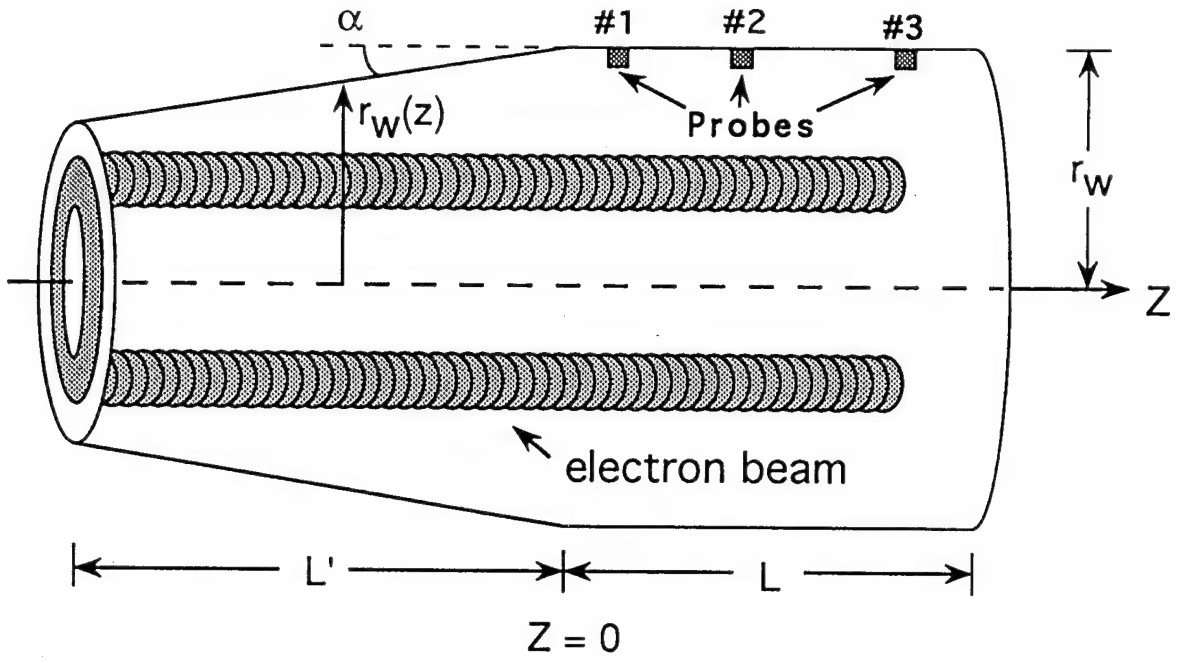

FIG. 1

54

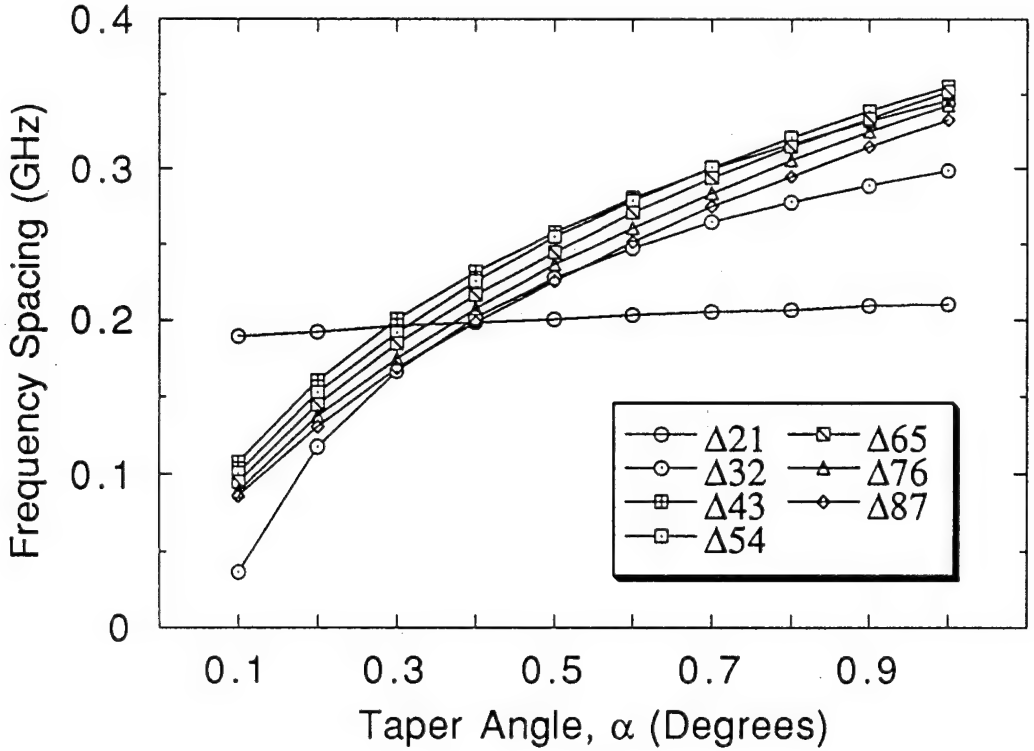
0.4
0.3
0.2
0.1
0
Frequency Spacing (GHz)
0.1
0.3
0.5
0.7
0.9
Taper Angle, α (Degrees)
Δ21
Δ32
Δ43
Δ54
Δ65
Δ76
Δ87

FIG. 2

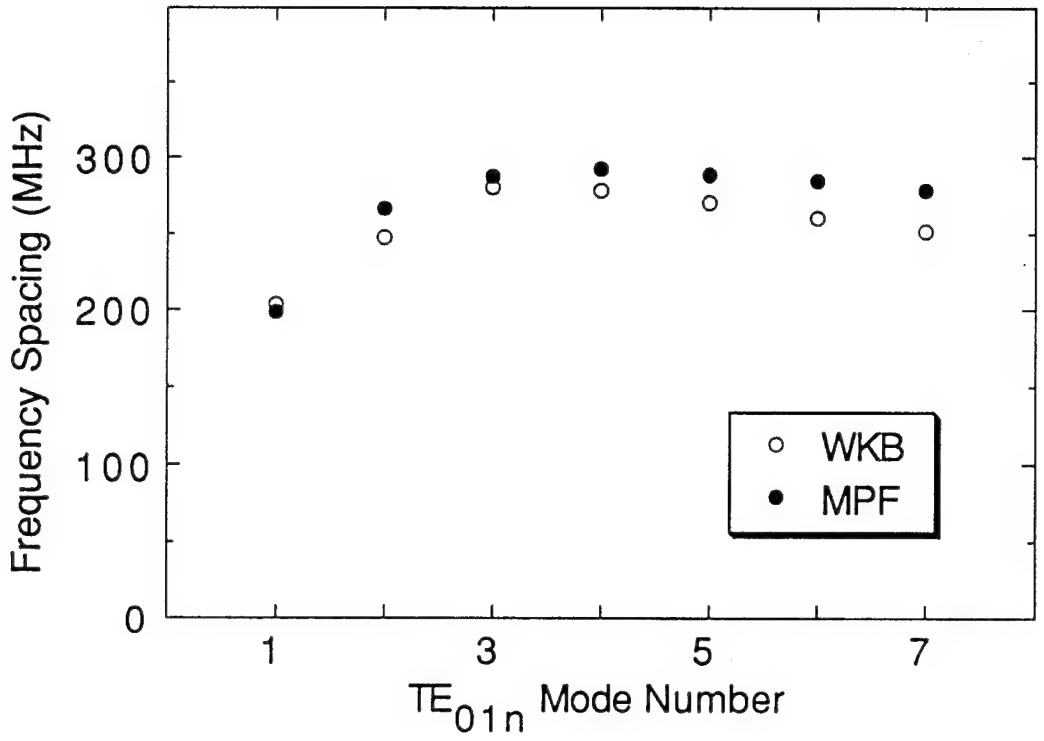
Frequency Spacing (MHz)
300
200
100
0
1
3
5
7
TE_{01n} Mode Number
WKB
MPF

FIG. 3

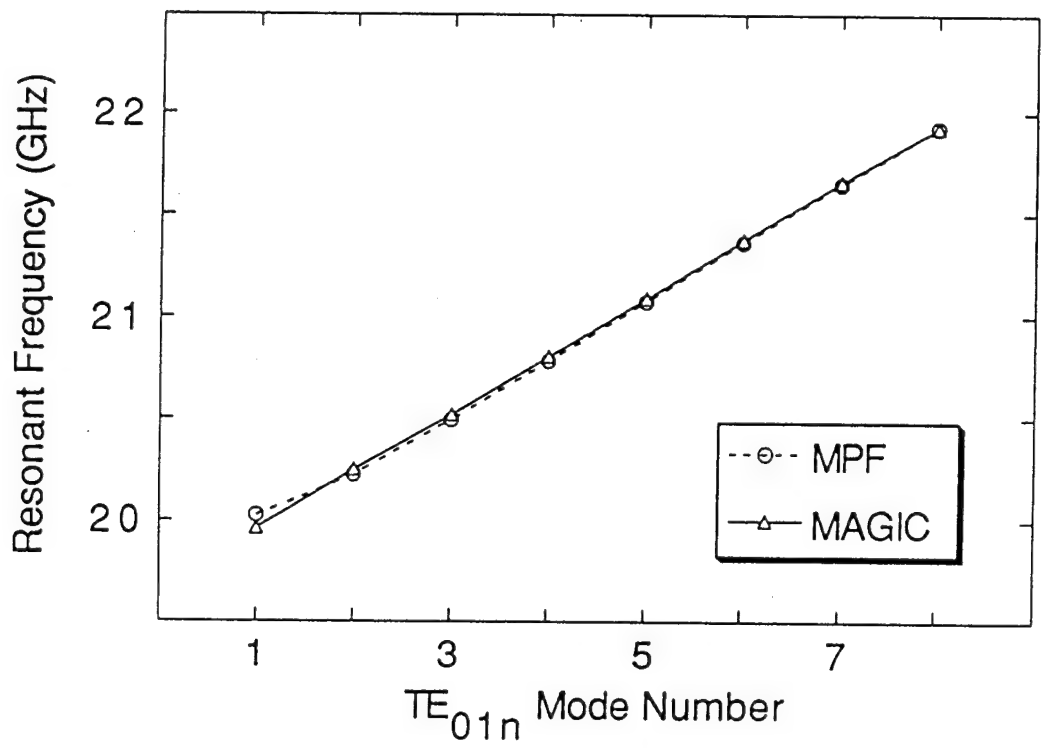
Resonant Frequency (GHz)
22
21
20
1
3
5
7
TE01n Mode Number
MPF
MAGIC

FIG. 4

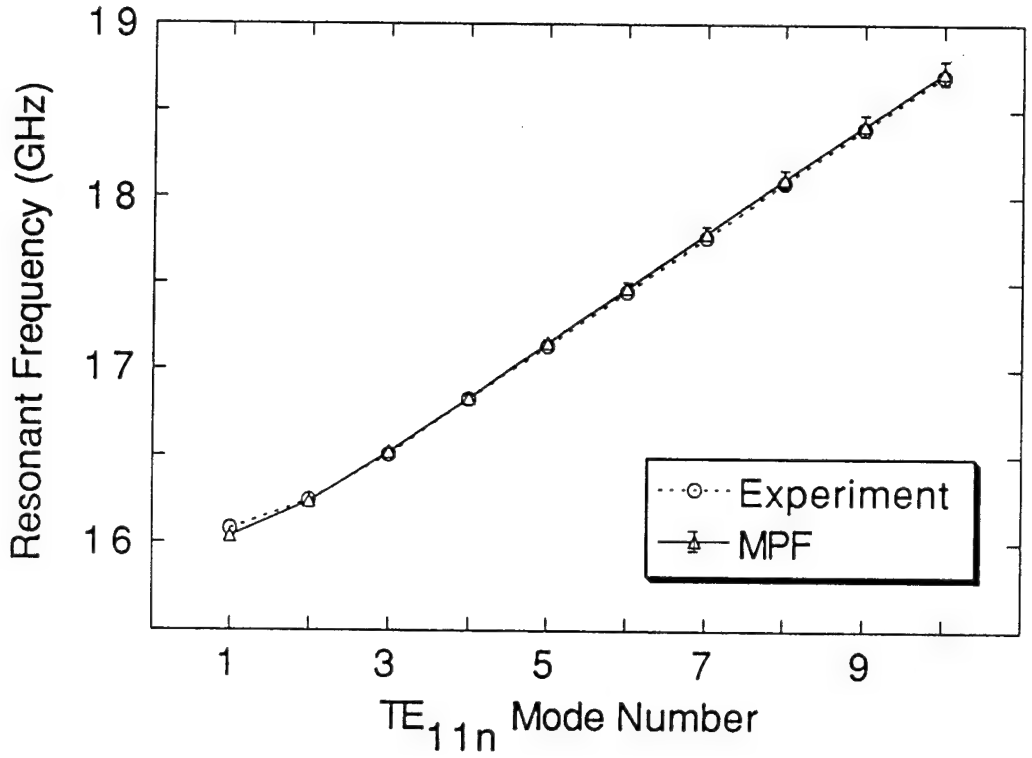
Resonant Frequency (GHz)
19
18
17
16
1
3
5
7
9
TE11n Mode Number
Experiment
MPF

FIG. 5

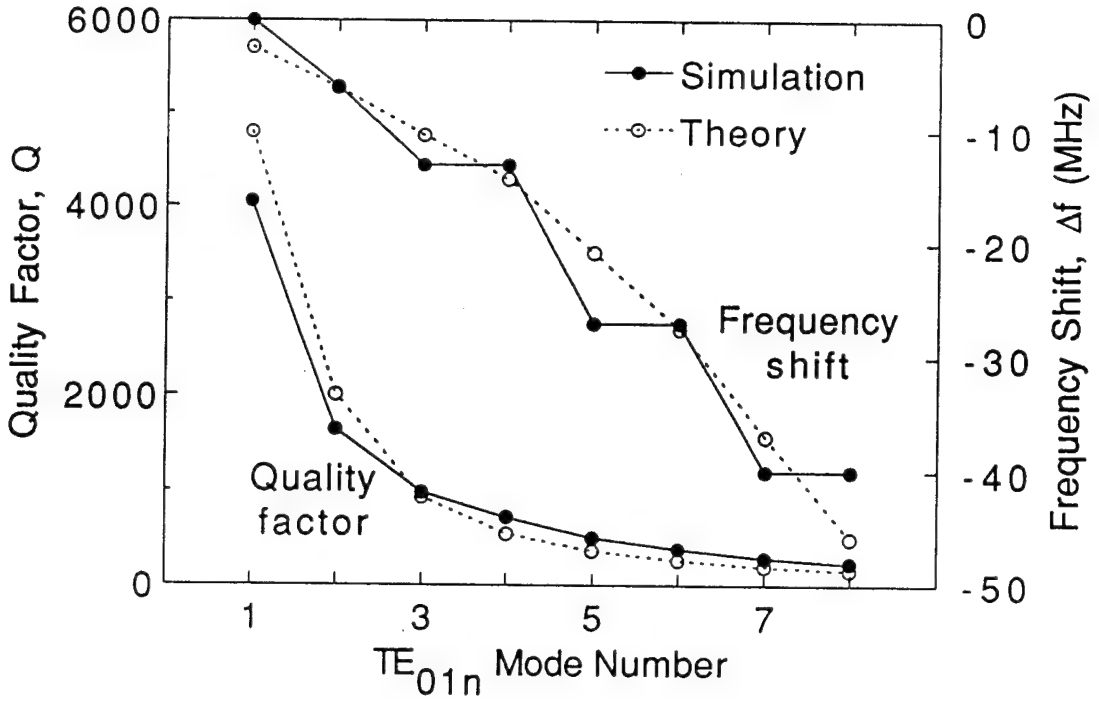
6000
4000
2000
0
Quality Factor, Q
0
-10
-20
-30
-40
-50
Frequency Shift, Δf (MHz)
Simulation
Theory
Frequency shift
Quality factor
1
3
5
7
TE01n Mode Number

F/G. 6

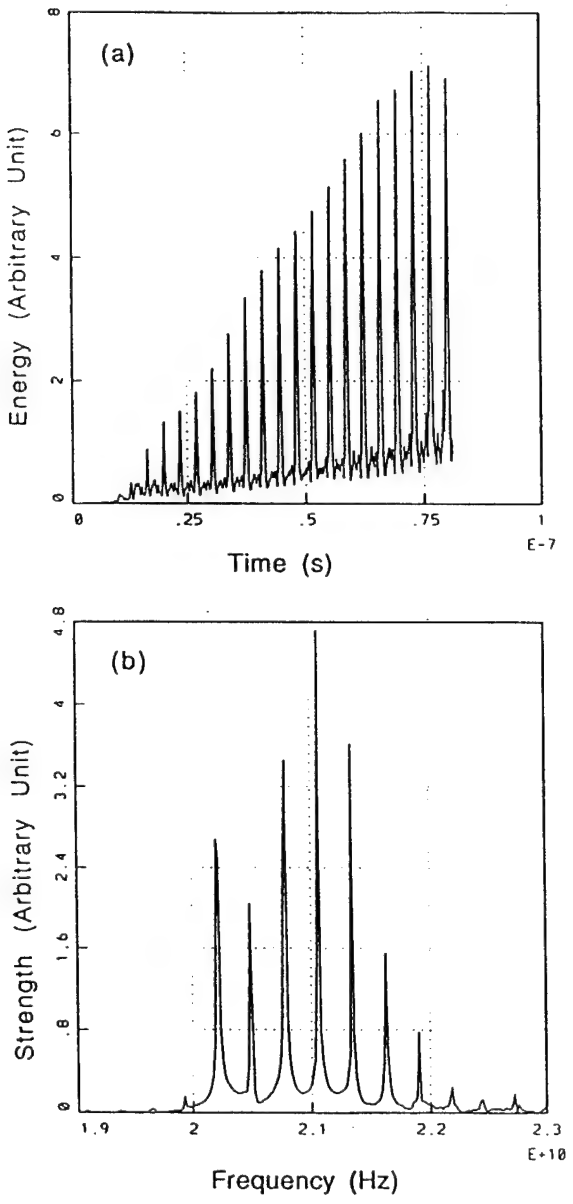
(a)
Energy (Arbitrary Unit)
0
2
4
6
8
0
.25
.5
.75
1
E-7
Time (s)
(b)
Strength (Arbitrary Unit)
0
.8
1.6
2.4
3.2
4
4.8
1.9
2
2.1
2.2
2.3
E+10
Frequency (Hz)

FIG. 7

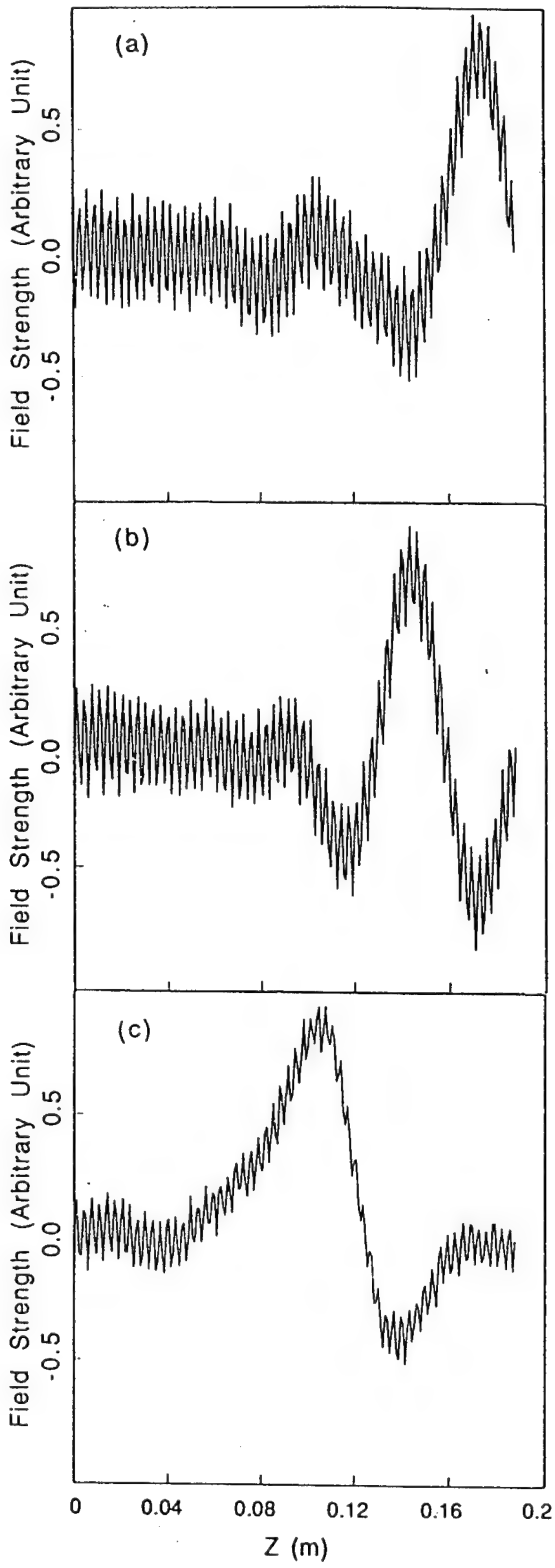
(a)
(b)
(c)
Field Strength (Arbitrary Unit)
-0.5
0.0
0.5
0
0.04
0.08
0.12
0.16
0.2
Z (m)

FIG. 8

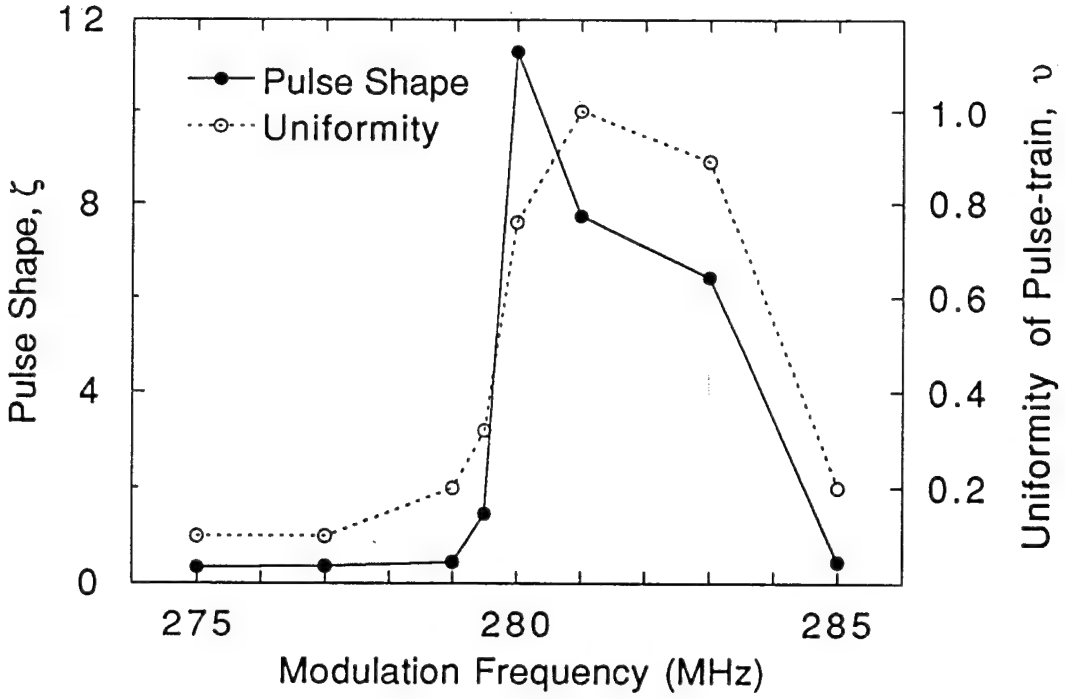
12
8
4
0
Pulse Shape, ζ
Pulse Shape
Uniformity
1.0
0.8
0.6
0.4
0.2
Uniformity of Pulse-train, υ
275
280
285
Modulation Frequency (MHz)

FIG. 9

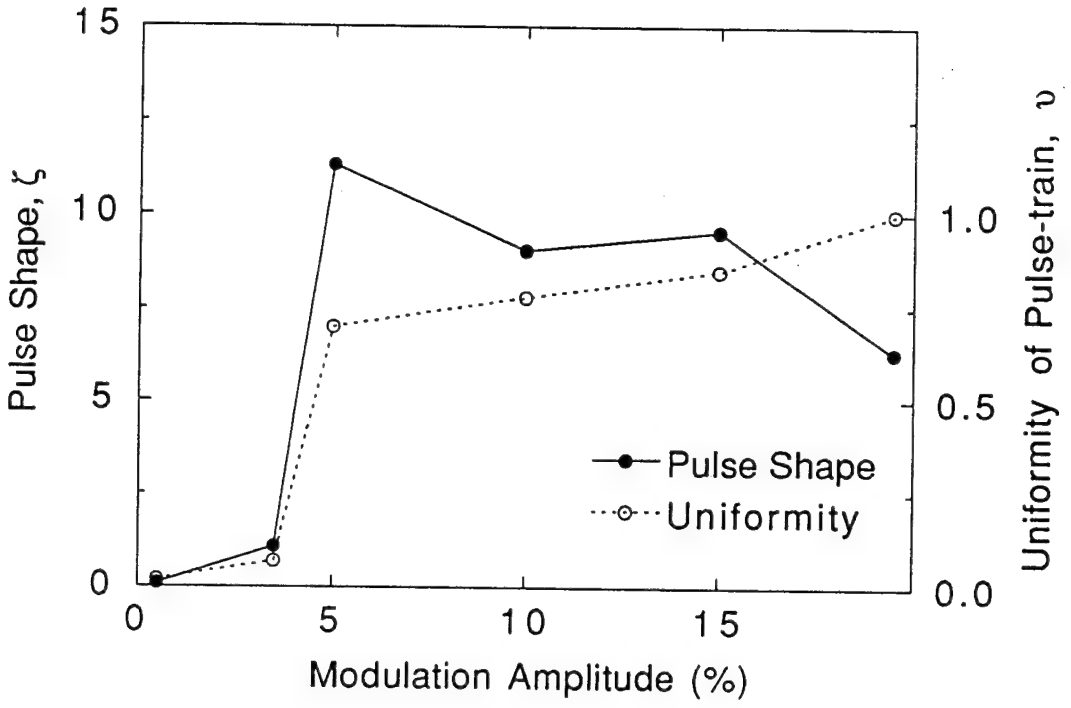
15
10
5
0
Pulse Shape, ζ
0
5
10
15
Modulation Amplitude (%)
1.0
0.5
0.0
Uniformity of Pulse-train, υ
Pulse Shape
Uniformity

FIG. 10

SECTION IV

Experimental Work on Closed Cavity Mode Locking

Abstract - Section IV

A two-cavity mode locked oscillator device has been designed and partially tested. One cavity is of the re-entrant type, and is used for premodulation of the electron beam density. The design of this cavity has been completed and field simulations using MAGIC are included. The cavity nominal resonant frequency is 300 MHz with a tuning range (via movable paddles) of 60 MHz. The second cavity is an endfired tapered gyrotron which has been built and cold tested. The gyrotron cavity features a movable rf probe to sample the pulsed radiation without incurring distortions due to the output electrodynamic structure. A high power rf source to modulate the beam has been obtained and tested. This supply generates 1 kW average power over a 40 MHz band about 300 MHz. The beam test facility required to run the mode locking device is fully functional and has been experimentally tested. Beam tests from the MIG gun have been carried out up to 40 keV at currents in excess of 7 A. Measurements of the perpendicular-to-parallel velocity ratio (α) of the beam typically indicate a value above one. A decrease in α at higher beam currents is observed.

I. INTRODUCTION

The experiment supported by this Air Force grant and currently underway at the University of Southern California involves the mode locking of axial TE_{11n} modes in a closed tapered cavity gyrotron. TE_{11n} modes are used for two reasons. First, these modes have optimal coupling to the small radius electron beam (the Varian model 8063 magnetron injection electron gun produces a beam with guiding center radius ~ 2 mm at 6 kG). All electrons are near the electric field maximum. Second, the TE_{11n} set are the dominant modes in the circular cavity. Thus, higher order transverse modes should not be excited. The cavity is tapered to reduce the dispersion of the electrodynamic structure. The quasi-linear work required the electron beam to shift the modal frequencies to an equidistant spectrum. Greater flexibility in the beam properties can be obtained by tapering the cavity to achieve the appropriate spectrum of cavity resonances.

The existing experimental infrastructure and technical results are outlined in the following sections. A beam test stand has been constructed and a drift tube built to allow high voltage test of the MIG gun (see Fig. 1). This drift tube incorporates a valve/bellows assembly for protection of the electron gun, a set of two capacitive probes mounted on a double-sided flange, and a water-cooled collector isolated from the tube by a dc break. The designs of these components are included. Calibrations of the probes have been made and collector simulations by MAGIC have been done. The design of the gyrotron cavity and prebunching cavity for the closed cavity experiment is given. Measurements have been made of the magnetic field both in the main solenoid and in the trim coil region. These measurements are compared with POISSON simulations. The trim coil is mounted on two movable trays which allow three dimensional positioning. Measurements and results from the high voltage test and beam test are included. Preliminary measurements of 24 GHz radiation from the beam test are also reported. Positive cold test results from the tapered cavity have been obtained.

I. INFRASTRUCTURE

A beam test stand has been constructed and a drift tube built (see Fig. 2(a)) to allow high voltage test of the MIG gun. This drift tube incorporates a valve/bellows assembly (see also Fig. 3(a)) for protection of the electron gun, a set of two capacitive probes mounted on a double-sided flange (see also Fig. 3(b)), and a water-cooled collector isolated from the tube by a dc break (see also Fig. 3(c)).

The design of the electron beam collector was closely guided by POISSON and MAGIC PIC simulations. In order to provide the flexibility to move the collector in the axial direction, a cup-shape polepiece is incorporated. The function of the polepiece is to create an abruptly divergent magnetic field at the entrance of the collector region so that electrons can be diverted toward the collector wall where

cooling is provided. The POISSON simulation generates a magnetic field distribution according to the electromagnet manufacturer's specifications and the proposed polepiece design. This simulation result is then transferred to the MAGIC PIC code as the prescribed field for electron trajectory simulation. The resultant electron spatial distribution will then give the information on the efficacy of the overall collector design. The criteria for success is that after passing through the polepiece the electrons will deposit their kinetic energy on the collector body where a proper cooling is provided. The polepiece thickness and the size of the bore hole play an important role in the electrons behavior inside the collector. The iteration between varying the pole piece shape and checking the electron trajectories is continued until a proper design is achieved. Figure 4 shows the simulated electron trajectory with MAGIC PIC code for a polepiece which is 0.8" thick with a bore hole of 1.23" in diameter. The electrons are observed to be distributed over a broad area on the collector wall (~ 100 cm^2.) The power density can be estimated to be $\approx$ 4.0 kW/cm^2. In this simulation the electron beam energy is 10 keV. Energies up to 40 keV were also tested with good results.

In order to simultaneously achieve high vacuum capability and good mechanical stability, a ceramic ring structure was chosen to provide the necessary electrical isolation of the collector from the tube body (Fig. 2a). This dc break involved brazing alumina rings to 30 mil thick Kovar disks. These disks were in turn electron beam welded to stainless steel flanges. While Kovar was needed to provide a good brazing interface, the mass of the material was minimized. This in turn minimized the possible perturbation of the magnetic field in the collector entrance.

The collector body was made of 304 stainless steel tube with 3.0" OD and 0.1" wall thickness. Collector cooling is provided with a water jacket consisted of 7-turn 1/4" copper tubes. With a cooling water flow rate of 0.1 gpm, the collector can handle a beam power of 400 W continuously.

Capacitive probes are used as beam diagnostics in this experiment. The capacitive probe measures directly the electron beam line charge density. With the knowledge of total beam current, the electron axial velocity can be deduced. The important parameter α ($\alpha = \frac{v_\perp}{v_{//}}$) can then be determined by a knowledge of the beam energy. The probe assembly consists of two sets of 50Ω SMA vacuum feedthroughs on a ConFlat flange as depicted in Fig. 2(a). The feedthroughs are separated by 180^o on the circumference. A small metal disc is welded on the tip of each feedthrough center conductor to increase the probe capacitance. The discs are flush with the drift tube inner surface and electrically isolated from the tube. The probe signal is linearly proportional to the electron beam line charge density when operated in a high impedance mode (1 MΩ).

In the calibration set-up (photograph Fig. 3(b)), the actual electron beam was replaced by a metal tube with a similar radius. The metal tube was pulsed to a high voltage to send a displacement current to the probes. Figure 5 shows the calibration results with two different cable length; 5 feet and 13.1 feet. One of the probes is found to be slightly misaligned after the fabrication and is believed to be the reason

for the difference in probe response. Since different cable lengths represent different total capacitance, the slopes are therefore different.

A schematic of the mode locked gyrotron design is shown in Fig. 2(b). The tapered wall section of the gyrotron cavity ($< 0.6^{o}$ taper angle) serves to reduce dispersion in the waveguide structure. In this way the frequency spacing between modes is almost equal even in the absence of a mode locking signal. The cavity is placed inside a vacuum jacket which allows quick interchange of cavities or output waveguide. Because of the broadband nature of the output radiation, we expect the dispersion induced by the oversized output waveguide to be important. A trade-off will be maintained between low dispersion and single mode propagation. The mode locking signal is provided by external modulation of the electron beam. This modulation is generated by a re-entrant bunching cavity. This signal can provide either velocity or current density modulation, depending on the input signal strength and the length of the drift section. Straightforward klystron theory indicates that at a modulation frequency of 300 MHz, a substantial drift tube length (~50 cm) is required for the 10 - 20% density modulation required for mode locking. The output radiation exits the device through a broadband window at the collector end. The nominal beam parameters are 40 keV, 10 A, α=1.0, with a 100 μs pulse length.

The electromagnet has been tested and the axial magnetic field measured. The electromagnet is powered with four 30 kW DC power supplies. In the measurement shown in Fig. 6, dc current from each power supply was 80 A which generated a peak magnetic field $\approx$ 3.2 kG. The current was measured with resistive shunts. The magnetic field was measured at a 0.5" axial increment throughout the whole electromagnet and compared with POISSON simulation. Figure 6 shows both the measurement and the simulation results. It was observed that some discrepancy existed in region at 15" away from one end of the magnet. The variation was about 2% of the peak magnitude. The actual cause is not yet clearly understood. The electromagnet has also been running with 90% power for $\approx$ 5 hours at a cooling water flow rate of 20 gpm. No thermal problems were observed.

The trim coil has been designed, fabricated and delivered. The coil consists of 5 pancake sections of electromagnets. A copper sheet provides heat conduction from the center of each section toward the edge where it is then was removed by cooling tubes. The trim coil is 5" long with a center bore of 7". A photograph of the assembled trim coil with iron pole pieces in the support mount is shown in Fig. 7(a). A trim coil support which is capable of XYZ motion and adjustment has been designed and constructed. A photograph of this structure is shown in Fig. 7(b).

Using this test stand, we have successfully demonstrated high voltage, full current operation. High voltage tests revealed two problems. The first was arcing in the compensated resistive voltage divider. Tighter connections solved this problem. The second was arcing in the modulator at full voltage operation (40 kV). The arc event (perhaps due to high humidity from the recent rainstorms) caused damage to the logic cards driving the grid modulator for the switch tubes. The FETs on the four cards

were replaced and normal operation resumed. Extra shielding was added between the switch tube anode and the lead shields surrounding the tubes. No modulator arcing has been observed since.

Figure 8 shows oscilloscope output of the current waveforms supplied to the cathode (8a) which are measured from a current transformer inside the modulator, before voltage division for the mod-anode; and current collected after traversing the drift tube, measured by a current transformer with ten times less sensitivity at the collector. Roughly 5.75 A of the 6.09 A supplied to the cathode arrives at the collector. These numbers indicate that virtually all of the electrons emitted by the MIG electron gun arrive at the collector since about 4% of the cathode current (0.25 A) is lost at the voltage divider. Measurements of tube body current confirm this conclusion. This data was taken at a beam voltage of 30 kV and a magnetic field of about 5.5 kG. The pulse length of 5 ms could be extended substantially (collector cooling worked well and gun performance seemed good) but excess pressure rise in the tube was noted because a temporary leak (bad ConFlat connection) had compromised the 10^{-9} torr bakeout. The turbomolecular pump was also unavailable at this time because of a worn bearing. Current overshoot in Fig. 8(a) could be adjusted by a pulse top correction on the grid modulator, but a roll-off of the gun voltage build-up was observed.

The capacitive probes were used to measure the average beam alpha as a function of beam voltage, divider tap position, beam current, and magnetic field. A sample output of this diagnostic is shown in Fig. 9. Noise problems were not excessive and signal strengths were such that repeatable measurements could be made. Results from a measurement at high gun filament heater power are shown in Fig. 10. The gun magnetic field was adjusted so that no more than 10% of the maximum collector current was stripped on the tube body. Velocity ratios (α) over 1.2 were reached with current over 6.0 A. Generally, higher beam current means a lower α, due to space charge depression between the cathode and mod anode. This is observed at high tap position in Fig. 10 where not even an adjustment of trim coil magnetic field can prevent a decrease in α.

Because of the small radius cathode on the 8063 MIG gun, the required magnetic field at the cathode can best be determined by simulation. Using EGUN2, it has been found that the magnetic field strength should be about 1 kG with a variation of 100 G over the emitter strip (increasing toward the anode). This field profile was not obtained in the present test since a slight modification was made to the magnet pole piece at the gun end which provided an insufficient solenoid magnetic field strength at the cathode. Hence most of the field was supplied by the trim coil, and the field taper was clearly not optimal. Further tests with a different pole piece will check if a can be further increased. Simulations also indicate that beam velocity spread is a rather strong function of the magnetic field profile at the gun.

Second harmonic gyrotron emission has been observed from the beam test tube. The tube has a diameter of 0.3" and a cutoff frequency just over 22 GHz. Using a magnetic field of 4.4 kG and a beam voltage of 26 kV, a sequence of second harmonic modes were observed. Figure 11 shows crystal detector output of this radiation. The frequency was measured by an EIP pulse counter as well as by a cavity

wavemeter. Frequencies in the interval 22.5 to 24.5 GHz were seen. Because of the length of the drift tube, many axial modes were excited in close proximity (in parameter space). The strong coupling between them allowed only one mode in the steady state. Power measurements were unavailable since the detector and couplers were all operated out of band. Since the detector response rolls-off around 20 GHz, we have a lower threshold for the power by assuming the calibration holds at the observed oscillation frequencies. The detector output indicates a power level over 1W after passing through a weakly coupled capacitive probe and 20 feet of semi-rigid co-axial cable. This result makes clear the fact that or test stand is ideal for doing harmonic gyrotron work. The water-cooled dc magnets have large bore, can be run continuously for long periods of time, contain individually addressable coils, and produce peak fields corresponding to gyrotron fundamental output just below 20 GHz. The 8063 MIG gun produces a small beam (guiding center position less than 2 mm at a 7 kG field) which allows cutoff drift tubes above 25 GHz.

The laboratory in which this work was performed is at the University of Southern California and is fully functional. It consists of a room with approximately 400 square feet of space with a chemical fume hood at one end. A 3 ft x 12 ft optical bench supports the solenoidal magnet and trim coil. The University of Southern California and the Powell Foundation have together provided some $160,000 of start-up funds to equip the laboratory. A 40 kV, 12 A high voltage modulator has been acquired to drive the electron sources. This modulator has a voltage droop of less than one percent over a 50 μs pulse and is capable of providing pulse lengths exceeding 150 μs. This pulse length enables observation of long-time behavior of the microwave pulse and could be essential if mode locking times are long. The laboratory is completely equipped with vacuum pumps, gauges and processing equipment. Also available are microwave sources and components in Ku band and X band. This equipment was used in performing the cold test and beam test for the mode locking experiment. A sweep oscillator is available which generates over 40 mW from 10 MHz to 20 GHz. This will generate the low frequency mode locking signal as well as enabling cold test of the two experimental cavities. A high power rf amplifier is available to amplify the 300 MHz mode locking signal. A lab computer for data acquisition and control is available, and a 7 kG magnet and four 30 kW dc power supplies are on-line. A laboratory schematic is shown in Fig. 12.

In addition there are substantial computational facilities available. On campus at USC there are various Sun Workstations, DEC and Alliant computers for general and parallel computing. These facilities are supported by the university. The university has recently obtained a Silicon Graphics supercomputer. The bulk of the computation was done at NSF supported supercomputer centers. Currently the principal investigator has research accounts at the San Diego Supercomputer Center (SDSC). The work at SDSC has included the closed cavity mode locking research as well as nonlinear calculations on quasi-optical gyrotrons.

II. TAPERED CAVITY DESIGN AND COLD TEST

A tapered cavity supporting TE_{11n} modes with a nominal cutoff frequency of 16 GHz was built and cold-tested. The tapered section is made of copper with length L' = 10.17 cm. A straight section of brass was made for cold test with length L = 8.52 cm. A copper version of this straight section with a probe mount was built for the actual experiment. The taper angle, α, is measured to be 0.5^{o}. This setup is pictured in Fig. 12. The cavity section is broken into three parts: the oscillator cavity (straight), the taper, and another straight piece of beam tunnel. This allows the gyrotron cavity length to be varied without changing the outer vacuum envelope. Since the probe fixture pierces the envelope, any cavity changes must keep the probe in the same place. The probe has motion of about 1 cm in the axial direction and can be fully retracted from the cavity. A waveguide transition couples the cavity fields to the output waveguide. The vacuum window, (not shown in the figure) is a halfwave window (at 18 GHz) made out of quartz. In the cold test, three probe positions are chosen to sample the various modes. The field amplitudes of modes n=2 and 6 are near their maximum at probe # 1, modes n=1, 7 and 8 are near their maximum at probe # 2, and modes n=3, 4 and 5 are near their maximum at probe # 3.

The cold test measurement results and the MPF predictions are in good agreement. The experimental sources of error include $\pm$10 MHz from the frequency measurement and a slightly elliptical cross-section of the tapered section. The uncertainty in MPF calculation is found by using the probable maximum and minimum taper angles corresponding to dimensional uncertainties.

Tapered cavities with various sizes of apertures in the untapered end have also been simulated and tested. Resonant frequency shifts with respect to closed cavity resonances were studied. Simulation shows that for a given aperture size, the quality factor Q roughly decreases as $1/n^2$. A simple heuristic indicates the dependence should be: $Q \sim 1/n^2\lambda^3$, where λ is the modal resonant wavelength. The resonant frequencies should be down shifted by approximately $\Delta f \sim f/2Q$, where f is the modal resonant frequency. The simulation results for a circular aperture of radius $0.95r_w$ have compared favorably with the heuristic relations.

III. PREBUNCHING CAVITY

The closed cavity mode locking experiment requires modulation of the electron beam. This is accomplished by modulating the axial electron velocity in a bunching cavity (similar to that of a klystron). As is familiar from klystron theory, this bunching can either result in charge density modulation or remain velocity modulation, depending on the bunching parameter. In either case a cylindrical re-entrant modulation cavity will be used to couple the mode locking signal to the beam. Here the rf electric field is directed along the direction of the beam flow. L_1 is the gap separation (where most of the electric field energy resides), d is the length of the drift section separating the modulator

cavity from the gyrotron. The presence of the drift section will allow ballistic bunching of electrons as in the klystron. This can be minimized, if necessary, by choosing a very short length d.

The modulator cavity can be designed using previous results from klystrons. The cavity dimensions are smaller than a wavelength of the low frequency input rf signal. Thus the resonant wavelength is approximately:

$$\lambda = r_1 \pi \sqrt{2 \frac{L}{L_1} \ln\left(\frac{r_2}{r_1}\right)} \qquad (4)$$

where L is the cavity length, and r_1 and r_2 are the inner and outer radii of the coaxial cavity. This type of cavity is well understood and presents no peculiarity other than a constraint on the diameter imposed by the electromagnet structure and the necessity for a fairly large tuning range. An "end-gap" variation was chosen with the gap occurring at the cavity entrance with respect to the direction of beam flow. Noting roughly the relation of gap width to capacitance and cavity length to inductance and the analogy to the series RLC circuit, the basic cavity dimensions can be calculated by applying equation (4). Note that this equation is derived on the basis of a gap at the cavity center. This expression assumes that $L >> L_1$. Rough dimensions taken from this expression, when modified for "endgap" operation, have yielded cavities that display resonance within 15% of the theoretical center frequency in MAGIC simulations.

To achieve the necessary level of modulation, the magnitude of the axial electric field experienced by the 40 keV electron beam while transiting the cavity must be large. In this case a pulse train of UHF "bursts" of up to 1 kW peak power will be used to drive the bunching cavity. Various methods of achieving a usable tuning bandwidth were examined an a "paddle' style design was selected. Here conducting paddles at cavity wall potential are introduced into perturbed fringe fields generated by a taper modification of the classic klystron cavity gap. This arrangement and other design considerations were studied and simulations performed using MAGIC. Results of this work and other supporting development work are presented.

Several high power premodulating cavity designs produced commercially and in research were studied to the extent non-proprietary information was available. Initially, of particular interest, was a two-stage sub-harmonic prebuncher designed by Boeing for a free electron laser. This design utilized two high power UHF cavities constructed from 304 stainless steel and plunge tuned in the vicinity of the gap. This assembly was designed to produce bunching effects on the Boeing 20 MeV S-band linac. Here the tuning range of the prebunching cavities was extremely limited with the plunge tuners providing only precision tuning of the operating frequency. These cavities exhibited a moderate quality factor.

Another cavity design of interest was provided by Litton. This cylindrical cavity utilized a single large plunging style paddle providing asymmetrical capacitive gap interaction, increasing the capacitance

of the parallel plate gap as the paddle was plunged inward thus driving down the resonant frequency. Detailed tuning range information for this design was not available.

Two types of tuning were considered, a piston style volume "end tuner" and various gap interactive appendages. This piston concept is attractive because inductive tuning provides a less sensitive coupling variation over the course on the piston motion and more precise tuning can theoretically occur. This resolution feature is outweighed by sheer difficulty of construction. In order to hold vacuum, a very large welded bellows is necessary which limits the axial motion of the piston, negating the long travel capability and its higher tuning resolution. Mention is made in textbooks regarding the use of capacitive joints between the cavity walls and tuning member to eliminate potential extraneous resonances in this tuning scheme. Piston binding issues eliminated consideration of commercial linear motion feedthroughs to actuate the tuning member.

Direct gap tuners were briefly considered, where the width of the classic parallel plane gap is varied using a diaphragm or direct translation of one side or the other. These variations were dismissed fairly quickly due to the known unpleasant behavior of parallel plane gaps in their tuning extremes. Large gap spacing provides ineffectual coupling and small gap spacing can exhibit hypersensitive coupling. Between these extremes lies a narrow tuning range. Arcing due to decreased shunt resistance and thermal drift in cw applications can occur in small gap tuning.

Finally, the family of gap interactive appendages was considered and ultimately selected for study with MAGIC. Tuning mechanisms designed in this style all possess conducting members with rf continuity to the cavity side walls. The tuning member is introduced into the fringe field of the gap parallel planed capacitor, generally effecting a virtual increase in the area of the capacitor plate(s) and resulting increase in capacitance, driving the resonant frequency downward. Some of these designs incorporate a tuning member which can be fully withdrawn. Most designs retract the tuning member into some sort of stowed position. Consideration of the volume displacement and gap interaction contributed by the tuning member(s) in the stowed position is difficult with asymmetric appendages, and almost all designs utilize them. A variant of this approach is pursued further here.

In the design selected, a pair of large curved "paddles" are rotationally actuated from the end wall by a pair of rotary motion vacuum feedthroughs as depicted in figure 14. These pivot points lie on opposite sides of the gap and the paddles pivot about their endpoints in opposite directions into the stowed position. Moving in from the stowed position, the paddles rotate about their endpoints in opposite directions, coming in to form a near ring adjacent to the gap. Incorporating an approximate 3.5 : 1 taper in the secondary parallel plane will perturb the capacitor fringe fields to maximize interaction with the paddles and also allow the paddles to extend inside the outer radius of the gap if necessary. This design lends itself to the use o commercially available rotary motion feedthroughs sturdy enough to withstand the 250^{o} C bakeout as well as the 3-7 kG magnetic field inside the magnet. This is the design

simulation presented here. Cavity excitation is accomplished with a B-field loop antenna protruding into the cavity from the end wall opposite the gap end of the cavity.

MAGIC is restricted to problems with a high degree of symmetry and employs finite difference equations to solve Maxwell's equations for each of a specified number of cells, determined by grid size. The basic cavity simulation represents a Cartesian slice of a cylindrically symmetric system. All cavity features are assumed to be rotationally symmetric about the cavity axis and no other features are allowed. The cavity must maintain an approximate 5:1 aspect ratio with respect to Cartesian grid sizes for numeric stability.

The cavity simulation utilizes a ring excitation antenna located inside the gap and just outside the radius of the beam tube and is energized by a wave packet current. This packet is a time domain function obtained by Fourier Transform of the step function spectrum in the frequency domain, centered at the expected resonant frequency, but with all frequencies in the band of interest excited at unity magnitude for an objective evaluation of cavity resonance.

MAGIC simulations of this cavity have been performed and the resonant frequency is found to agree within 15% of the theoretical prediction when the gap is in the cavity center. When the gap is at the cavity end MAGIC gives a substantially lower frequency. This allows the gap length to be increased to increase the resonant frequency to the desired 280 MHz value. In addition, MAGIC tests have elucidated the fringe fields in the vicinity of the electron beam and the velocity modulation imparted to the beam. The cavity "cold test" was done using a novel "wave packet" current in the antenna. This time dependent current is constructed so that only an interval of frequencies are excited, each with approximately the same amplitude. Figure 15 shows the conductor geometry of the prebunching cavity as well as the antenna position for cold test. Figure 16 shows the results obtained after a 100 ns wave packet current pulse is applied to the antenna. The resonance is obtained at 280 MHz. The width of the resonance is not accurate since only a 400 ns simulation was carried out (these finite time sample provides a 2.5 MHz uncertainty which is almost the width of the resonance peak). These simulations do not include the paddles.

Further simulations were performed which included the tuning effect of the paddles. The paddles were included by using a conducting ring surrounding the gap. Figure 17 shows the tapered cavity geometry with the paddle in the withdrawn position. The cavity spectrum is shown in Fig. 18 with a resonance clearly visible at 350 MHz. This is the upper limit of the paddle tuning range. The geometry of paddles in the deployed position is shown in Fig. 19. The paddle length has been chosen so that the paddles fit into the tapered center conductor. This is to push the resonance down as low as possible. It may be that the tuning range will not extend this low due to breakdown at the paddle edges. The spectrum associated with this paddle position is shown in Fig. 20. At this position the resonance has been pushed down to 225 MHz, well below that required.

Figure 21 shows an outline drawing of the final prebunching cavity design. All vital dimensions have been specified in accordance with physical constraints imposed by the magnet and results of MAGIC simulations. Initially the cavity post and tapered sections were quite massive, resulting in unacceptable overall weight for the cavity in an experiment that is already on the verge of boresight sag. This massive arrangement also offered difficulties in alignment during assembly for welding. Continuity was also an issue as the initial design used set screws to attach the tapered section to the cavity post, with no axial forces between the post and tapered section.

The design that emerged after an effort to remove material and settle some vacuum issues utilizes largely hollow post and tapered sections with screws used to attach the post to the end wall and to attach the tapered section to the post. Access to the latter is provided through holes in the end wall 2.75" O.D. ConFlat flange. These screws provide the aforementioned desirable axial forces between the components for better continuity. Alignment is augmented by machined guides on the post and collector-wall and with the much lighter components should be easier to achieve.

All of the high power equipment necessary to drive the cavity has arrived in the lab consisting of a Henry Radio high power amplifier, two directional couplers, high power circulator, two high power terminations, and semi-rigid cables. The acceptance test on the amplifier was carried out successfully, operating at full 1 kW power in cw mode and demonstrating 40 MHz tuning range.

The following is a summary of students who contributed to the research effort:

Postdoctoral: R. Liou . . . . . experiment

Graduate:
J. Plewa (M.S. Spring 1993) . . . . . experiment
V. Kasibhotla (passed qualifier Spring 1993) . . . . theory, design codes
H. Wu (passed qualifying exam Spring 1994) . . . . experiment, MAGIC
K. Drummond . . . . . cavity design, MAGIC

Undergraduates:
R. S. Burnside . . . . . .prebunching cavity design and simulation
M. Young (EE) . . . . . .magnetic field measurements
J. Mai (EE) . . . . . cavity drawings, inventory control
B. Kuo (EE) . . . . . construction & test of voltage divider
I. Campbell (EE) . . . . . .equipment purchase, magnet support structure
Y. Yuen (EE) . . . . . . mode locking code work

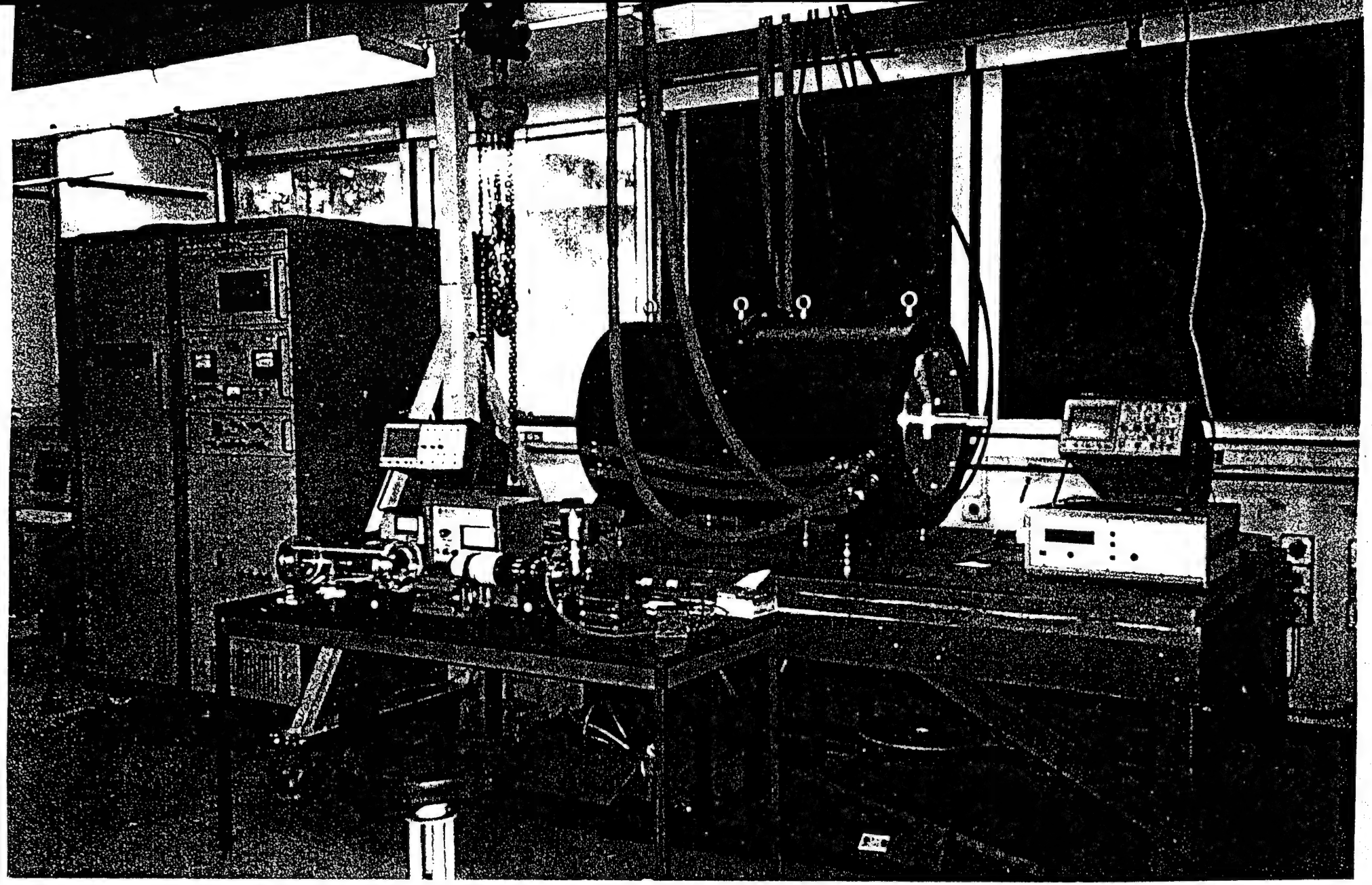

FIG. 1

(a)

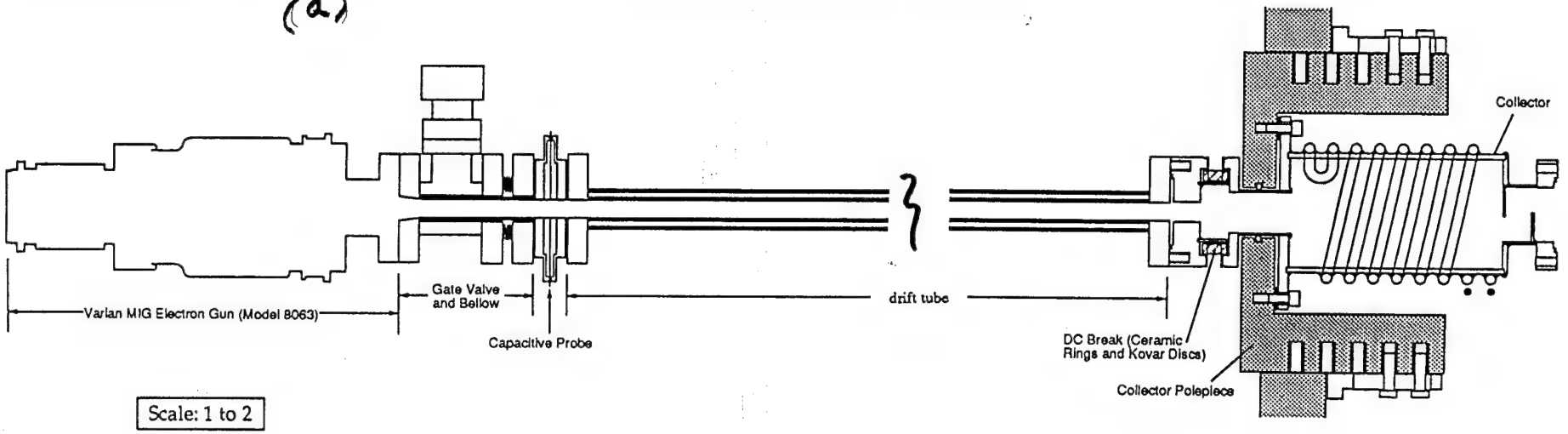

Scale: 1 to 2

(b)

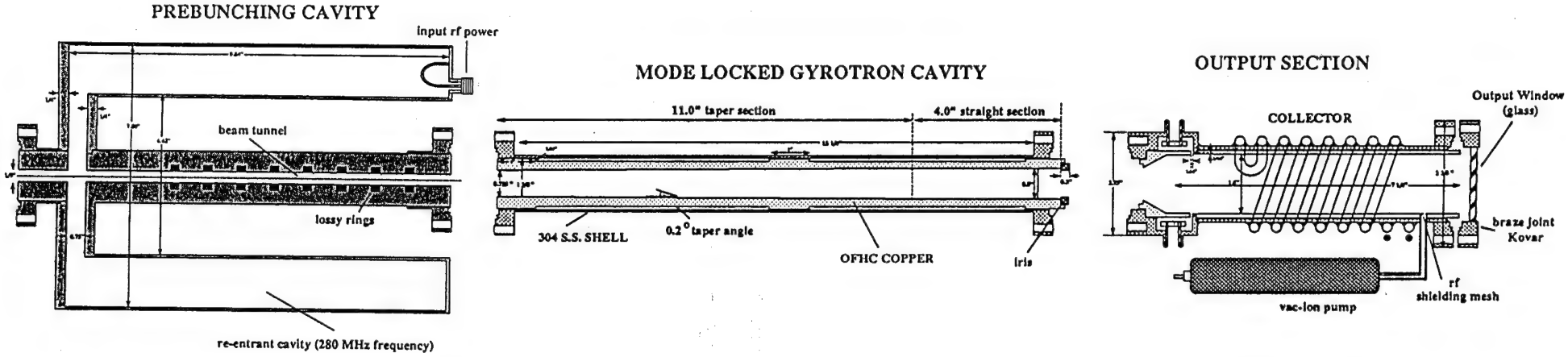

FIG. 2

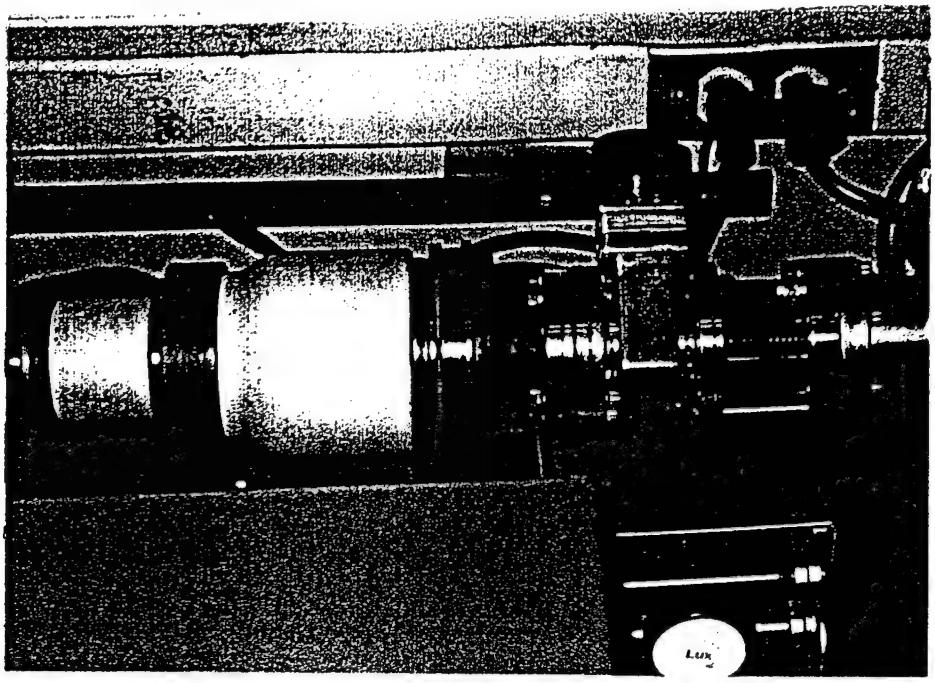

(a)

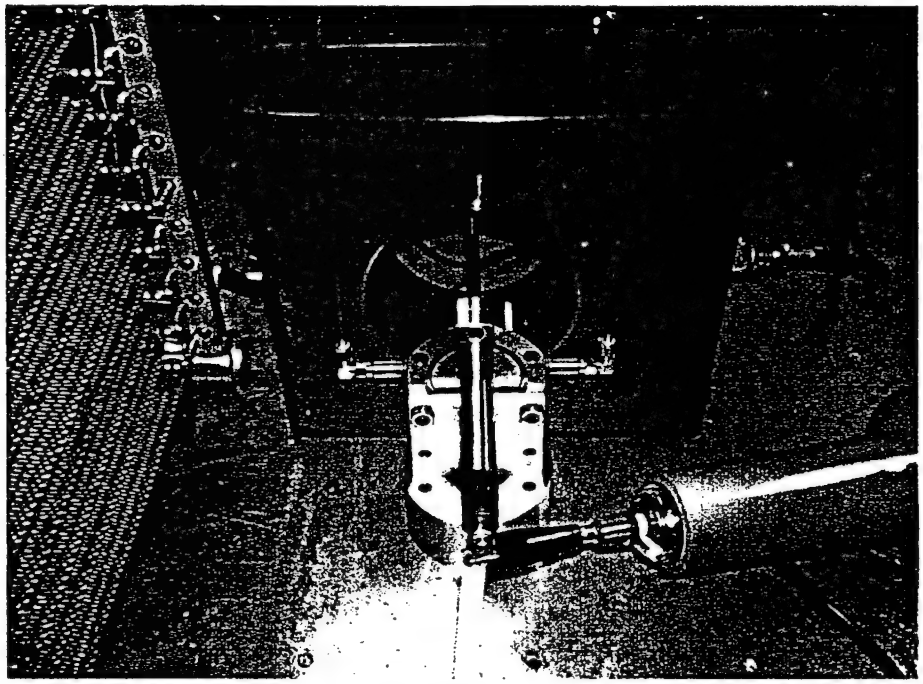

(b)

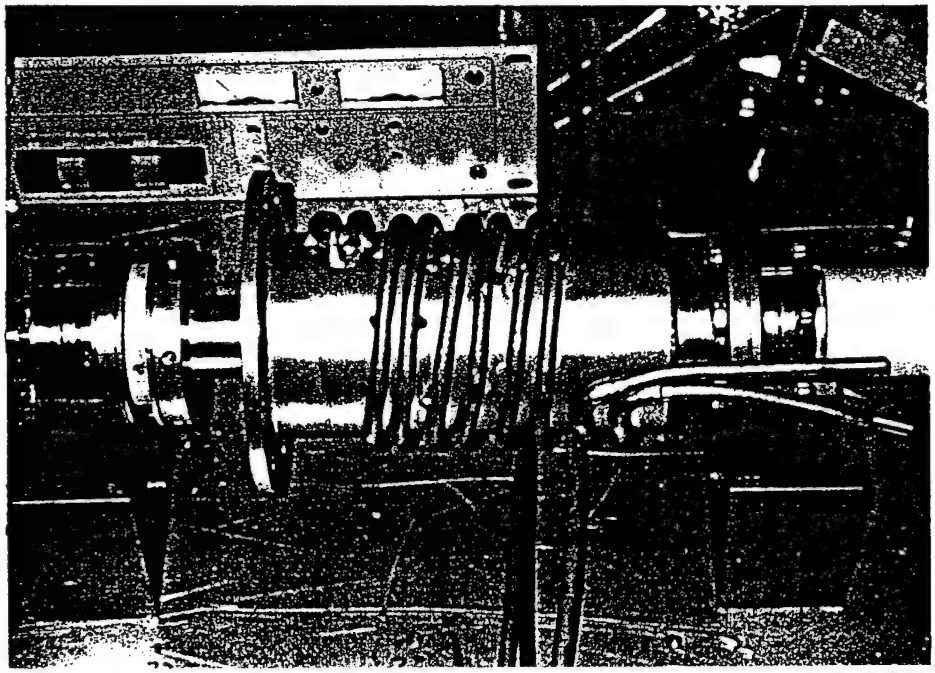

(c)

FIG. 3

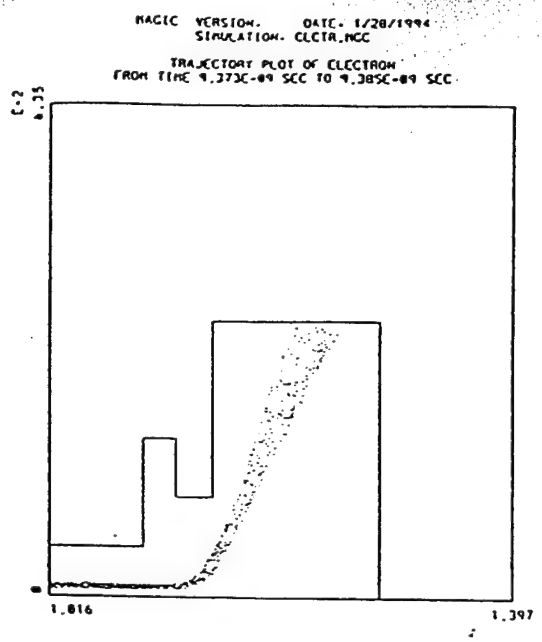

FIGURE 4

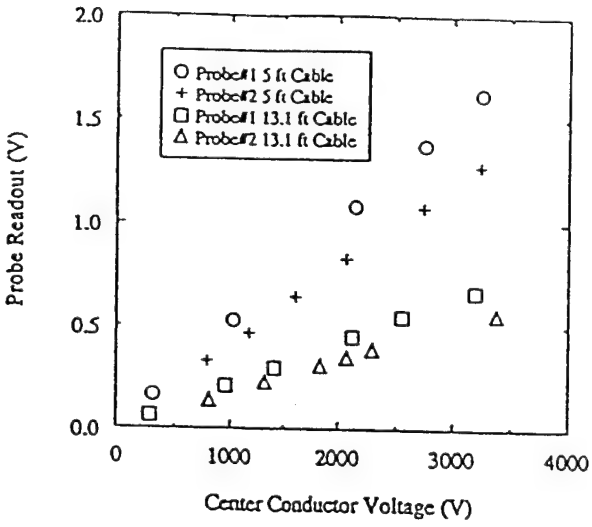

FIGURE 5

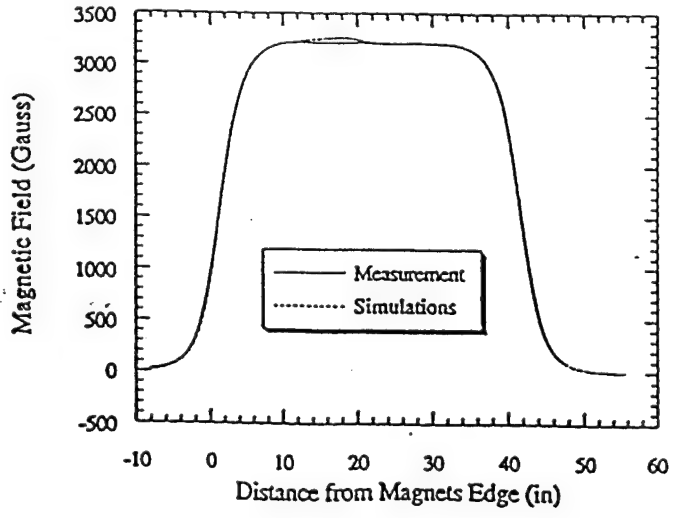

FIGURE 6

(a)

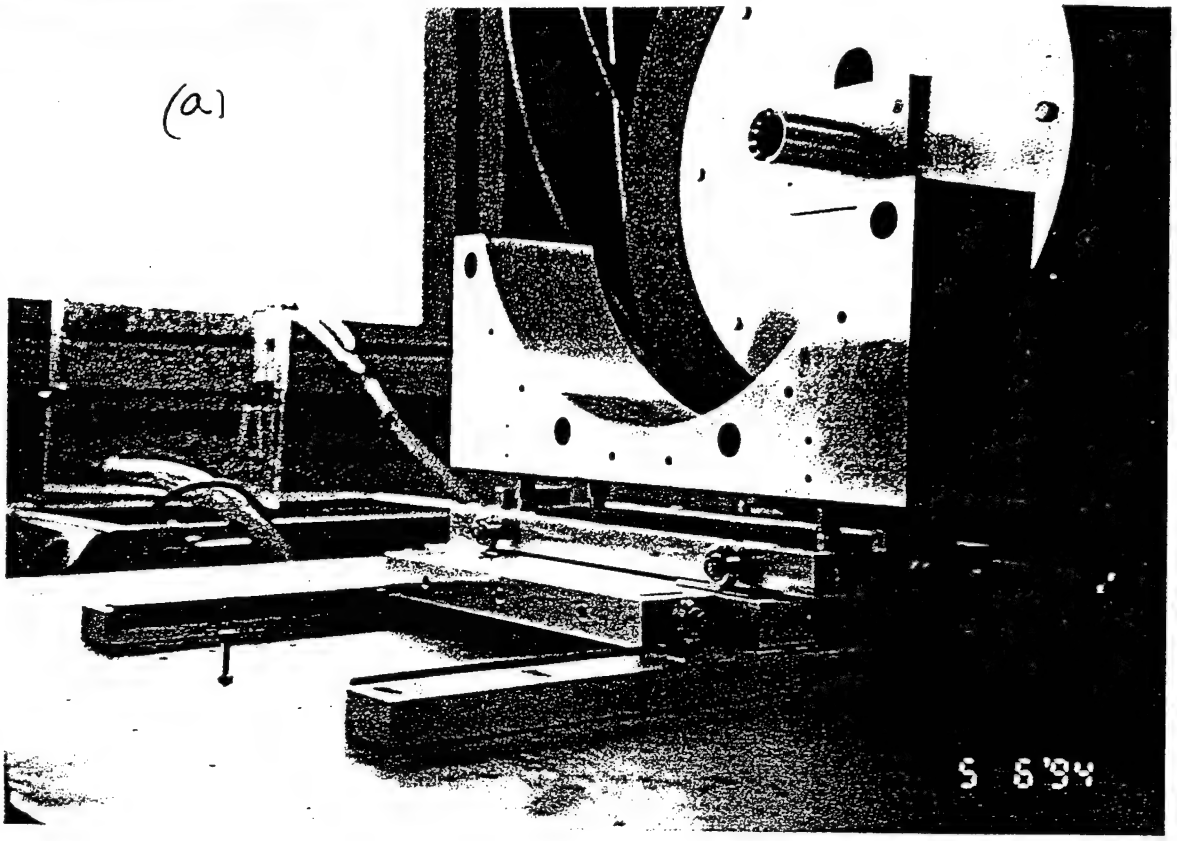

(b)

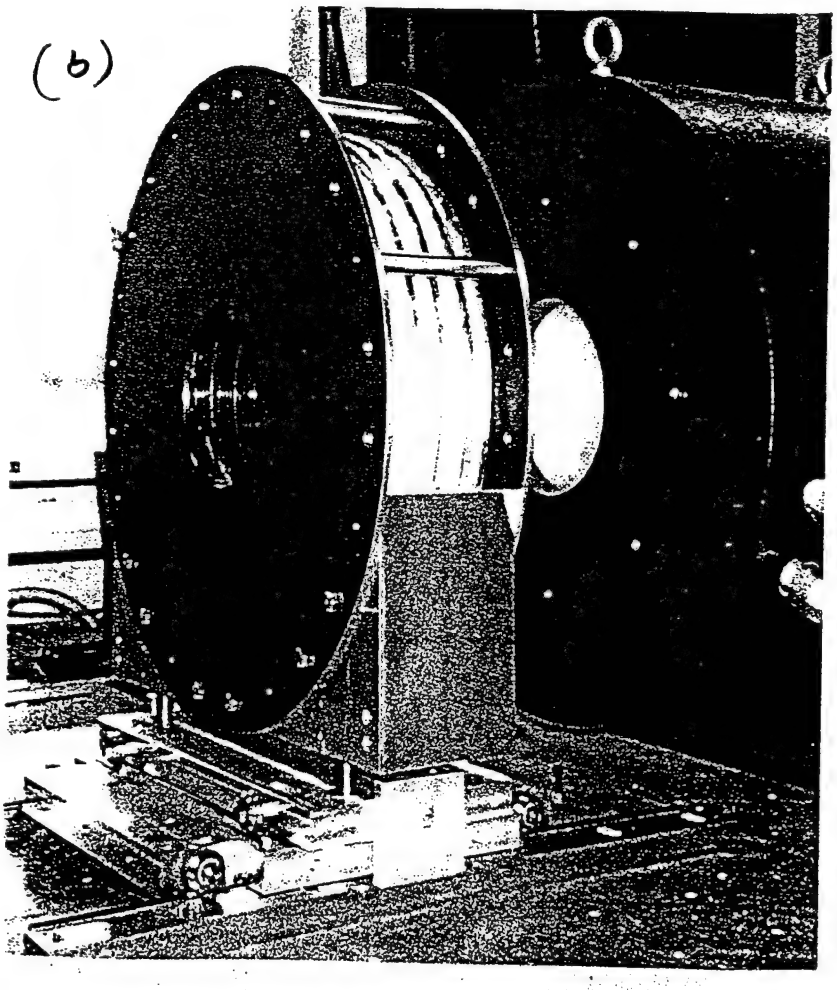

FIG. 7

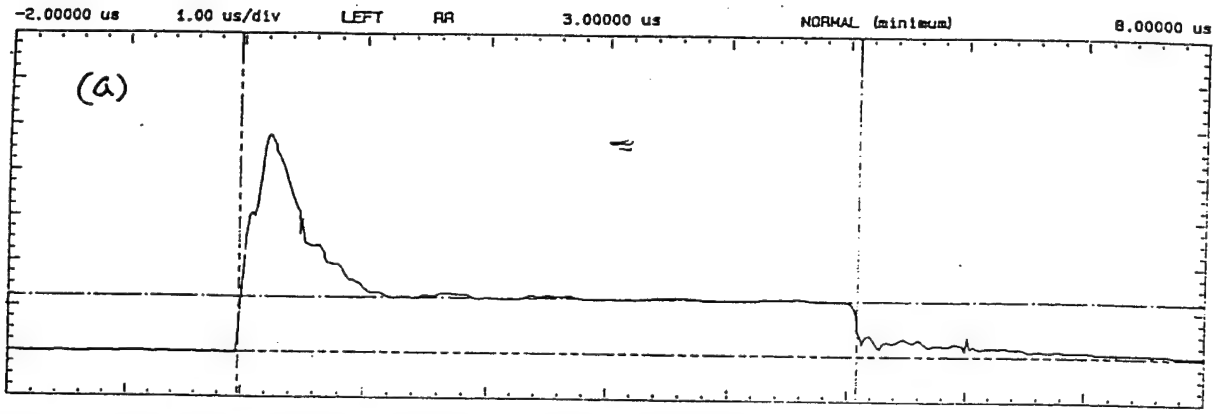

	Sensitivity	Offset	Timebase	Delay	Sampling
WMemory 1	500 mV/div	1.50000 V	1.00 us/div	-2.00000 us	Repetitive

Trigger Mode: Edge
On the Positive Edge of Channel1
Trigger Level(s)
Channel1 = 118.750 mV (noise reject ON)
HoldOff = 1.82000 us

Markers
Y2marker(m1) = 609.375 mV
Y1marker(m1) = 0.00000 V
delta Y = 609.375 mV

X2marker(m1) = 5.10000 us
X1marker(m1) = -20.000 ns
delta X = 5.12000 us
1/delta X = 195.313 kHz

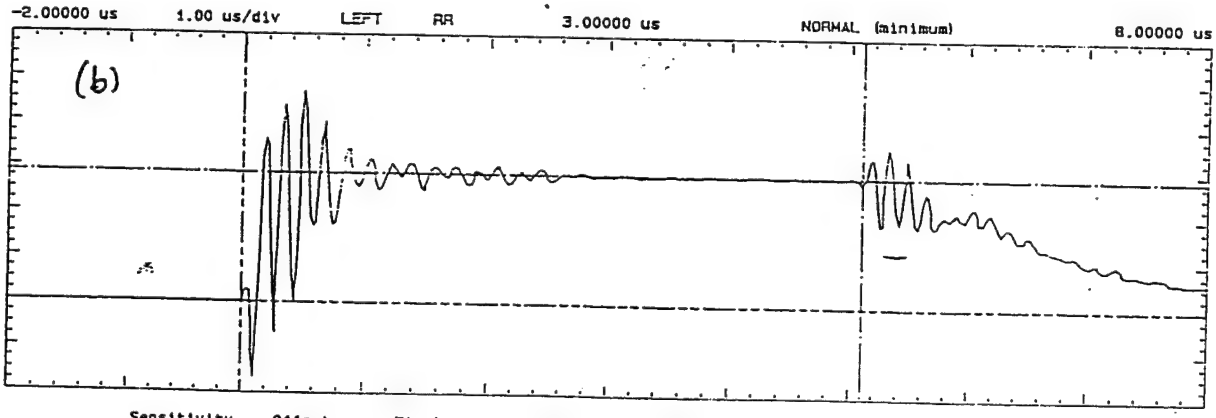

	Sensitivity	Offset	Timebase	Delay	Sampling
WMemory 2	20.0 mV/div	40.0000 mV	1.00 us/div	-2.01981 us	Repetitive

Trigger Mode: Edge
On the Positive Edge of Channel1
Trigger Level(s)
Channel1 = 118.750 mV (noise reject ON)
HoldOff = 1.82000 us

Markers
Y2marker(m2) = 57.5000 mV
Y1marker(m2) = 0.00000 V
delta Y = 57.5000 mV

X2marker(m2) = 5.10000 us
X1marker(m2) = -20.000 ns
delta X = 5.12000 us
1/delta X = 195.313 kHz

FIGURE 8

Printed: 07 APR 1995 at 10:57:46

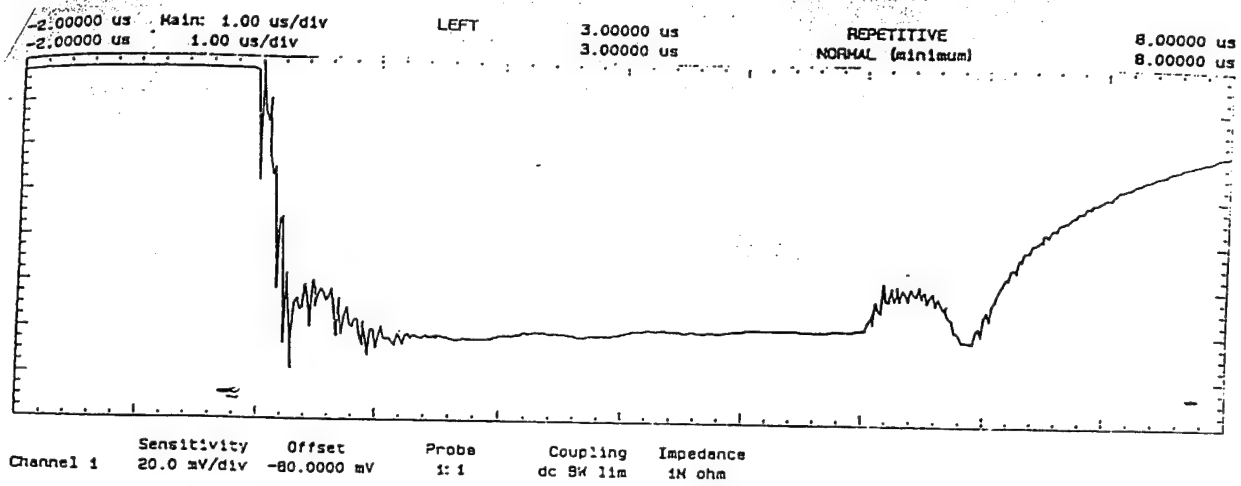

FIGURE 9

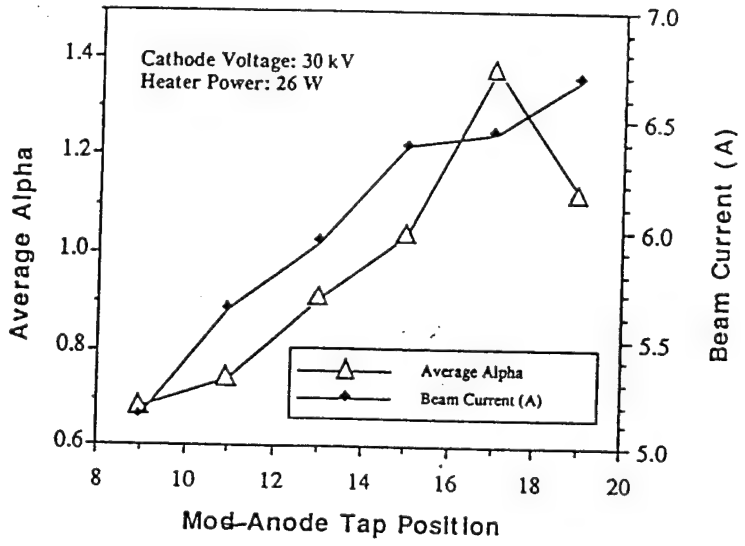

FIGURE 10

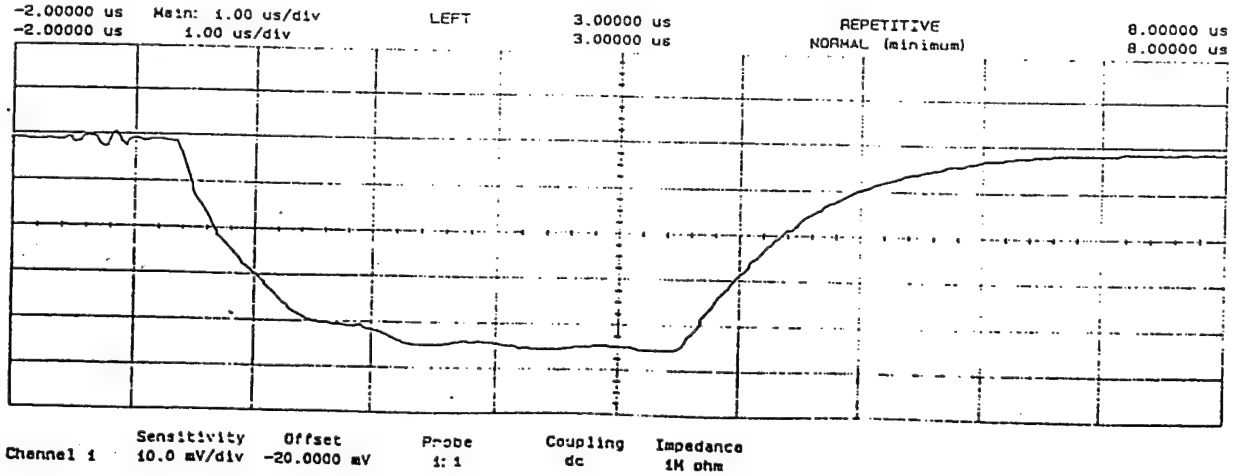

FIGURE 11

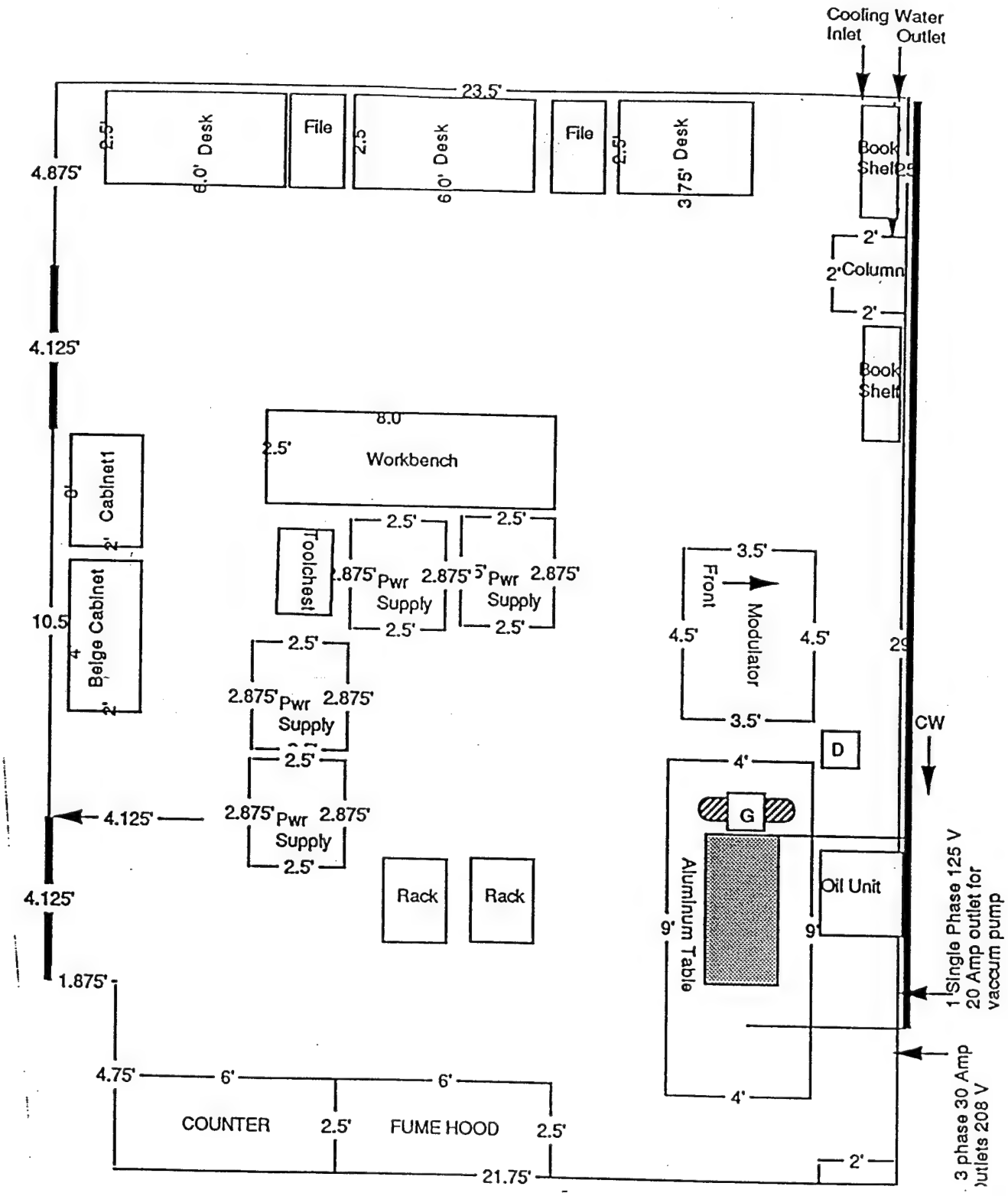
Cooling Water Inlet
Outlet
23.5'
2.5'
6.0' Desk
File
2.5
6.0' Desk
File
2.5'
3.75' Desk
Book Shelf
4.875'
2'
2' Column
2'
4.125'
Book Shelf
8.0
2.5'
Workbench
Cabinet1
2'
Toolchest
2.5'
2.5'
2.875' Pwr Supply 2.875'
2.875' Pwr Supply 2.875'
2.5'
2.5'
3.5'
Front
Modulator
4.5'
4.5'
3.5'
10.5'
Belge Cabinet
2'
2.5'
2.875' Pwr Supply 2.875'
2.5'
CW
D
4'
4.125'
2.875' Pwr Supply 2.875'
2.5'
G
Aluminum Table
9'
9'
Oil Unit
4.125'
Rack
Rack
1.875'
1 Single Phase 125 V 20 Amp outlet for vaccum pump
4.75'
6'
6'
COUNTER
2.5'
FUME HOOD
2.5'
4'
2'
21.75'
3 phase 30 Amp outlets 208 V

FIG. 12

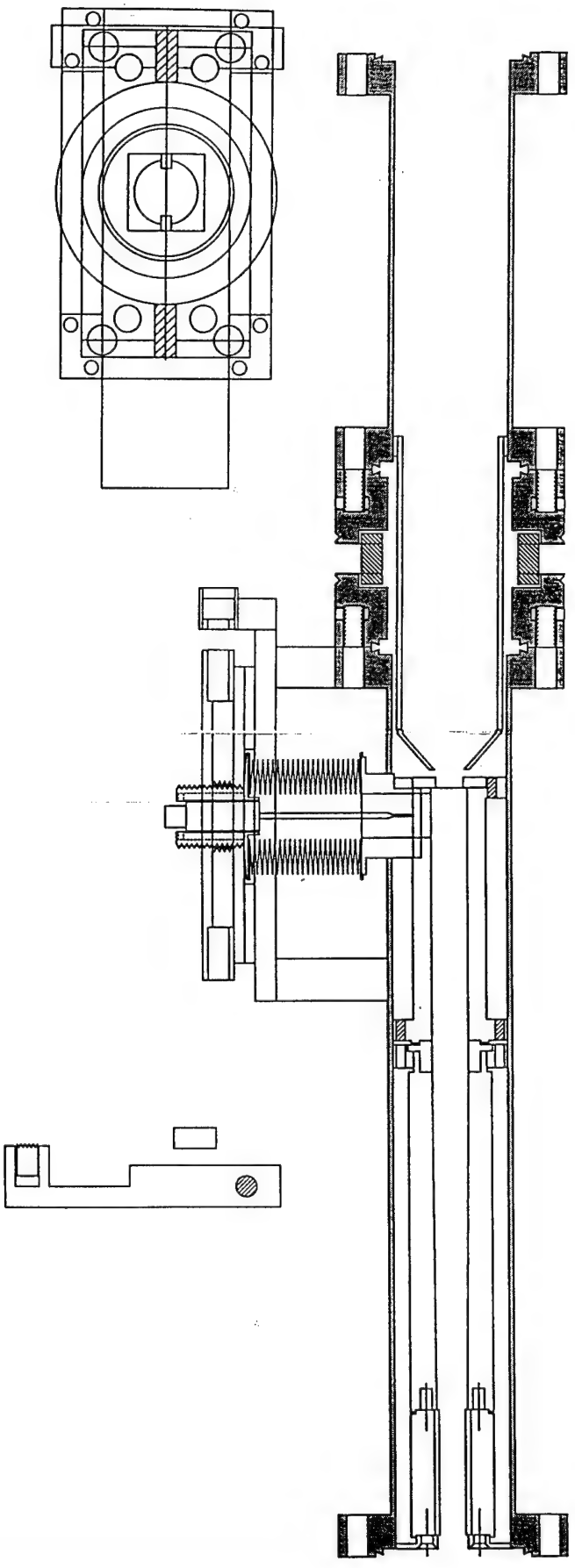

FIG. 13

"on-axis view"

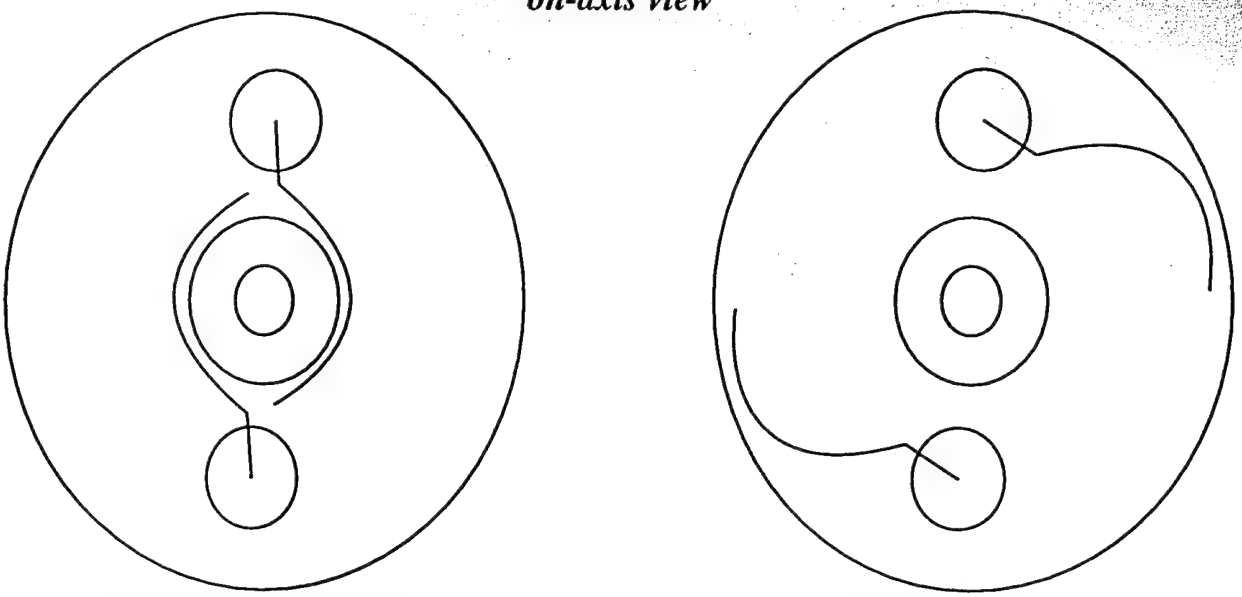

Paddles Deployed

Paddles Stowed

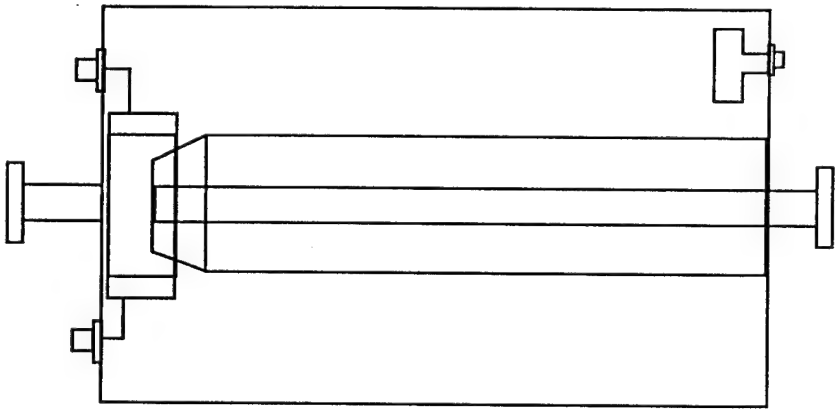

"side view"

Figure 14

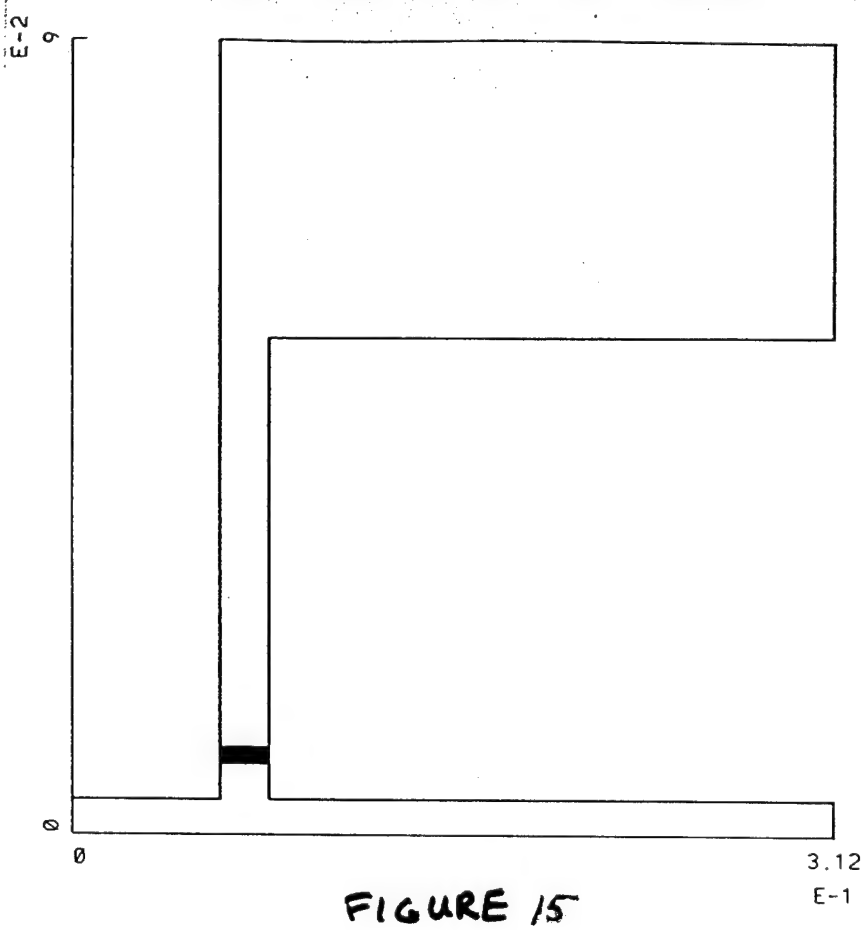

FIGURE 15

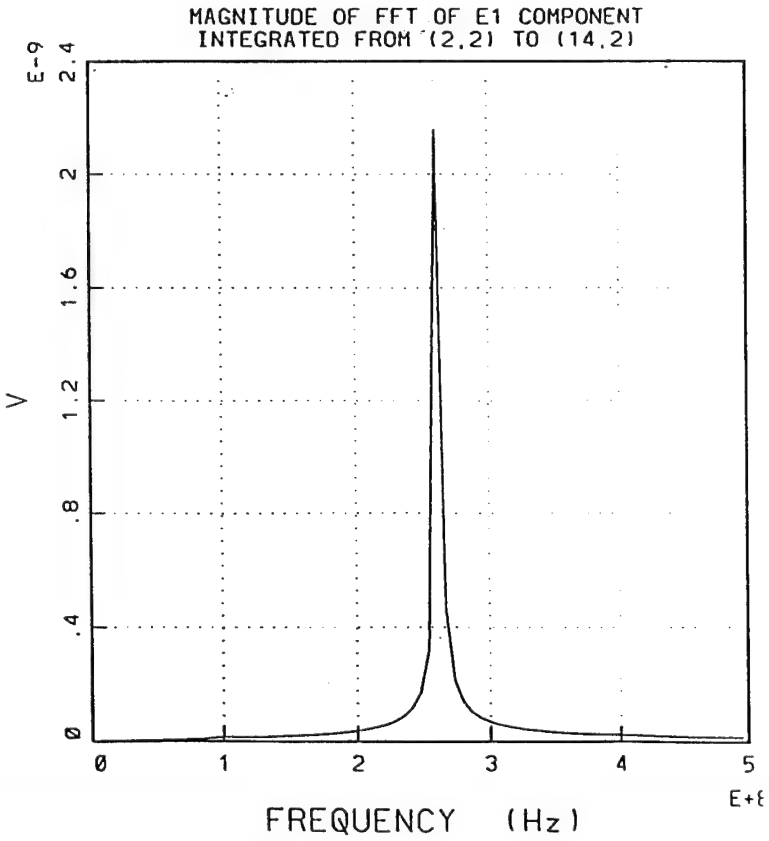

FIGURE 16

MAGIC VERSION: JANUARY 1995 DATE: 9/1/1995
SIMULATION: TUNED

VIEW OF GRID, CONDUCTORS, AND SYMMETRY BOUNDARIES

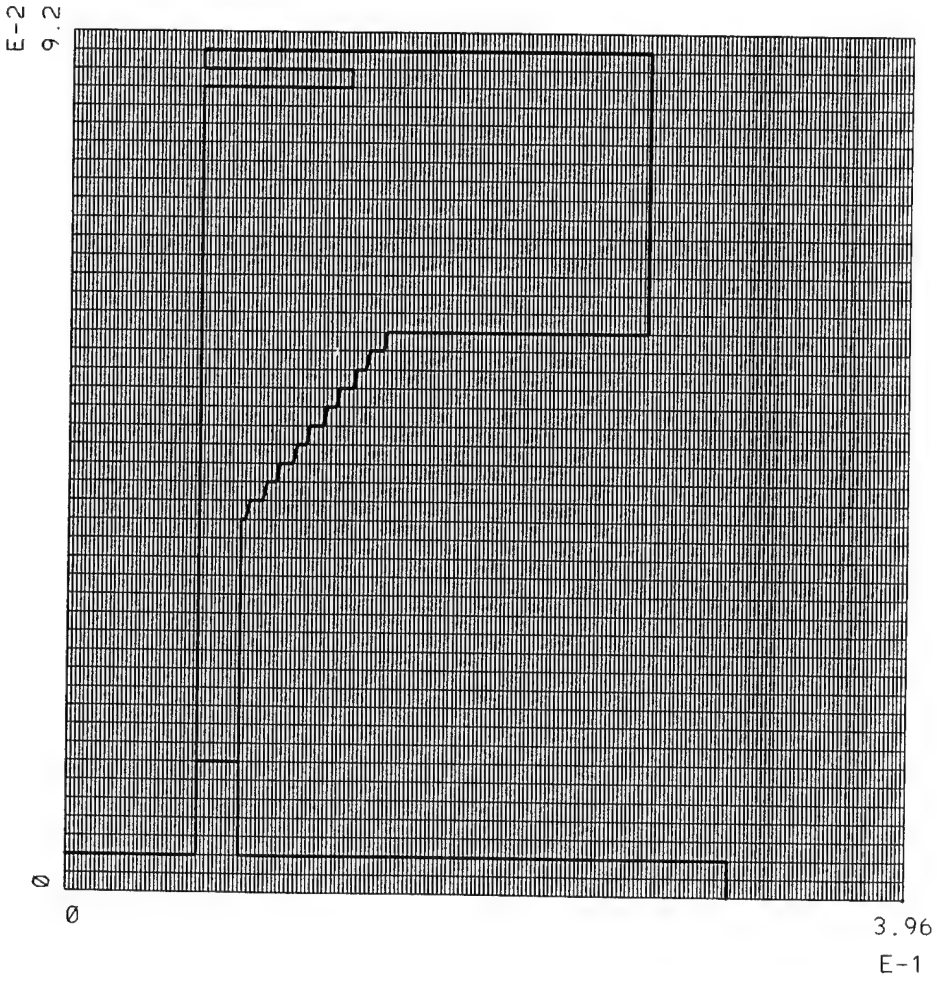

FIG. 17

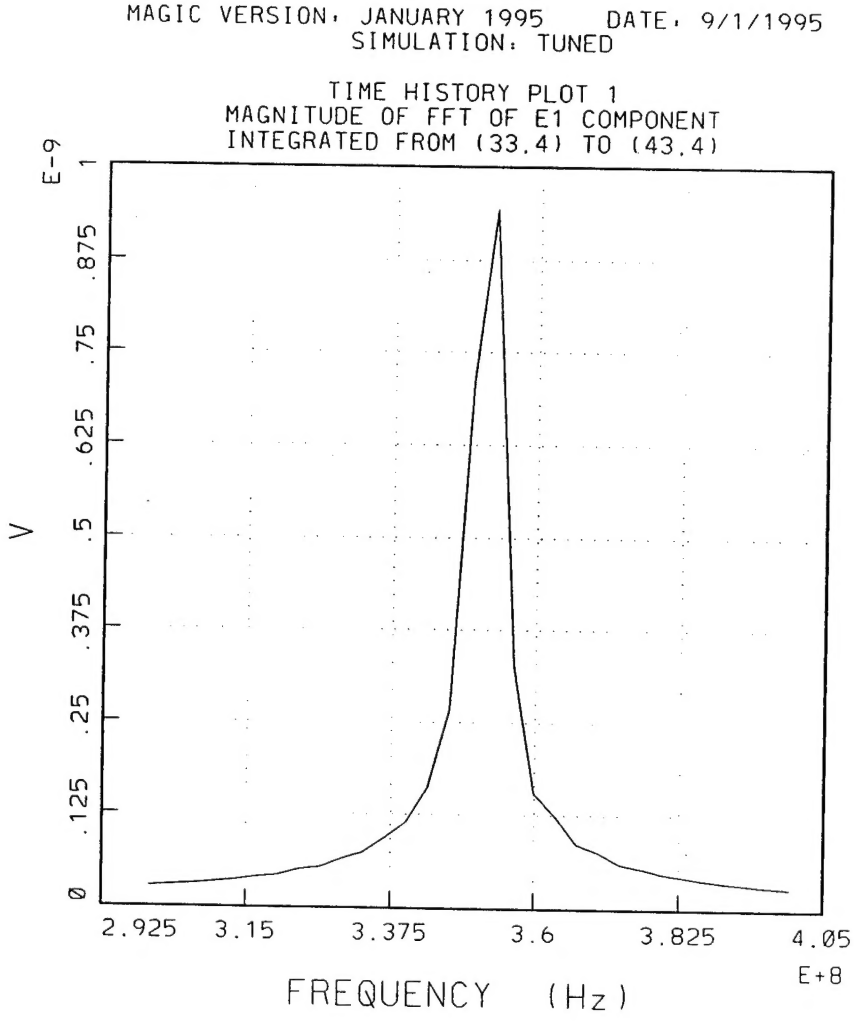
MAGIC VERSION: JANUARY 1995 DATE: 9/1/1995
SIMULATION: TUNED
TIME HISTORY PLOT 1
MAGNITUDE OF FFT OF E1 COMPONENT
INTEGRATED FROM (33,4) TO (43,4)
E-9
V
1
.875
.75
.625
.5
.375
.25
.125
0
2.925
3.15
3.375
3.6
3.825
4.05
E+8
FREQUENCY (Hz)

F16.18

MAGIC VERSION: JANUARY 1995 DATE: 9/1/1995
SIMULATION: RING

VIEW OF GRID, CONDUCTORS, AND SYMMETRY BOUNDARIES

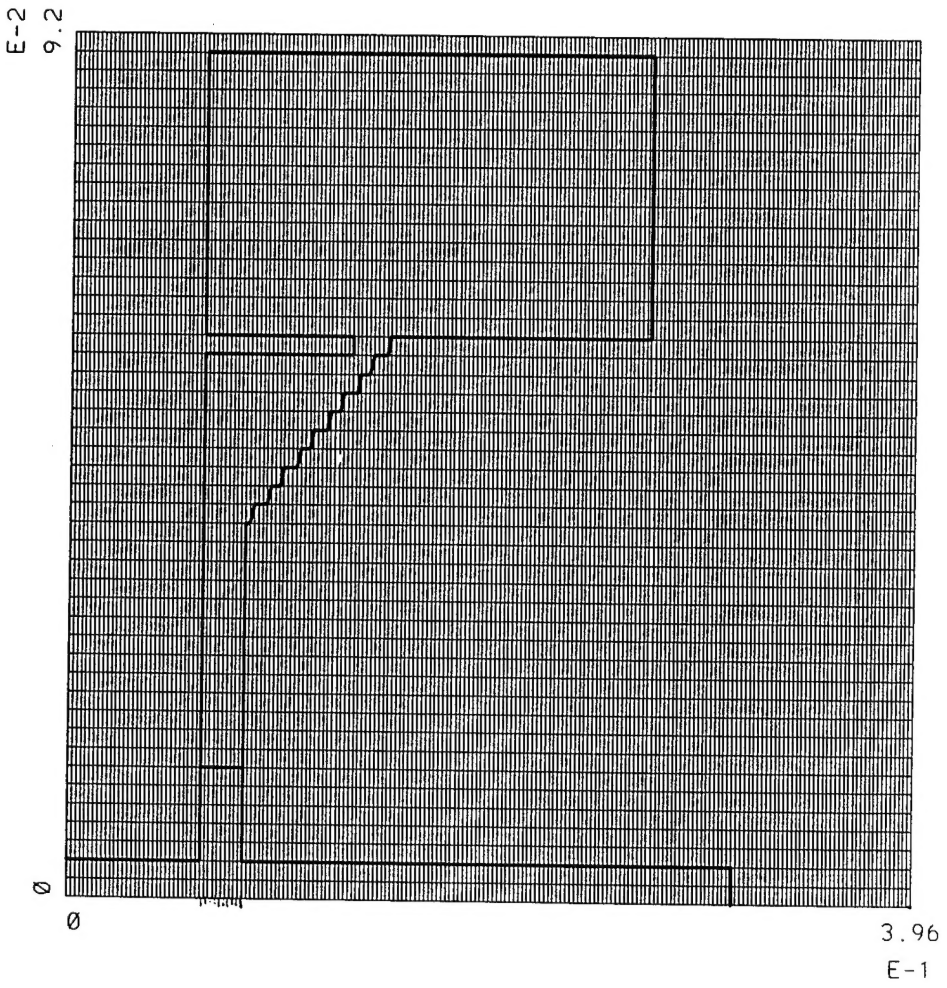

FIG. 19

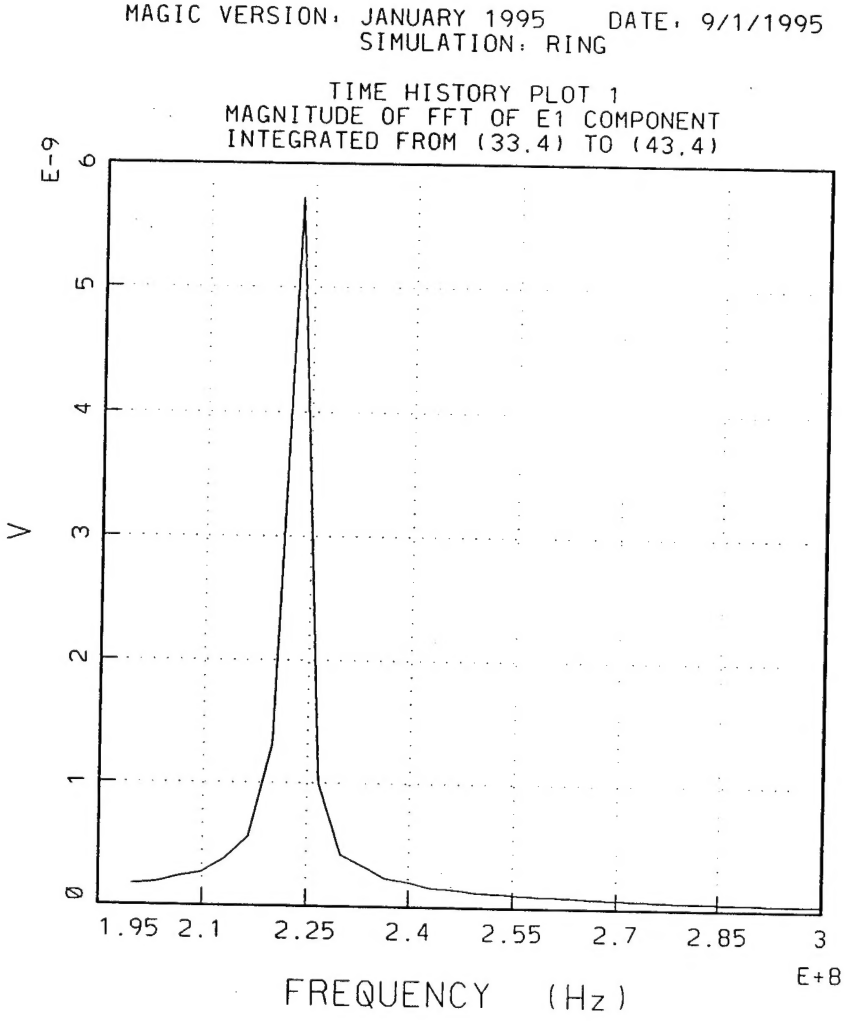
MAGIC VERSION: JANUARY 1995 DATE: 9/1/1995
SIMULATION: RING
TIME HISTORY PLOT 1
MAGNITUDE OF FFT OF E1 COMPONENT
INTEGRATED FROM (33,4) TO (43,4)
E-9
V
0
1
2
3
4
5
6
1.95
2.1
2.25
2.4
2.55
2.7
2.85
3
E+8
FREQUENCY (Hz)

FIG. 20

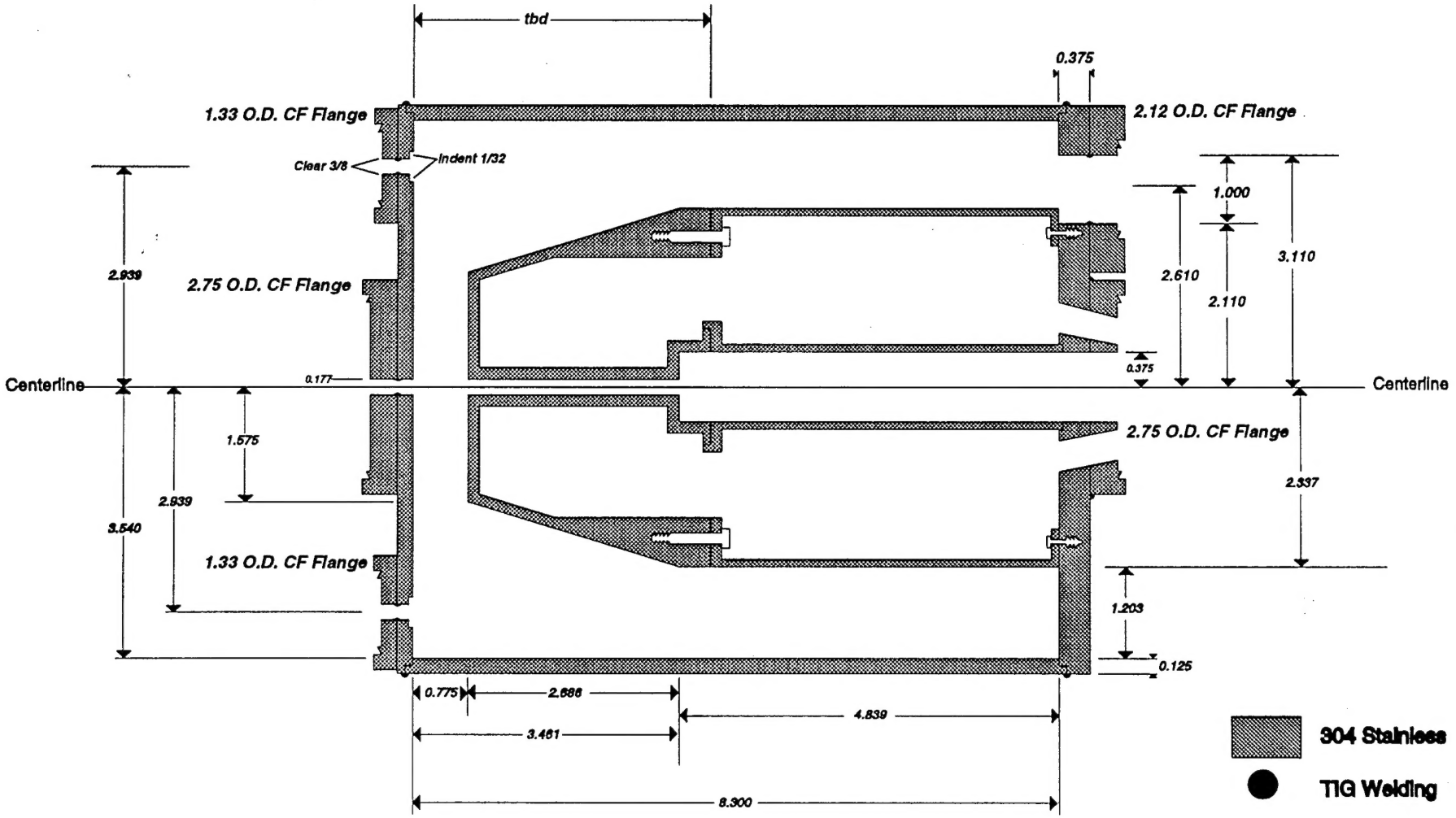

SCALE 1:2
UNITS: Inches

FIG. 21

Premodulating Cavity		
top.ai	Richard S. Burnside	1/5/96